ATOMIC LAYER DEPOSITION

Mikko Ritala, Markku Leskelä
Department of Chemistry, University of Helsinki, FIN-00014 Helsinki, Finland

Contents

1. Introduction . . . 103
2. Alternative Names . . . 104
3. Basic Features of ALD . . . 104
 3.1. ALD Cycle . . . 104
 3.2. Benefits of ALD . . . 106
 3.3. Limitations of ALD . . . 108
4. ALD Reactors . . . 108
 4.1. Overview . . . 108
 4.2. Flow-Type ALD Reactors with Inert Gas Valving . . . 109
 4.3. Flow-Type ALD Reactors with Moving Substrates . . . 112
5. ALD Precursors . . . 113
 5.1. Requirements for ALD Precursors . . . 113
 5.2. Choice of Precursors . . . 121
 5.3. Overview of Precursors and Their Combinations Used in ALD . . . 121
6. Film Materials and Applications . . . 125
 6.1. Electroluminescent Display Phosphors . . . 126
 6.2. Insulators . . . 128
 6.3. Transparent Conductors . . . 133
 6.4. Passivating and Protecting Layers . . . 134
 6.5. Transition Metal Nitride Diffusion Barriers . . . 135
 6.6. Metals . . . 137
 6.7. Solar Cell Absorbers . . . 138
 6.8. Optical Coatings . . . 138
7. Characterization of ALD Processes . . . 138
 7.1. Film Growth Experiments . . . 139
 7.2. Reaction Mechanism Studies . . . 144
8. Summary . . . 152
 References . . . 153

1. INTRODUCTION

Atomic layer deposition (ALD) is a chemical gas phase thin film deposition method based on alternate saturative surface reactions. As distinct from the other chemical vapor deposition techniques, in ALD the source vapors are pulsed into the reactor alternately, one at a time, separated by purging or evacuation periods. Each precursor exposure step saturates the surface with a monomolecular layer of that precursor. This results in a unique self-limiting film growth mechanism with a number of advantageous features, such as excellent conformality and uniformity, and simple and accurate film thickness control.

ALD was developed and world widely introduced with a name of atomic layer epitaxy (ALE) (for other names, see Section 2) in the late 1970s by Suntola and co-workers in Finland [1–4]. The motivation behind developing ALD was the desire to make thin film electroluminescent (TFEL) flat panel displays [2, 5–9]. This is a demanding application since electric fields in the range of megavolts per centimeter are applied across

Handbook of Thin Film Materials, edited by H.S. Nalwa
Volume 1: Deposition and Processing of Thin Films
Copyright © 2002 by Academic Press
All rights of reproduction in any form reserved.

ISBN 0-12-512909-2/$35.00

polycrystalline or amorphous luminescent and insulator films (Sections 6.1. and 6.2). Nevertheless, ALD was successful in meeting the requirements of high dielectric strength, low pinhole density, and uniformity over the large-area substrates, and it has been employed in TFEL production since the early 1980s [7–11].

Soon after the successful introduction of ALD, its applicability to epitaxial compound semiconductors was demonstrated by several groups [12–15], and since that semiconductors, especially the III–V compounds, have been the most extensively examined materials [16–25]. However, though many outstanding results have been achieved, the overall success in that field has remained limited with no reported commercial applications. Meanwhile, new nonepitaxial applications were taken into research more slowly but steadily. Solar cells, microelectronics, optics, protective applications, and gas sensors have been among the areas examined.

Since the mid 1990s, rapidly increasing interest toward ALD has arisen from the silicon-based microelectronics. This increase is a direct consequence of the ever-decreasing device dimensions and the increasing aspect ratios in the integrated circuits (IC). The thin film deposition techniques used for a long time in the IC industry are foreseen to meet major conformality problems during the next few years, and ALD is currently considered as one of the most potential substitutes for them. At the same time, the films are shrinking so thin that the major concern of ALD, the low deposition rate, is becoming less important.

In addition to thin films on planar substrates, ALD has also been examined in surface processing of porous materials. A great deal of this work has concentrated on chemical modification of high surface area silica and alumina powders for heterogeneous catalysts [26–33] but also nanoporous silicon layers [34, 35] and alumina membranes [36, 37] have been processed.

As the current interest in ALD is largely centered on nonepitaxial films, this review chapter mainly focuses on these materials and the related chemistry. The growth of epitaxial semiconductors has been thoroughly reviewed elsewhere [16–25] and is touched here only from the chemistry point of view. In addition, the ALD processing of high surface area powders has been summarized in a number of articles [30–33] and is considered here only as a valuable source of information on the growth mechanisms (Section 7.2.2). In addition to these and other, more general review articles [5–9, 38–42], the proceedings of the biannually held topical international symposia [43–46] give a good overview of the development of the ALD method.

We start with a few notes on the alternative names of ALD, followed by an introduction of the basic features, benefits, and limitations of the method. After examining ALD reactors, precursors will be discussed. This is followed by a summary of ALD made film materials. Finally, the various ways of optimizing and characterizing ALD processes are surveyed.

2. ALTERNATIVE NAMES

At the time of its introduction, the method was given a name atomic layer epitaxy (ALE) [1, 2] where the term "epitaxy," coming from the Greek and meaning "on-arrangement," was used to emphasize the sequentially controlled surface reactions upon the previously deposited layer [7, 38]. However, as "epitaxy" is more commonly used in describing a growth of a single crystalline film on a single crystalline substrate with a well-defined structural relationship between the two, unfortunate confusions have arisen when applying the name ALE in the case of amorphous or polycrystalline films. For this and other reasons, many synonyms, all basically referring to the same method, have been suggested for ALE during the years (Table I). Among these, ALD appears to have become the most widely used one and is to be understood as a general name of this method covering all kinds of films, whereas ALE should now be reserved for epitaxial films only. Though the words "atomic" and "layer" have also been questioned (Table I), their continuous use is strongly motivated by the desire to keep the terminology consistent, thereby assisting the follow-up of the literature.

3. BASIC FEATURES OF ALD

3.1. ALD Cycle

In ALD, the film growth takes place in a cyclic manner. In the simplest case, one cycle consists of four steps: (i) exposure of the first precursor, (ii) purge or evacuation of the reaction chamber, (iii) exposure of the second precursor, and (iv) purge or evacuation. This cycle is repeated as many times as necessary

Table I. Alternative Names to the ALD Method

Name	Acronym	Comments
Atomic layer deposition	ALD	General, covers all kinds of films In a close connection with the original name
Atomic layer epitaxy	ALE	The original name, but should be reserved for epitaxial films only
Atomic layer growth	ALG	Like ALD but less used
Atomic layer chemical vapor deposition	ALCVD	Emphasizes the relation to CVD
Molecular layer epitaxy	MLE	Emphasizes molecular compounds as precursors
Digital layer epitaxy	DLE	Emphasizes the digital thickness control
Molecular layering	ML	Dates back to old Russian literature
Successive layerwise chemisorption		
Sequential surface chemical reaction growth		
Pulsed beam chemical vapor deposition		

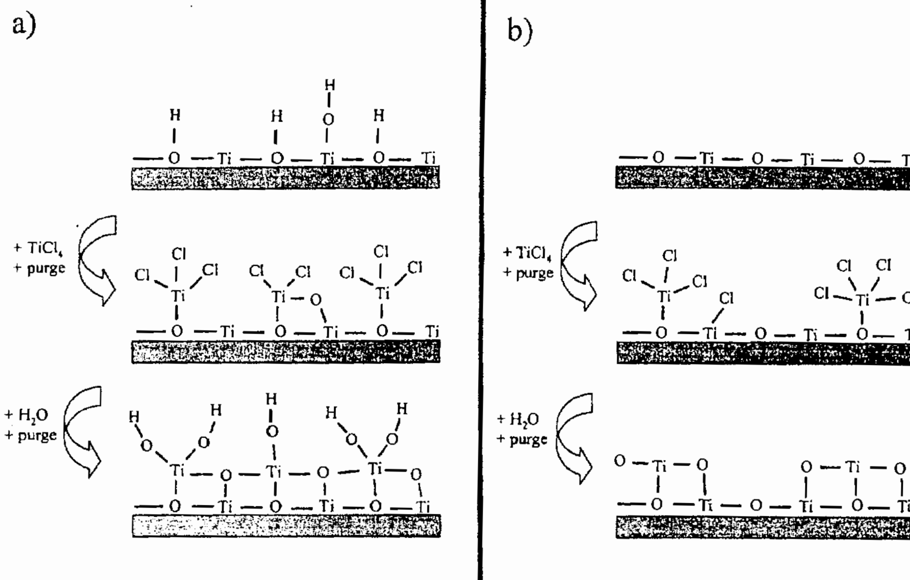

Fig. 1. An ALD film deposition cycle shown schematically with the $TiCl_4$-H_2O process as an example. To illustrate the importance of surface species possibly remaining after the water pulse, or more generally, after the nonmetal precursor pulse, two hypothetical reaction routes have been sketched: (a) hydroxyl group terminated and (b) dehydroxylated surface after the water pulse.

to obtain the desired film thickness. Depending on the process, one cycle deposits 0.1- to 3-Å film thickness.

The actual reactions taking place under each exposure step depend largely on the presence or the absence of reactive functional groups on the surface of the growing film. In the case of oxides, for example, surface hydroxyls often terminate the surface after exposure to water. Here, the ALD process is schematically illustrated by an example of the growth of TiO_2 from $TiCl_4$ and H_2O (Fig. 1). To emphasize the importance of the hydroxyl groups, two alternative reaction routes have been sketched out, one with a hydroxyl group terminated surface (Fig. 1a) and the other with a completely dehydroxylated surface (Fig. 1b). In reality, the hydroxyl coverage is temperature dependent, and thus the two routes may be mixed.

When dosed onto the surface terminated with functional (here hydroxyl) groups, the precursor molecules react with these groups (Fig. 1a) releasing some of their ligands. If there are no functional groups on the surface, the incoming molecule can only chemisorb, either intact or dissociatively (Fig. 1b). As a consequence of a finite number of the reaction or chemisorption sites on the surface. in maximum only a monomolecular layer of the precursor becomes firmly bound to the surface. The following purge (or evacuation) period removes all the excess precursor molecules and volatile byproducts leaving only the monolayer on the surface. For simplicity, from here on, this monolayer will be called a chemisorption layer regardless of whether it is formed via exchange reactions (Fig. 1a) or true chemisorption (Fig. 1b). Subsequently, the other precursor is dosed in and reacts with the chemisorption layer liberating the ligands and producing the desired solid. At the same time, the surface is converted back to its original state, i.e., in our example either hydroxyl terminated (Fig. 1a) or bare oxide surface (Fig. 1b). The second purge period completes the deposition cycle which is then repeated.

Ideally, each exposure and purge step is complete. The precursor molecules chemisorb or react with the surface groups saturatively so that after the formation of the chemisorption monolayer no further adsorption takes place, and the purge periods remove all the excess precursor and volatile byproduct molecules. Under these conditions, the film growth is self-limiting: the amount of the film material deposited during each cycle is the same and is determined only by the density of the chemisorption or reaction sites at the surface. The self-limiting growth mechanism gives ALD a number of advantageous features (Table II) which are discussed in more detail in the next section.

Most of the ALD processes are based on the above described exchange reactions between molecular precursors. Another possible reaction type is additive with elemental precursors but because only a few metals are volatile enough, the applicability of these reactions is limited. The third reaction type, quite rare as well, involves a self-limiting adsorption of a precursor followed by its decomposition by an appropriate energy pulse (Section 5.3.4).

In a majority of the ALD processes reported, the reactions are activated only thermally under isothermal conditions. However, additional activation methods have also been examined. These include light irradiation with lasers [15, 17, 19, 47–51] or lamps [52–57] for promoting photolytic or photothermal reactions, and upstream generation of reactive radicals by thermal cracking [58–69] or with plasma discharges [70–75].

The alternate pulsing is definitely the most characteristic feature of ALD but almost as distinctive is the self-limiting growth mechanism. However, some deviations from the absolutely self-

Table II. Characteristic Features of ALD with the Consequent Advantages

Characteristic feature of ALD	Inherent implication on film deposition	Practical advantage
Self-limiting growth process	Film thickness is dependent only on the number of deposition cycles	Accurate and simple thickness control
	No need of reactant flux homogeneity	Large-area capability
		Large-batch capability
		Excellent conformality
		No problems with inconstant vaporization rates of solid precursors
		Good reproducibility
		Straightforward scale-up
	Atomic level control of material composition	Capability to produce sharp interfaces and superlattices
		Possibility to interface modification
Separate dosing of reactants	No gas phase reactions	Favors precursors highly reactive toward each other, thus enabling effective material utilization
	Sufficient time is provided to complete each reaction step	High quality materials are obtained at low processing temperatures
Processing temperature windows are often wide	Processing conditions of different materials are readily matched	Capability to prepare multilayer structures in a continuous process

limited growth conditions may be accepted with certain precautions. The reactions may be somewhat incomplete leaving the chemisorption layer short from saturation, or there may be some precursor decomposition in addition to the chemisorption. As long as the reactions causing these nonidealities proceed in a surface controlled rather than a mass transport controlled manner, the coverage of the chemisorption layer and thereby the deposition rate remain everywhere the same, thus maintaining the advantageous characteristics of ALD. Alternatives to accepting these nonidealities would be to increase the exposure time to complete the reactions, or to lower the deposition temperature to avoid the decomposition, but these would be accompanied by negative effects of increased process time and reduced film quality.

A common misconception is that ALD growth always proceeds in a layer-by-layer manner but this is often not the case as only a fraction of a monolayer may be deposited in each cycle. Reasons for the less than a monolayer per cycle growth are the limited number of reactive surface sites [33, 42] and the steric hindrances between bulky ligands in the chemisorption layer [8, 76]. As a consequence, even if saturatively formed, the chemisorption layer contains too few metal atoms for forming a full monolayer of the film material. On the other hand, also surface reconstructions may cause a decrease in the growth rate [77, 78], though in the apparently exceptional case of the 2 ML $cycle^{-1}$ growth of AlAs they appear to have the opposite effect [19, 79–81].

Yet another misconception is that ALD would produce atomically smooth films. This indeed may often be the case with epitaxial or amorphous films, but the nucleation and the grain growth involved in the formation of polycrystalline films usually lead to a measurable surface roughness which increases along with film thickness (Section 7.2.1) [39, 82–87].

3.2. Benefits of ALD

Table II summarizes the relationships between the characteristic features of the ALD process and the resulting benefits. The benefits are now discussed with selected examples. It is worth emphasizing already here that the achievement of these benefits requires appropriate chemistry fulfilling the special requirements set for ALD processes (Section 5).

As the film growth proceeds in a self-limiting manner, each cycle deposits exactly the same amount of material, and thus the film thickness may be accurately controlled simply by the number of deposition cycles. However, it must be recognized that during the very first cycles when the surface is converted from the substrate to the film material, the surface density of the chemisorption or reactive sites and, accordingly, the growth rate may change.

The self-limiting growth mechanism also ensures that the precursor fluxes do not need to be uniform over the substrate. What is only needed is a flux which is large enough so that the chemisorption layer becomes saturated, all the excess will be subsequently purged away. As a result, ALD provides perfect conformality and trench-fill capability (Fig. 2) [88] as well as good large-area uniformity [88, 89] and large-batch capability. Batches as large as 82 substrates of a size 15.5×26.5 cm^2 [41] or 42 times 40×50 cm^2 substrates [90] may be processed in the existing ALD reactors, and this is certainly not the upper limit. The self-limiting growth mechanism also ensures good reproducibility and relatively straightforward scale-up.

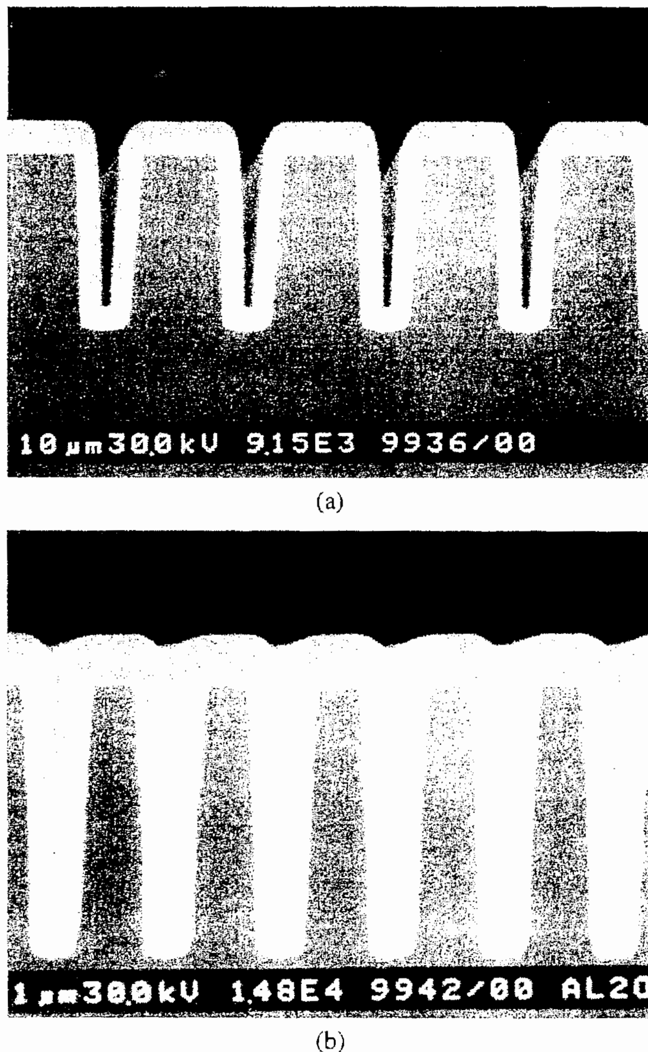

Fig. 2. Cross-sectional SEM images of a 300-nm Al_2O_3 film deposited onto a patterned silicon substrate showing (a) perfect conformality and (b) trench-fill capability [88]. Note that on the top surface of the silicon wafer there is a thermal silicon oxide layer below the Al_2O_3 film. Reprinted with permission from M. Ritala et al., Perfectly conformal TiN and Al_2O_3 films deposited by atomic layer deposition, *Chem. Vapor Deposition* 5, 7 (1999), © 1999, Wiley-VCH Verlag GmbH.

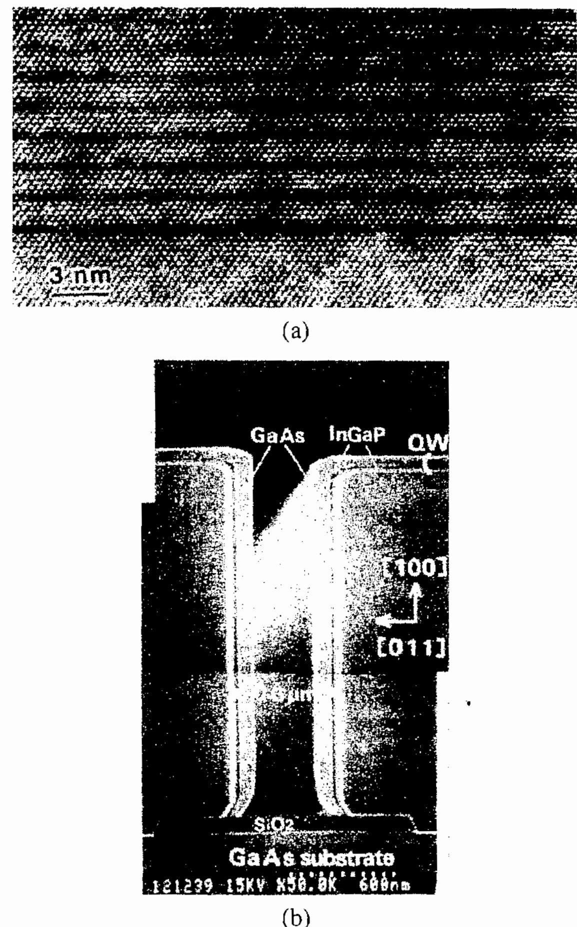

Fig. 3. (a) (110) cross-sectional transmission electron microscopy (TEM) micrograph of a 1-ML InAs – 5-ML GaAs superlattice. (b) Cross-sectional scanning electron microscopy (SEM) micrograph of an $In_{1-x}Ga_xP$/GaAs single quantum well structure on a (011) sidewall of a GaAs substrate [18]. Reprinted with permission from A. Usui, Atomic layer epitaxy of III–V compounds: Chemistry and applications, *Proc. IEEE* 80, 1641 (1992), © 1992, IEEE.

Precursor flux homogeneity is not required in timescale either. Therefore, solid sources which often have inconstant sublimation rates are more easily adopted in ALD than in chemical vapor deposition (CVD). The separate dosing of the precursors, in turn, naturally eliminates all possible detrimental gas phase reactions.

As the film is deposited in a layerwise manner, either a full monolayer or a fraction of a monolayer at a time, the material composition may be controlled down to a nanometer level, and in the most ideal cases even to an atomic level. This offers a simple way to create superlattices (Fig. 3a) [7, 18, 91, 92] and other multilayer structures with accurately controlled layer thicknesses, such as optical multilayers tailored for soft X-ray or visible range (Section 6.8), or nanolaminate insulators (Section 6.2). An outstanding demonstration of the accurate film thickness control and perfect conformality is shown in Figure 3b where a single quantum well structure has been grown into a trench. Note also the selective growth between the GaAs and SiO_2 surfaces.

Practice has shown that ALD made films often, though of course not always, possess superior quality as compared with films made by other methods at the corresponding temperatures. This can be related to the fact that in ALD each monomolecular layer reaction step is given enough time to reach completion while in other methods the continuous growth may prevent this by covering the unreacted species with new deposits.

Many ALD processes may be performed over a relatively wide temperature range. Therefore, a common growth temperature is often found for different materials, thereby making it possible to deposit multilayer structures in a continuous manner. This is utilized, for example, in manufacturing of the TFEL displays where the insulator-luminescent material-

insulator three-layer structure (Section 6.1) is grown in one continuous process.

3.3. Limitations of ALD

The major limitation of ALD is evidently its slowness since at best a monolayer of the film is deposited during one cycle. Typically, deposition rates of 100–300 nm h^{-1} are obtained and 1 $\mu m\,h^{-1}$ appears to be the upper limit for most processes, though a record rate of 2 $\mu m\,h^{-1}$ was achieved for epitaxial GaAs in a specially designed reactor (Section 4.3) [93]. However, the low growth rate does not necessarily mean low productivity when the latter is considered in terms of film volume (= thickness × area) produced per time unit. By making use of the good large-batch and large-area processing capabilities of ALD, the low growth rate may be effectively compensated for. On the other hand, there are certain application areas, in particular integrated circuits, where single substrate processing is increasingly preferred because of the cost risks related to losing a batch of valuable substrates. Luckily, at the same time, the film thicknesses have shrunk down to a level where the low growth rate of ALD is losing its significance when weighted against the potential benefits.

One limitation to a widespread use of ALD has been the lack of good and cost-effective processes for some important materials. Among these are, for example, metals, Si, SiO_2, Si_3N_4, and several ternary and multicomponent materials. Many of these materials have been made by ALD (Table V in Section 6) but the processes are still far from ideal in a sense that long cycle times are required.

4. ALD REACTORS

4.1. Overview

Just like CVD, ALD processes may also be performed in many kinds of reactors over a wide pressure range from atmospheric to ultrahigh vacuum (UHV). ALD reactors can be divided into two groups: inert gas flow reactors operating under viscous or transition flow conditions at pressures higher than about 1 Torr, and high- or ultrahigh-vacuum reactors with molecular flow conditions. The former resemble CVD reactors while the latter are like molecular beam epitaxy (MBE) reactors. In any case, when the special features and the needs of ALD are taken into consideration in the reactor design, some significant differences emerge as discussed in this section.

The main parts of an ALD reactor are:

1. transport gas supply (if any),
2. sources of one or several of the following types: gas, liquid, and solid sources,
3. flow and sequencing control of the sources,
4. reaction chamber,
5. temperature control of the heated sources and the reaction chamber (and the substrate, if heated separately),
6. vacuum pump and related exhaust equipment.

Provisional items include:

7. *in situ* surface and gas phase analysis equipments, such as an ellipsometer and mass spectrometer, for process characterization and control (Section 7.2),
8. load-locks for changing substrates or sources,
9. separate preheating chamber for the substrates.

The last one is especially effective in maximizing throughput in large-batch processing. Besides equipping with a load-lock, often it may be desirable to make the ALD reactor a part of a larger cluster tool for an inert transfer of the substrates from one process step to another.

As already noted, in ALD no strict precursor flux homogeneity is required. This gives freedom in the reactor design and assists in constructing large-batch reactors. On the other hand, cost-effectiveness of the process requires that both exposure and purge sequences are rapidly completed. For this reason, flow-type reactors are preferred especially in production scale use: purging of a properly designed reactor under viscous flow conditions is much more rapid than evacuation of a high-vacuum chamber. Another crucial aspect related to purging or evacuation is that the chamber and the lines which are to be purged or evacuated should have small volume and uniformly heated walls. Otherwise, long purge periods may be required to desorb precursor molecules adsorbed on "cold spots" on the walls. This is especially important in the growth of oxides where water is often used as an oxygen source.

The desire for high precursor utilization efficiency is also an important aspect for the reactor design. In high-vacuum reactors, the precursor molecules make at best only a few collisions with the substrate surface before being pumped out and thus have a limited probability to react. On the other hand, in the flow-type reactors, and in the traveling-wave reactors (Section 4.2.4) in particular, a precursor molecule makes multiple hits while being transported through the reactor. As a consequence, reaction probability and thereby precursor utilization efficiency are increased, and the saturation of the chemisorption layer is accelerated which makes the process faster.

MBE types of reactors are basically easy to operate in the ALD mode since they are usually equipped with shutters by means of which precursor fluxes from the Knudsen effusion cells can be chopped. When volatile reactants are used, their pulsing is realized with valves. What is still needed to make an ALD process is a proper choice of substrate temperature and evacuation periods between the alternate precursor pulses to ensure the self-limiting growth conditions. The major benefit of the MBE type of reactors is the rich variety of *in situ* analytical techniques which may be implemented for detailed reaction mechanism studies. Large chambers also make it easy to employ various sources of extra energy for activating the reactions (Fig. 4). On the other hand, the need of long exposure and evacuation times limits the throughput.

CVD reactors with liquid and gas sources only are also relatively easy to operate in the ALD mode. For pulsing the precursors, simple solenoid or pneumatic valves may be used. However, if the valves are far from the reaction chamber and there

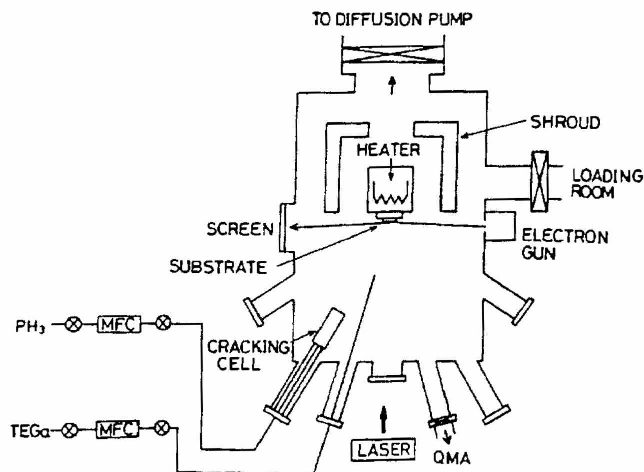

Fig. 4. An example of a high-vacuum ALD reactor incorporating RHEED (electron gun and screen) and a quadrupole mass analyzer (QMA) for *in situ* characterization, and a laser and a thermal cracking cell for activating the reactions [49]. Reprinted with permission from M. Yoshimoto, A. Kajimoto, and H. Matsunami, Laser-assisted atomic layer epitaxy of GaP in chemical beam epitaxy, *Thin Solid Films* 225, 70 (1993), © 1993, Elsevier Science.

Fig. 5. A photograph of an ASM Microchemistry F-950 ALD reactor for production of flat panel displays and solar cells. (Courtesy ASM Microchemistry, Espoo, Finland.)

are long tubings in between, their effective purging calls for special attention. Even more problematic is the pulsing of solid sources which need to be heated far above room temperature where no mechanical valves can be used. In the flow-type ALD reactors described in the next two sections, these issues have been specially addressed.

4.2. Flow-Type ALD Reactors with Inert Gas Valving

The ALD reactors commercially available [90] and those in industrial use in TFEL manufacturing are all of a flow type with inert gas valving [3, 4, 38]. These reactors are carefully designed to minimize the pulse and purge times and to maximize the precursor utilization efficiency. They are available in both small size for research and large size for production [90] (Fig. 5). The main points of these reactor designs are now examined. The discussion is limited mainly to those features which are special to ALD whereas more common issues, like mass flow controllers, pumps, heaters, and their controllers etc., are not dealt with. For a detailed model of mass transport in the flow-type ALD reactors, see Ref. [94].

4.2.1. Transport Gas

Inert gas, most often nitrogen, is used for transporting the precursor vapors and purging the reaction chamber. A continuous flow of the inert gas is regulated with mass flow controllers. The flow rate is optimized together with the total pressure and the reactor geometry to give the best combination of speed, transportation and utilization efficiency of the reactants, inert gas valving (Section 4.2.3), and the consumption of the inert gas itself. In small research reactors, the flow rate is about 0.5 slm whereas the largest production reactors require 20–50 slm. The operating pressures are typically in the range of 1–10 Torr.

A crucial aspect of the transport gas is purity because it is the main source of impurities in an ALD process. In the minimum, 99.999% purity should be used. In Section 4.2.4, a calculation of the effects of the impurities is presented.

4.2.2. Sources

The source chemicals may be divided into two groups depending on if their vapor pressures at room temperature, or close to it, are higher or lower than the total pressure inside the reactor (1–10 Torr). The high vapor pressure sources; i.e., gases and highly volatile liquids, are led into the reactor from their external cylinders or vessels by pulsing with fast valves. No bubblers or transport gases are necessary since the source vapors enter the reactor as a consequence of the pressure difference. Once entered into the reactor, the vapor is transported further by the carrier gas flow inside the reactor. However, as large scale manufacturing requires large doses, carrier gas transportation already from the source vessel may become necessary.

For low vapor pressure source chemicals, two options exist. The first one is to have them in external vessels which, together with the source lines and the required valving systems, are properly heated to ensure effective transportation. The second option is to place the source chemicals inside the reactor where they are heated to temperatures where appropriate vapor pressures are obtained. In research reactors, for instance, a vapor pressure around 0.1 Torr has been found to be a good starting point for a new precursor. To realize pulsing of solid sources inside the reactor, a clever inert gas valving system (next section) was developed [3, 4].

4.2.3. Inert Gas Valving

An exact mathematical description of the inert gas valving system has been given elsewhere [3, 4, 38], so here only the basic principle is introduced. The inert gas valving is based on a

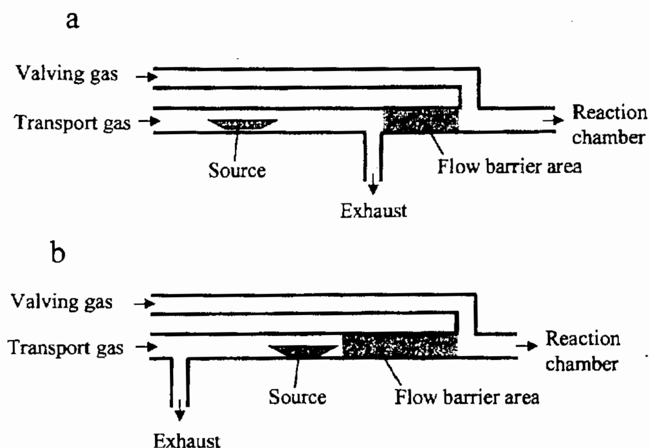

Fig. 6. A schematic of the inert gas valving system where the direct connection to the exhaust is (a) between the source and the reaction chamber, or (b) behind (upstream of) the source. The shading shows the area where the flow barrier is formed when set on.

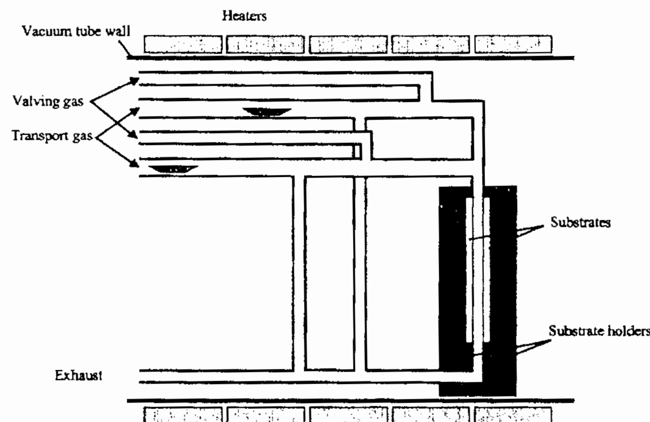

Fig. 7. Schematics of a small research ALD reactor with two inert gas valved source lines and a traveling-wave reaction chamber inserted to a main vacuum tube (not to scale). The intermediate space contains inert gas at a pressure slightly higher than that inside the tubings and the reaction chamber.

design where each source tube is connected both to a reaction chamber and directly to an exhaust so that the exhaust connection is either between the source and the chamber (Fig. 6a) or behind the source (Fig. 6b). Each tube is also equipped with two inert gas flows: one is the transport gas and the other is the valving gas. The valving gas enters the source tube between the source and the reaction chamber. A practical way to realize the two flows is to employ coaxial tubes [3, 4].

When the source is in its off state, the valving gas flow is on and the transport gas flow is off. The valving gas flow divides into two parts, one purging the reaction chamber and the other one setting up a laminar flow barrier (shaded areas in Fig. 6). The flow rate of the valving gas in the flow barrier is adjusted to counterbalance the diffusion rate of the precursor toward the chamber so that the precursor vapor pressure in the chamber does not exceed a predetermined level, for example, one part per million (ppm) of its pressure in the source. In other words, the velocity of the valving gas in the barrier is set equal to or greater than the velocity by means of which the specified precursor isobar diffuses. When the source is turned on, the valving gas is turned off and the transport gas is turned on, thereby breaking the flow barrier. All this can be done rapidly with valves located at room temperature, no matter how hot the source itself is.

The source vapors are led into the reaction chamber through separate lines which all, i.e., also those through which vapors from the external gas or liquid sources are led in, are equipped with the inert gas valving system. Usually, the valving points are close to the chamber and the separate lines merge just in front of it so that the volume to be purged is minimized and well heated and there is hardly any film growth before the chamber.

The operation of the inert gas valving system is easily tested by pulsing only one precursor into the chamber while keeping the other one behind the flow barrier. No film deposition is observed when the barrier holds.

4.2.4. Reaction Chamber

The reactors may be equipped with two kinds of reaction chambers: a compact, cassette-like, traveling-wave reactor chamber, and a more open tubular chamber. They both may be combined easily with the inert gas valving system. The open chambers have the benefit that they can incorporate any arbitrarily shaped substrate. However, they are not as fast and as cost-effective as the traveling-wave reactors which therefore are preferred with planar substrates in both research and large scale production.

In the traveling-wave reactor geometry, the substrates are located face to face close to each other. The distance between two substrates is typically only a few millimeters leaving a narrow flow channel in between. As an example, Figure 7 shows schematics of a small reactor where there is only one substrate pair. A connection to two inert gas valved source lines is shown as well. In practice, there are usually more source lines to facilitate deposition of multicomponent films or multilayer structures. Favorably, the substrates are located close to the point where the source lines merge since this minimizes the chamber wall area subjected to the film growth. The whole assembly of the source lines and reaction chamber is inserted into a vacuum tube outside which heaters are located. The temperature increases stepwise from the gas inlets toward the reaction chamber so that each solid source may be set independently to an appropriate temperature.

In large-batch reactors, there may be tens of substrates arranged in pairs so that the gases flow over the front but not on the backsides of the substrates (Fig. 8). Instead of the one flow channel in the small reactor, in the large reactor there are several of them parallel with each other. Connections to the sources are basically similar to the small reactor. Together with the self-limiting film growth mechanism, these similarities between the research and large scale reactors assist in scale-up of ALD processes.

When pulsed into the reaction chamber, the precursor molecules are transported by the carrier gas along the flow

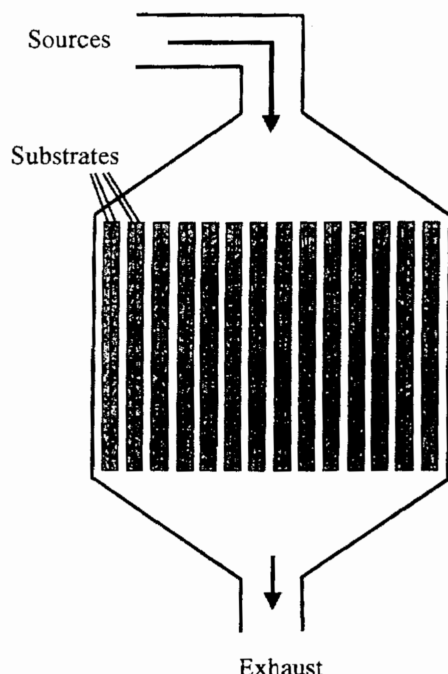

Fig. 8. Reaction chamber of a large scale ALD reactor incorporating several substrates in pairs so that narrow flow channels are left between each pair.

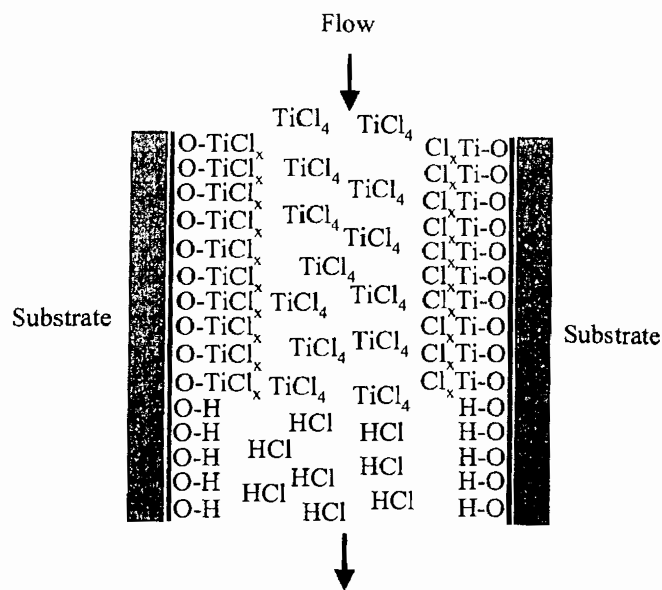

Fig. 9. Propagation of a $TiCl_4$ pulse along a flow channel over substrate surfaces which the preceding water pulse has left hydroxyl group terminated. The multiple hit conditions ensure that the hydroxyl groups become effectively consumed in exchange reactions at the $TiCl_4$ pulse front. HCl molecules formed as reaction byproducts travel in front of the $TiCl_4$ pulse and thus may readsorb and block reaction sites from $TiCl_4$.

channel between the substrates. The flow velocity and pressure are adjusted to maintain essentially pluglike flow conditions which keep the adjacent precursor pulses separated—like waves—and ensure effective and rapid purging of the small volume left between the substrates. In the small research reactors with two 5×5 cm^2 substrates (Fig. 7), purge times as short as 0.1 s are enough for separating the precursor pulses. If the pulses were not well separated, films with nonuniform thickness would be obtained, and in the worst case particles might form in gas phase reactions.

While traveling along the narrow flow channel, the precursor molecules undergo multiple collisions with the substrates. As a result of these multiple hit conditions, the precursor molecules have a high probability to find an open chemisorption or reaction site and thus become effectively utilized. At the same time, the surface becomes rapidly saturated: often 0.2 s is enough for the saturation in the previously described research reactor. A low operation pressure favors high hitting frequency but reduces the precursor transport capability of the carrier gas. The optimal pressure is thus a compromise of the two factors.

The special conditions in the traveling-wave reactors have a number of interesting consequences. In the beginning of the precursor pulse, its vapor pressure in the flow channel is very much location and time dependent [95]. At first, only the leading edge of the substrate; i.e., the edge closest to the inlet, receives precursor molecules. Because of their high hitting frequency, and preferably also high reactivity, the precursor molecules become rapidly exhausted from the pulse front to the open surface sites. Thus, the latter parts of the substrate do not receive any precursor molecules before the leading parts have become covered. In other words, the precursor pulse front rolls like a wave over the substrate saturating the surface on its way (Fig. 9). Experimentally, this can easily be seen and verified by underdosing one precursor and by observing two distinct regions on the substrate: one covered with a uniform film and another one covered with no film. The higher the precursor reactivity, the sharper the border between the two areas. In research reactors, borders as sharp as a few millimeters are observable. In principle, the steepness of the border could be used in studying the reactivities of the precursors. Quantitative evaluation would, however, require constant doses throughout the experiment which, especially with solid sources, may often be difficult to realize.

The sharp border between the growth and nongrowth areas points out the possibility of maximizing the precursor utilization. The closer the border is set to the substrate, the less precursor is wasted to the growth on the downstream side chamber walls or to the exhaust. However, at the same time the risks related to variations in precursor doses are increased.

In the traveling-wave reactor geometry, the surface hitting densities estimated from the partial pressures with the basic equations of the kinetic gas theory lose their meaning quite a lot. This is illustrated by considering the effects of impurities in the carrier gas. Taking again the research reactor (Fig. 7) as an example, we have, approximately, a total pressure of 5 Torr and 200 stdcm^3 min^{-1} carrier gas flow rate to the flow channel limited by the two 5×5 cm^2 substrates. A typical moisture content of 1 ppm in the carrier gas means a partial pressure of 5×10^{-6} Torr which at room temperature implies a hit-

ting density of 2.4×10^{15} water molecules $cm^{-2} s^{-1}$. For water, a high reactivity toward a surface covered with metal precursors may be assumed and therefore the sticking coefficient should approach unity. Then, the amount of oxygen corresponding to a typical ALD oxide film growth rate (3.0×10^{14} oxygen atoms cm^{-2} $cycle^{-1}$) would become adsorbed in about 0.1 s already from the residues in the carrier gas. However, from the flow rate of the carrier gas, one can calculate that in the same time (0.1 s), only 9×10^{12} H_2O molecules enter the flow channel. When averaged over the 50-cm^2 substrate area, this gives only 1.8×10^{11} oxygen atoms cm^{-2} which is more than 3 orders of magnitude less than that estimated from the hitting density. Clearly, the ordinary hitting density calculations cannot be applied.

What actually happens is that the moisture impurities become adsorbed at the upstream edge of the substrate, i.e., right after the point where the precursor flow lines merge and film growth starts (cf. Fig. 7). Assuming a coverage of 1×10^{14} molecules cm^{-2} and a cycle time of 1.0 s, this means that 0.9-cm^2 area adsorbs the incoming moisture impurities. In practice, a somewhat larger area, typically 5 cm^2, may be disturbed close to the leading edge but besides the impurities other factors also contribute to this area. In any case, the upstream edge of the substrate serves as an effective internal getter for the impurities. By moving the substrates a bit further away from the merging point of the separate precursor lines, the getter region would be eliminated from the substrate but then films would grow more extensively on the chamber walls. Therefore, in research it is more convenient to accept the leading edge area and to consider only the area outside that as representative for the true ALD growth.

A less favorable consequence of the multiple hit conditions is that also the reaction byproducts, like HCl, have a high probability to adsorb. As they are formed in the reactions at the front edge of the precursor pulse, the byproducts travel in front of this pulse (Fig. 9) and thereby they have a possibility to decrease the growth rate by blocking reaction sites from the precursor molecules [96, 97]. This effect may explain the differences which are sometimes observed in the growth rates obtained with the traveling-wave and other kinds of reactors.

In addition to the limitations on substrate shape, the traveling-wave reactors are also restricted in respect to the utilization of extra energy sources like plasma, hot filaments, or light. Because of the compact construction of the reaction chamber, there hardly is any room for the implementation of the extra energy sources, especially in the large-batch reactors. The multiple wall collision conditions, in turn, make it difficult to transport reactive radicals from their remote sources over the entire substrates. Therefore, these reactors are quite limited to thermally activated reactions only.

4.3. Flow-Type ALD Reactors with Moving Substrates

The alternate precursor dosing as required in ALD may be realized not only by chopping precursor fluxes to the stationary substrates as above, but also by moving substrates between separate precursor fluxes which are either constantly on or accordingly pulsed. While a high-vacuum version of such a reactor was used in the very first ALD experiments in 1974 [1, 5, 7], also with this approach flow-type systems have subsequently become dominating. In these reactors, inert gases are used for transporting the precursors and for setting up shrouds between the zones with the different precursors.

The most popular type of moving substrate reactors is based on the rotating susceptor design [3, 4, 13, 20, 63, 93, 98–100], an example of which is shown in Figure 10. A fixed part with

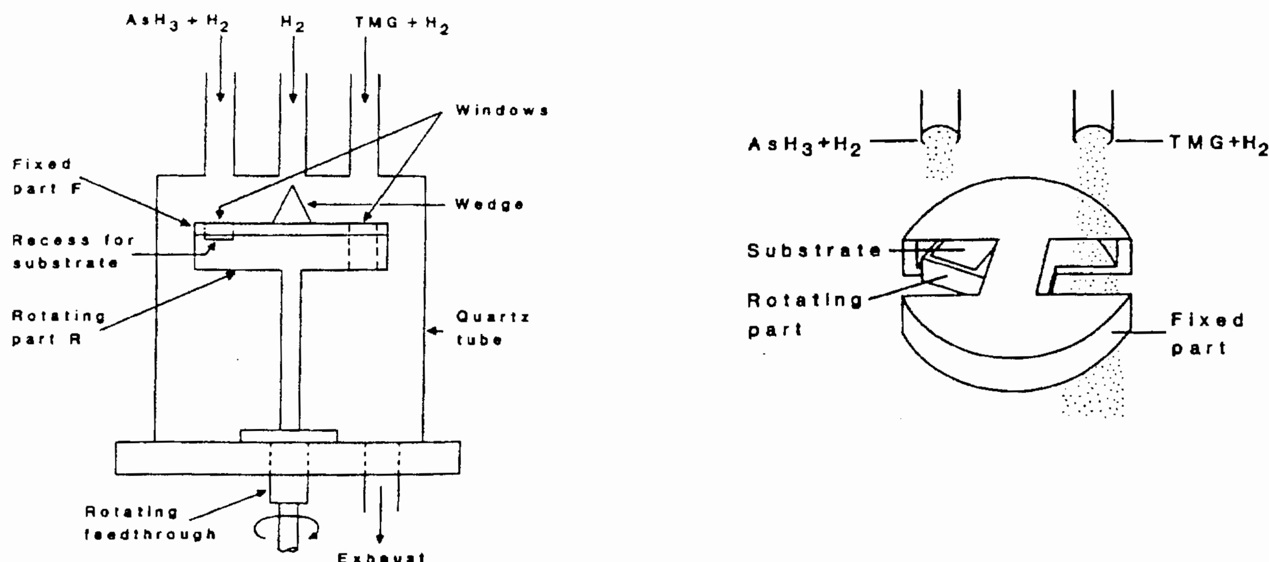

Fig. 10. Schematics of a rotating susceptor ALD reactor [98]. The susceptor consists of fixed and rotating parts. The precursor streams are directed into windows in the fixed part below which the substrate rotates and cuts through the streams. A wedge and a large H_2 flow from the center tube prevent mixing of the two precursors. Reprinted with permission from M. A. Tischler and S. M. Bedair, Self-limiting mechanism in the atomic layer epitaxy of GaAs, *Appl. Phys. Lett.* 48, 1681 (1986), © 1986, American Institute of Physics.

two openings covers the rotating susceptor. The source gases are continuously directed to the openings and flow unimpeded through the fixed part except when the substrate cuts through the streams. The exposure times are controlled by the rotational speed and, if needed, they may be elongated by pausing the substrate. A carrier gas flown with a high rate at the center and guided by the wedge on the fixed part prevents mixing of the source gases. The fixed part also shears off a part of the boundary layer above the substrate. With a small clearance between the fixed and moving parts, the rotation speed could have been increased up to 120 rpm which corresponds to 85 ms exposure times and gives a high, self-limited (1 ML $cycle^{-1}$) growth rate of 2 $\mu m\, h^{-1}$ for GaAs [20, 93]. On the other hand, the rotating susceptor reactors have limitations in that they are difficult to adopt into processes which require complex sequencing of several sources, like a growth of multilayer structures or compositionally varied multicomponent films.

5. ALD PRECURSORS

Chemistry, especially the choice of proper precursors, is certainly the key issue in a successful design of an ALD process. In this section, we first examine the properties required for the ALD precursors. Next, some practical aspects of choosing the precursors are discussed. Finally, a comprehensive survey of the precursors used in ALD is carried out.

5.1. Requirements for ALD Precursors

Requirements for ALD precursors are summarized in Table III. The precursor chemistry of ALD is convenient to compare with CVD. There are many similarities but because of the certain characteristics of ALD, differences exist as well. However, the unique features of ALD are not reflected that much in the individual compounds which are usually the same as those used in CVD (see Table IV). Rather, it is how they are combined together which makes the difference. For ALD, the most aggressively reacting precursor combinations are looked for while in CVD too aggressive reactions must be avoided.

5.1.1. Volatility

The volatility requirement is of course common to ALD and CVD but as the self-limiting growth mechanism makes ALD less susceptible to small variations in precursor fluxes, solid precursors are more easily adopted to ALD than to CVD. Solids do possess some disadvantages, however. First, because solids are often loaded inside the ALD reactor in a limited source volume, the sources must be reloaded frequently, possibly after each run, which is laborious especially in industry. Second, if the particle size is too small, the particles may be transported by the carrier gas, even if operated under reduced pressure, to the substrates where they cause detrimental defects. For these reasons, liquid or gaseous precursors should be preferred, if available.

Table III. Requirements for ALD Precursors

Requirement	Comments
Volatility	For efficient transportation, a rough limit of 0.1 Torr at the applicable maximum source temperature Preferably liquids or gases
No self-decomposition	Would destroy the self-limiting film growth mechanism
Aggressive and complete reactions	Ensure fast completion of the surface reactions and thereby short cycle times Lead to high film purity No problems of gas phase reactions
No etching of the film or substrate material	No competing reaction pathways Would prevent the film growth
No dissolution into the film or substrate	Would destroy the self-limiting film growth mechanism
Unreactive volatile byproducts	To avoid corrosion Byproduct readsorption may decrease the growth rate
Sufficient purity	To meet the requirements specific to each process
Inexpensive	
Easy to synthesize and handle	
Nontoxic and environmentally friendly	

The required precursor vapor pressure is reactor specific and depends on many factors, like source geometry, substrate area, and flow rates. In research scale flow-type reactors, for example, a vapor pressure of 0.1 Torr is usually appropriate and ensures effective transportation (cf. Section 4.2.2). In large scale production, higher doses and accordingly higher precursor vapor pressures are often desired. The minimum requirements to the precursor volatility are thus set by these vapor pressures and the highest applicable source temperatures (e.g., 500°C).

Precursor vapor pressure data are not always available, and especially with low volatility solids such measurements may be quite troublesome. In these cases, thermogravimetric (TG) measurements can be used for examining the volatility [101] and for estimating the required source temperatures [102]. One option is to use the conventional constant heating rate measurements. From the weight loss curves of compounds which have already been used in ALD, one can identify certain temperatures, such as those corresponding to 10 or 50% weight losses, and one can plot these as a function of the source temperatures used in a given type of an ALD reactor (Fig. 11). On basis of this data set and a similar TG measurement, a source temperature may be estimated for any new compound to be used in a similar reactor. Another possibility is to perform isothermal weight loss measurements over a range of temperatures. After calibration with a compound with a known vapor pressure, vapor pressures of the compounds of an interest may be estimated [102].

Table IV. A Summary of the Precursor Combinations Used and Examined in ALD Thin Film Processes[a]

Metal precursor	Nonmetal and other precursors	Film material	Reference
Elements			
Zn	S	ZnS	[1, 2, 116]
	Se	ZnSe	[116–120]
	$Se(C_2H_5)_2$, prepyrolyzed	ZnSe	[121]
	Te	ZnTe	[118, 122]
Cd	S	CdS	[123]
	Se	CdSe	[116]
	Te	CdTe	[122, 124–127]
Halides			
$AlCl_3$	H_2O	Al_2O_3	[2–4, 107, 128–136]
	O_2	Al_2O_3	[137, 138]
	ROH	Al_2O_3	[129, 139]
	$H_2O/ROH + P_2O_5/(CH_3O)_3PO$	$Al_2O_3:P$	[140, 141]
	NH_3	AlN	[142]
	AsH_3	AlAs	[143]
GaCl	NH_3	GaN	[144]
	PH_3	GaP	[145]
	$P_4 + As_4$	$GaP_{1-x}As_x$	[146, 147]
	AsH_3	GaAs	[14, 145, 148–153]
$GaCl_3$	NH_3	GaN	[154]
	AsH_3	GaAs	[143, 155, 156]
	$CuCl + H_2S$	$CuGaS_2$	[157]
GaBr	AsH_3	GaAs	[158]
GaI	AsH_3	GaAs	[158]
InCl	PH_3	InP	[145]
	$((CH_3)_3C)PH_2$	InP	[129]
	AsH_3	InAs	[148, 153]
$InCl_3$	H_2O/H_2O_2	In_2O_3	[86, 115, 159]
	$H_2O/H_2O_2 + SnCl_4$	$In_2O_3:Sn$	[86, 159, 160]
	H_2S	In_2S_3	[161]
$SiCl_4$	H_2O	SiO_2	[162–167]
	NH_3	Si_3N_4	[168]
	H_2S	Cl dopant in SrS and CaS	[169]
Si_2Cl_6	Si_2H_6	Si	[60, 170]
	Atomic H[b]	Si	[61]
	N_2H_4	Si_3N_4	[171]
$GeCl_4$	Atomic H[b]	Ge	[62]
$SnCl_4$	H_2O	SnO_2	[34, 35, 172–174]
	$H_2O + SbCl_5$	$SnO_2:Sb$	[175]
$SbCl_5$	H_2O	Sb_2O_5	[175]
$TiCl_4$	H_2-plasma	Ti	[74]
	H_2O	TiO_2	[82, 96, 107, 176–182]
	H_2O_2	TiO_2	[183, 184]
	NH_3 (+ Zn)	TiN	[88, 111, 112, 185, 186]
	$(CH_3)_2NNH_2$	TiN	[114]
TiI_4	H_2O_2	TiO_2	[187–190]
	NH_3	TiN	[186, 191]
$ZrCl_4$	H_2O	ZrO_2	[83, 133, 192–195]
ZrI_4	H_2O_2	ZrO_2	[196]

Table IV. (Continued)

Metal precursor	Nonmetal and other precursors	Film material	Reference
$HfCl_4$	H_2O	HfO_2	[84, 131, 195, 197, 198]
$NbCl_5$	NH_3 (+ Zn)	NbN	[103, 112, 185]
	$(CH_3)_2NNH_2$	NbN	[114]
$TaCl_5$	H_2-plasma	Ta	[74]
	H_2O	Ta_2O_5	[3, 4, 104–106, 130, 131, 135, 195, 199–202]
	$NH_3 + H_2O$	TaO_xN_y	[113]
	NH_3	Ta_3N_5	[113, 185]
	NH_3 + Zn	TaN	[113]
	$(CH_3)_2NNH_2$	Ta_3N_5	[114]
TaI_5	H_2O_2	Ta_2O_5	[203]
$MoCl_5$	Zn	Mo	[204]
	NH_3 (+ Zn)	MoN, Mo_2N	[114, 185]
	$(CH_3)_2NNH_2$	MoN, Mo_2N	[114]
WO_xF_y	H_2O	WO_3	[205]
WF_6	Si_2H_6	W	[206]
	NH_3	W_2N	[207]
$MnCl_2$	H_2S	Dopant in ZnS	[3, 4, 8]
MnI_2	H_2S	Dopant in ZnS	[208]
CuCl	H_2	Cu	[209, 210]
	Zn	Cu	[110]
	$GaCl_3 + H_2S$	$CuGaS_2$	[157]
$ZnCl_2$	H_2S	ZnS	[2–4, 85, 211–213]
	H_2Se	ZnSe	[214]
	H_2S + Se	$ZnS_{1-x}Se_x$	[108]
	HF	ZnF_2	[215]
$CdCl_2$	H_2S	CdS	[123, 213]
Alkyl compounds			
$Al(CH_3)_3$	H_2O	Al_2O_3	[36, 37, 88, 89, 133, 134, 162, 194, 216–224]
	H_2O_2	Al_2O_3	[184, 225–229]
	N_2O	Al_2O_3	[228]
	NO_2	Al_2O_3	[217]
	O_2-plasma	Al_2O_3	[75]
	NH_3	AlN	[230–233]
	PH_3	AlP	[234]
	AsH_3	AlAs	[13, 17, 47, 58, 79, 80, 235, 236]
$Al(CH_3)_2Cl$	H_2O	Al_2O_3	[237]
	NH_3	AlN	[238]
$Al(CH_3)_2H$	PH_3	AlP	[239]
	AsH_3	AlAs	[79, 240]
$Al(C_2H_5)_3$	H_2O	Al_2O_3	[241]
	NH_3	AlN	[242, 243]
	AsH_3	AlAs	[17, 47]
$Al(CH_2CH_2(CH_3)_2)_3$	AsH_3	AlAs	[244]
$Ga(CH_3)_3$	NH_3	GaN	[245–249]
	N_2-H_2-plasma	GaN	[71]
	PH_3	GaP	[234, 239, 250, 251]
	AsH_3	GaAs	[12, 13, 15, 17, 48, 70, 78, 79, 93, 98, 99, 235, 236, 252–256]
	$((CH_3)_3C)AsH_2$	GaAs	[99, 257, 258]
$Ga(CH_3)_2(C_2H_5)$	AsH_3	GaAs	[252]

Table IV. (Continued)

Metal precursor	Nonmetal and other precursors	Film material	Reference
$Ga(C_2H_5)_3$	NH_3	GaN	[243, 259, 260]
	NH_3, thermally cracked	GaN	[63]
	PH_3	GaP	[49]
	AsH_3	GaAs	[17, 19, 47, 50, 252]
	$((CH_3)_3C)AsH_2$	GaAs	[258, 261]
	$((CH_3)_2N)_3As$	GaAs	[262]
$Ga(C_2H_5)_2Cl$	AsH_3	GaAs	[263]
$Ga(CH_2CH_2(CH_3)_2)_3$	AsH_3	GaAs	[19]
$Ga(CH_2C(CH_3)_3)_3$	$((CH_3)_3C)AsH_2$	GaAs	[258]
$In(CH_3)_3$	H_2O	In_2O_3	[264]
	PH_3	InP	[78, 265, 266]
	$((CH_3)_3C)PH_2$	InP	[267, 268]
	AsH_3	InAs	[48, 269]
	$((CH_3)_3C)AsH_2$	InAs	[270]
$((CH_3)_2(C_2H_5)N)In(CH_3)_3$	AsH_3	InAs	[257]
$In(CH_3)_2Cl$	AsH_3	InAs	[92]
$In(CH_3)_2(C_2H_5)$	NH_3	InN	[246–248]
$In(C_2H_5)_3$	PH_3	InP	[250, 251]
	AsH_3	InAs	[91]
$Sn(CH_3)_4$	NO_2	SnO_2	[271]
$Sn(C_2H_5)_4$	NO_2	SnO_2	[271]
$Zn(CH_3)_2$	H_2O	ZnO	[272]
	$H_2O + Al(CH_3)_3$	ZnO : Al	[272]
	$H_2S + H_2O$	$ZnO_{1-x}S_x$	[273]
	H_2S	ZnS	[274–276]
	$H_2S + H_2Se$	$ZnS_{1-x}Se_x$	[276–278]
	H_2Se	ZnSe	[276, 279–282]
	$(C_2H_5)_2Te$	ZnTe	[283]
	$(CH_3)(CH_2CHCH_2)Te$	ZnTe	[283]
$Zn(C_2H_5)_2$	H_2O	ZnO	[52, 89, 272, 284–293]
	$H_2O + B_2H_6$	ZnO : B	[289–292, 294]
	$H_2O + Al(CH_3)_3$	ZnO : Al	[272]
	$H_2O + Ga(CH_3)_3$	ZnO : Ga	[293]
	$H_2S + H_2O$	$ZnO_{1-x}S_x$	[288]
	H_2S	ZnS	[288, 295, 296]
	$(C_2H_5)_2S_2$	ZnS	[297]
	$(C_2H_5)_2Se_2$	ZnSe	[297]
$Cd(CH_3)_2$	H_2S	CdS	[298–302]
	H_2Se	CdSe	[279]
	$(C_2H_5)_2Te$	CdTe	[283]
	$(CH_3)(CH_2CHCH_2)Te$	CdTe	[283, 303]
	$((CH_3)_2CH)_2Te$ + temperature modulation	CdTe	[53]
$Hg(CH_3)_2$	CH_3(allyl)Te	HgTe	[303]
Alkoxides			
$Al(OC_2H_5)_3$	H_2O/ROH	Al_2O_3	[129]
$Al(OCH_2CH_2CH_3)_3$	H_2O/ROH	Al_2O_3	[129]
	H_2O/ROH + P_2O_5	Al_2O_3 : P	[141]
$Ti(OC_2H_5)_4$	H_2O	TiO_2	[304, 305]
$Ti(OCH(CH_3)_2)_4$	H_2O	TiO_2	[306–308]
	$Bi(C_6H_5)_3 + H_2O$	$Bi_xTi_yO_z$	[309]
$Zr(OC(CH_3)_3)_4$	H_2O	ZrO_2	[310]

Table IV. (Continued)

Metal precursor	Nonmetal and other precursors	Film material	Reference
$Nb(OC_2H_5)_5$	H_2O	Nb_2O_5	[136, 192, 202, 311]
$Ta(OC_2H_5)_5$	H_2O	Ta_2O_5	[133, 136, 192, 197, 202, 312, 313]
	NH_3	TaO_xN_y	[314]
$Pb(OC(CH_3)_3)_2$	H_2S	PbS	[315]
$Pb_4O(OC(CH_3)_3)_6$	H_2S	PbS	[315]
β-diketonato complexes			
$Mg(thd)_2$ [c]	H_2O_2	MgO	[316]
	O_3	MgO	[317]
$Ca(thd)_2$	H_2S	CaS	[87, 169, 318–321]
	HF	CaF_2	[215]
$Sr(thd)_2$	O_3	SrO ($SrCO_3$)	[322]
	$O_3 + Ti(OCH(CH_3)_2)_4 + H_2O$	$SrTiO_3$	[322]
	H_2S	SrS	[169, 296, 318, 323–325]
	H_2S + Se	$SrS_{1-x}Se_x$	[109]
	HF	SrF_2	[215]
$Ba(thd)_2$	H_2S	BaS	[318, 326]
$Ga(acac)_2$ [d]	O_3/H_2O	Ga_2O_3	[35, 327]
$In(acac)_3$	H_2S	In_2S_3	[288]
$Pb(thd)_2$	H_2S	PbS	[315]
$Y(thd)_3$	O_3, O_2	Y_2O_3	[328, 329]
	H_2S	Y_2O_2S	[330]
$La(thd)_3$	H_2S	La_2S_3, La_2O_2S	[331]
	O_3	La_2O_3	[332, 333]
	$Co(thd)_2 + O_3$	$LaCoO_3$	[332]
	$Ni(thd)_2 + O_3$	$LaNiO_3$	[333]
	$Mn(thd)_3 + O_3$	$LaMnO_3$	[334]
$Ce(thd)_4$	O_3	CeO_2	[335]
	H_2S	Dopant in CaS, SrS and BaS	[169, 296, 326, 336–338]
$Ce(thd)_3(phen)$ [e]	H_2S	Dopant in SrS	[339]
$Ce(tpm)_3$ [f]	H_2S	Dopant in SrS	[339]
$Ce(tpm)_4$	H_2S	Dopant in SrS	[340]
$Ce(tfa)_4$ [g]	H_2S	Dopant in SrS	[340]
$Mn(thd)_3$	O_3	MnO_x	[334]
	H_2S	Dopant in ZnS	[295, 296]
$Co(thd)_2$	O_3	Co_3O_4	[332]
$Ni(acac)_2$	O_3	NiO	[341, 342]
$Ni(thd)_2$	O_3	NiO	[333]
$Cu(thd)_2$	H_2	Cu	[186, 210, 343, 344]
$Ln(thd)_3$ [h]	H_2S	Dopants in CaS, SrS and ZnS	[296, 319, 336, 345–352]
Cyclopentadienyl compounds			
$Mg(C_5H_5)_2$	H_2O	MgO	[241, 353–355]
$Sr(C_5{}^iPr_3H_2)_2$ [i]	$Ti(OCH(CH_3)_2)_4 + H_2O$	$SrTiO_3$	[356–358]
	H_2S	SrS	[359]
$Sr(C_5Me_5)_2$ [j]	H_2S	SrS	[359]
$Ba(C_5Me_5)_2$	$Ti(OCH(CH_3)_2)_4 + H_2O$	$BaTiO_3$	[356, 357]
	H_2S	BaS	[359]
$Ba(C_5{}^tBu_3H_2)_2$ [k]	$Ti(OCH(CH_3)_2)_4 + H_2O$	$BaTiO_3$	[357]
$Mn(C_5H_5)_2$	H_2S	Dopant in ZnS	[295]
$Mn(C_5MeH_4)(CO)_3$	H_2S	Dopant in ZnS	[295]
$Zr(C_5H_5)_2Cl_2$	O_3	ZrO_2	[322]
$Ce(C_5Me_4H)_3$	H_2S	Dopant in SrS	[360]

Table IV. (Continued)

Metal precursor	Nonmetal and other precursors	Film material	Reference
Carboxylates			
$Zn(CH_3COO)_2$[l]	H_2S	ZnS	[212, 361, 362]
	H_2O	ZnO	[361, 363]
Hydrides			
$((CH_3)_3N)AlH_3$	NH_3 + temperature modulation	AlN	[365]
	AsH_3	AlAs	[366]
	$((CH_3)_2N)_3As$	AlAs	[262]
$((CH_3)_2(C_2H_5)N)AlH_3$	NH_3	AlN	[367–369]
	AsH_3	AlAs	[81, 370–372]
SiH_4	Temperature modulation	Si	[54, 55]
$SiCl_2H_2$	H_2	Si	[373, 374]
	Atomic H[b]	Si	[60, 64–66, 170]
	UV light	Si	[375]
	C_2H_2	SiC	[376, 377]
	NH_3-plasma	Si_3N_4	[72, 73]
	NH_3, thermally cracked	Si_3N_4	[59]
Si_2H_6	Temperature modulation	Si	[51, 57, 378]
	Thermal precracking and temperature modulation	Si	[67]
	Si_2Cl_6	Si	[60]
	C_2H_2	SiC	[379, 380]
	C_2H_4	SiC	[100]
Si_3H_8	Temperature modulation	Si	[65, 381]
$Si(C_2H_5)_2H_2$	Temperature modulation	Si	[382]
GeH_4	Temperature modulation	Ge	[55, 56]
$Ge(CH_3)_2H_2$	Atomic H[b]	Ge	[68, 69]
$Ge(C_2H_5)_2H_2$	Temperature modulation	Ge	[383]
Alkyl- and silylamides			
$Ti(N(CH_3)_2)_4$	NH_3	TiN	[384, 385]
	$NH_3 + SiH_4$	$Ti_xSi_yN_z$	[384, 385]
$Ti(N(C_2H_5)(CH_3))_4$	NH_3	TiN	[386]
$Ce(N(Si(CH_3)_3)_2)_3$	H_2S	Dopant in SrS	[387]
Others			
$Si(NCO)_4$	H_2O	SiO_2	[388]
	$N(C_2H_5)_3$	SiO_2	[389]
$CH_3OSi(NCO)_3$	H_2O_2	SiO_2	[390, 391]
$Pb((C_2H_5)_2NCS_2)_2$	H_2S	PbS	[315, 392]
$Ni(apo)_2$[m]	O_3	NiO	[341]
$Ni(dmg)_2$[n]	O_3	NiO	[341]
Two metal compounds			
$AlCl_3$	$Al(OC_2H_5)_3$	Al_2O_3	[393]
	$Al(OCH(CH_3)_2)_3$	Al_2O_3	[393]
	$Ti(OC_2H_5)_4$	$Al_xTi_yO_z$	[393]
	$Ti(OCH(CH_3)_2)_4$	$Al_xTi_yO_z$	[393]
$Al(CH_3)_3$	$Al(OCH(CH_3)_2)_3$	Al_2O_3	[393]
	$Ti(OCH(CH_3)_2)_4$	$Al_xTi_yO_z$	[393]
	CrO_2Cl_2	$Al_xCr_yO_z$	[394]
$ZrCl_4$	$Al(OC_2H_5)_3$	$Al_xZr_yO_z$	[393]
	$Ti(OCH(CH_3)_2)_4$	$Ti_xZr_yO_z$	[393]

Table IV. (Continued)

Metal precursor	Nonmetal and other precursors	Film material	Reference
	$Si(OC_2H_5)_4$	$Zr_xSi_yO_z$	[393]
	$Si(OC_4H_9)_4$	$Zr_xSi_yO_z$	[393]
$HfCl_4$	$Al(OC_2H_5)_3$	$Al_xHf_yO_z$	[393]
	$Ti(OCH(CH_3)_2)_4$	$Ti_xHf_yO_z$	[393]
$TaCl_5$	$Ta(OC_2H_5)_5$	Ta_2O_5	[393, 395]

[a] Classification goes according to the type of the metal precursor. Processes with two metal precursors with no separate nonmetal source are listed separately in the end of the table.

[b] Obtained by thermal dissociation of H_2.

[c] thd is 2,2,6,6,-tetramethyl-3,5-heptanedione. Alkaline earth and yttrium thd-complexes used may also contain a neutral adduct molecule or they may have been slightly oligomerized.

[d] acac is acetyl acetonate.

[e] phen is 1,10-phenanthroline.

[f] tpm is 1,1,1-trifluoro-5,5-dimethyl-2,4-hexanedione.

[g] tfa is 1,1,1-trifluoro-2,4-pentanedione.

[h] Ln is Ce, Pr, Nd, Sm, Eu, Gd, Tb, Tm.

[i] ^{i}Pr is $-CH(CH_3)_2$.

[j] Me is $-CH_3$.

[k] ^{t}Bu is $-C(CH_3)_3$.

[l] Converts to $Zn_4O(CH_3COO)_6$ when annealed [364].

[m] apo is 2-amino-pent-2-en-4-onato.

[n] dmg is dimethylglyoximato.

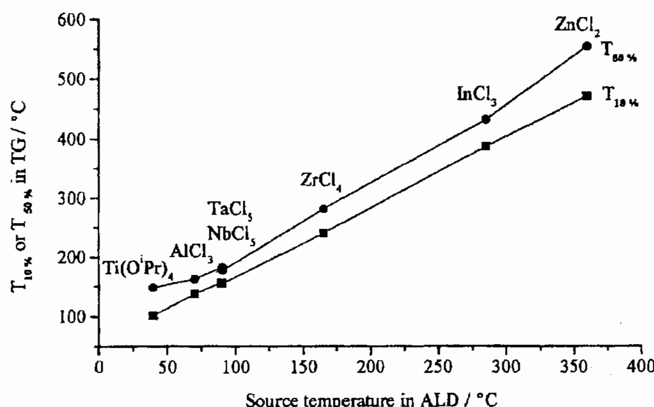

Fig. 11. Correlation between temperatures corresponding to 10 and 50% mass losses in TG measurements and source temperatures used in research scale ALD reactors [102]. The TG measurements were carried out in 1-atm nitrogen atmosphere with a heating rate of $10°C\,min^{-1}$.

TG measurements also reveal if the volatilization takes place in one step, or if there are decomposition reactions involved [101].

5.1.2. *Stability Against Self-Decomposition*

The self-limiting film growth via the surface exchange reactions is obviously achievable only under conditions where the precursors do not decompose on their own. A simple way to test if a precursor is thermally decomposing is to pulse only that compound in the reactor and to see if any film grows. As the decomposition reactions may often be catalyzed by the film material, it is advised to carry out the decomposition experiments not only on bare substrates but also on previously deposited films and to see if their thicknesses increase.

Because the decomposition is a thermally activated reaction, its rate increases exponentially with temperature. On the other hand, the longer the exposure time, the more pronounced the decomposition in comparison to the desired exchange reaction (Section 7.1.1). This explains why in processing of porous materials and in many surface chemistry studies, both with long exposure times of minutes, decomposition is observed at significantly lower temperatures than in film growth experiments with fast pulsing. Clearly, it is a material-, process-, and application-dependent choice where to set the uppermost limit for the acceptable decomposition rate.

In fortuitous cases, the product of the decomposition reaction is the same as that of the exchange reactions, like, for example, in the growth of oxides from metal alkoxides and water where also the thermal decomposition of the alkoxide deposits the same oxide. In such a case, quite a substantial contribution of the decomposition may be accepted, provided of course that the decomposition proceeds in a surface reaction rate limited manner, thereby maintaining the good uniformity and conformality (Section 7.1.2). On the other hand, if the decomposition reaction causes incorporation of contaminants into the film, it must be minimized to a level where the resulting contamination can be tolerated.

5.1.3. *Aggressive and Complete Reactions*

The alternate pulsing means that there are no risks of gas phase reactions in ALD. Therefore, precursors which react aggressively with each other can be used. In fact, such combinations should be preferred to ensure rapid completion of the reactions and thereby short cycle times as well as effective precursor utilization. This is in marked contrast with CVD where too reactive precursor combinations must be avoided. Thermodynamically, this means that the reactions used in ALD should have as negative a Gibbs free energy change ΔG as possible [39], while in CVD ΔG should still be negative but close to zero.

The reactions also need to be completed so that no impurities are left in the films. The aggressiveness of the reaction does not necessarily guarantee the completion. Especially at low temperatures, kinetic reasons may prevent the completion and thus some unreacted ligands from the metal precursors may be incorporated into the films. Likewise, nonmetal precursors such as H_2O or NH_3, for example, may leave $-OH$ or $-NH_x$ residues if the reactions are incomplete. The amount of these residues in the films decreases as the temperature is increased but if that is increased too much, the precursor decomposition may start to produce new kinds of contaminants.

5.1.4. *No Etching Reactions*

A negative consequence of the alternate supply of the precursors is that there are no competing reaction pathways for possible etching reactions where the film itself, substrate, or an underlying film is etched by one of the precursors. Such etching reactions have, for example, prevented the growth of Nb_2O_5 from $NbCl_5$ and H_2O and have been interpreted to involve a formation of volatile oxochlorides [103]:

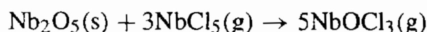

$$Nb_2O_5(s) + 3NbCl_5(g) \rightarrow 5NbOCl_3(g)$$

Similar etching is also observed in the analogous $TaCl_5$-H_2O process but only above a certain threshold temperature of about 300°C, and even then the etching is slow enough not to totally prevent the film growth but just to cause a decrease of the deposition rate with longer $TaCl_5$ pulse times [104–106]. A simple test to verify an existence of etching reactions is to expose a film to one precursor only and to observe a disappearance of the film or part of it.

A somewhat less detrimental type of gas–solid reaction is the one which involves an exchange of the film constituents, like a replacement of a metal cation in an oxide with another metal having a higher affinity toward oxygen [107]:

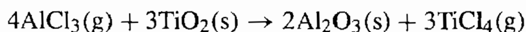

$$4AlCl_3(g) + 3TiO_2(s) \rightarrow 2Al_2O_3(s) + 3TiCl_4(g)$$

Such reactions are often self-terminated once the surface becomes covered by the exchange reaction product (Al_2O_3 in the preceding example), and therefore they may be tolerated unless very sharp interfaces are required. On the other hand, the same kind of replacement reactions may also be utilized in making, for example, metal sulfoselenides where sulfur atoms deposited through reactions between metal precursors and H_2S are in the next step partially replaced by elemental selenium, thereby avoiding the need to use the highly toxic H_2Se [108, 109] (cf. Section 5.3.2).

5.1.5. *No Dissolution to the Film or the Substrate*

The precursors should chemisorb on the surface upon which they are dosed but they are not allowed to dissolve into that material. Examples of precursor dissolution are rare but one is the attempt to deposit metallic copper from CuCl and elemental zinc, the latter being used as a reducing agent [110]. Metallic copper with only about 3 at.% zinc was indeed obtained but the film growth was evidently not self-limiting and growth rates were high, above 5 Å $cycle^{-1}$. The results were explained with the following mechanism in which the copper film is formed as desired by the reductive exchange reaction:

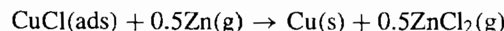

$$CuCl(ads) + 0.5Zn(g) \rightarrow Cu(s) + 0.5ZnCl_2(g)$$

However, once copper has been formed on the surface, the dissolution of zinc into copper starts to complicate the process. When dosed onto a copper surface with a CuCl chemisorption layer, Zn first reduces CuCl as before but then, rather than just adsorbing on the surface, zinc also dissolves into the copper,

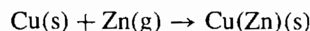

$$Cu(s) + Zn(g) \rightarrow Cu(Zn)(s)$$

The resulting Cu(Zn) alloy is not stable and during the following purge period Zn outdiffuses and evaporates

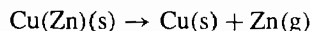

$$Cu(Zn)(s) \rightarrow Cu(s) + Zn(g)$$

The outdiffusion is slow, however, and also continues during the next CuCl pulse. This leads to a CVD-type of growth and thereby to a loss of the self-limiting growth mechanism:

$$CuCl(g) + 0.5Zn(g) \rightarrow Cu(s) + 0.5ZnCl_2(g)$$

The precursor may dissolve not only into the film material but also into the substrate. Processes where this can possibly take place are the growths of transition metal nitride films onto silicon substrates from the metal halides and ammonia with elemental zinc as an additional reducing agent (Section 5.3.6) [103, 111–114]. If dissolved into silicon, zinc forms detrimental electrically active defects. In fact, this has been regarded as such a major concern that the zinc-based processes have not been taken into a more detailed study even if they produce the highest quality nitrides (Section 6.5) and the occurrence of zinc dissolution into silicon still remains to be verified.

5.1.6. *Unreactive Byproducts*

Preferably, the precursors should produce unreactive byproducts which would be easily purged out of the reactor. Reactive byproducts may cause corrosion problems in the reactor or in the exhaust. In addition, they may readsorb on the film surface and block adsorption sites from the precursor molecules, thereby decreasing the growth rate (Section 4.2.4). In the worst case, the byproducts may etch the film. Nonetheless, in many successfully implemented ALD processes (e.g., $ZnCl_2$-H_2S,

$AlCl_3$-H_2O, $TiCl_4$-H_2O) hydrogen chloride is formed as a byproduct and routinely handled in properly designed reactors. Thus, the unreactivity of the byproducts may be considered only as a secondary, though still an important requirement while planning an ALD process.

5.1.7. Other Requirements

Precursor purity requirements are specific to each process and application, and also depend on the nature of the impurities. Naturally, semiconductors are more sensitive to impurities than, for example, protective coatings. If nonvolatile and unreactive with the precursor, the impurities are of less concern because they remain in the source.

The other requirements, such as low cost, easy synthesis and handling, nontoxicity and environmental friendliness, are all common to the CVD precursor requirements. However, all these and the above requirements may not always be fulfilled simultaneously, and often only these last ones can be sacrificed while developing a new ALD process. If toxic or otherwise dangerous compounds cannot be avoided, special care must of course be given to their handling before and after the process, and appropriate safety systems must be installed.

While considering the cost issue, it must be kept in mind that a price of any chemical is largely determined by its demand. Therefore, no compound should be rejected from research just because of its current price. Rather, one should have a look at its synthesis procedure and try to estimate how much the price might be lowered if the precursor would be taken into a large scale use. Furthermore, in many cases the contribution of the precursor chemicals to the final price of a thin film device is rather small.

5.2. Choice of Precursors

After examining the desired properties of the ALD precursors, we now present some basic ideas about how to proceed in selecting precursors for a new process. The necessary background information can be looked for from basically two sources: literature and thermodynamic calculations.

5.2.1. Literature Survey

For planning a new ALD process and choosing precursors for it, looking at the literature makes a good start. While searching the literature, all the alternative names of the method (Table I) should be taken into account. If no ALD process for the particular film material has been reported, processes of any material containing the constituent elements should be looked for to see which kind of precursors have been used. To assist the literature survey, ALD processes reported so far have been summarized in Table IV in Section 5.3.

In addition to ALD literature, CVD publications also contain valuable information, such as volatility data and reaction and decomposition temperatures. For example, notations of precursor combinations too reactive for CVD are often especially promising. Other potential sources of volatility data are publications on synthesis or thermal analysis of the compounds and catalogues and data sheets of commercial suppliers. Any comments on moisture or air sensitivity give hope for fast reactions, especially in the growth of oxides but also in more general terms, though at the same time they imply that special care must be devoted to the precursor handling.

5.2.2. Thermodynamic Consideration

Thermodynamics refers to equilibrium conditions while ALD is certainly a nonequilibrium process: the precursors are dosed into the reactor alternately and the byproducts are constantly pumped out. In addition, thermodynamics tells nothing about reaction rates. In any case, thermodynamic calculations provide valuable information about the compounds under consideration for ALD, provided of course that relevant thermodynamic data are available. Today, these calculations are easily made with relatively inexpensive commercial PC programs with integrated databases, but while evaluating the results the previously mentioned limitations of thermodynamics must carefully be kept in mind.

The simplest calculation is the vapor pressure of the compound. Additionally, the stable form, e.g., monomer vs dimer, in the gas phase at each temperature of an interest is easily checked.

To estimate a reactivity of a pair of precursors, ΔG for a suggested net reaction is calculated and is compared with other alternatives, all balanced to deposit an equal amount of the film. If otherwise possible and reasonable, the reaction with the most negative ΔG should be chosen. However, in some cases, like in the growth of In_2O_3 from $InCl_3$ and H_2O [115], reactions with even slightly positive ΔG have been used and have been explained to be possible because of the continuous feed of one precursor and the pump out of the byproducts. On the other hand, it also must be emphasized that in ALD the two precursors can meet each other only if there is a certain mechanism by means of which at least one of them can adsorb on the surface. Thermodynamic estimations of such mechanisms are of course impossible because of a lack of thermodynamic data for the intermediate surface species.

The occurrence of possible side reactions, like etching (Section 5.1.4), may also be estimated by thermodynamic calculations. One may either calculate ΔG for the suggested side reaction or perform equilibrium composition calculations for a system where the film or the substrate material is exposed to one precursor vapor.

5.3. Overview of Precursors and Their Combinations Used in ALD

Table IV summarizes the precursors and their combinations used in ALD as comprehensively as the authors know (compiled in June 2000). For the materials of the greatest interest in nonepitaxial applications (oxides, nitrides, sulfides, fluorides, metals) rather extensive referencing has been attempted, whereas for the widely examined epitaxial semiconductors, especially for the III–V compounds, only a few examples have been given for each precursor combination and review articles

[7, 16–25, 38] are recommended for broader coverage including also the semiconductor dopant precursors which are not dealt with here. Basically, all the processes which have resulted in film growth are included in Table IV, even if some of them are slow requiring unpractically long exposure times.

The evolution of ALD precursor chemistry has been reviewed [396] so only a rather concise summary is presented. Other recommended review articles can be found in Refs. [7, 8, 18, 19, 39], for example.

5.3.1. *Metal Precursors*

Elemental zinc and sulfur were used in the first ALD experiments for growing ZnS [1, 2]. Subsequently, zinc and cadmium have been used in reactions with sulfur, selenium, and tellurium (Table IV), but except for these and mercury the use of metal elements is limited because of their low vapor pressures.

Soon after the first demonstrations of ALD, metal chlorides were taken under study. Among the first processes examined were also two of the most successful ALD processes, namely, $ZnCl_2$-H_2S for ZnS and $AlCl_3$-H_2O for Al_2O_3 [2–4]. Though both these processes are based on solid chlorides and are therefore somewhat laborious in production, they have been used in industry from the very beginning of the ALD manufacturing of the TFEL displays. For doping of the ZnS : Mn phosphor, $MnCl_2$ is used, even if it has quite a low vapor pressure. Among the first chloride precursors examined were also the liquids $TiCl_4$ and $SnCl_4$, the former of which has also been adopted to the TFEL production for making $Al_xTi_yO_z$ insulators (Section 6.2.1). Subsequently, basically all possible volatile chlorides have been examined (Table IV). By contrast, of the other halides only TiI_4, ZrI_4, TaI_5, WF_6, and MnI_2 have been examined so far. Especially the iodides should be examined in more detail because the low metal-iodine bond energies suggest that iodide residues could be removed from the films more completely than chlorides.

As the interest toward ALE (here the name ALE is used to emphasize the epitaxial deposits) of the III–V materials arose, a natural starting point was to choose metal alkyls, like $Ga(CH_3)_3$, as precursors because at that time they were already well known and were broadly used in metal organic vapor phase epitaxy (MOVPE). However, this choice is not completely in line with the previously discussed requirements to ALD precursors because the reactions with the group V hydrides usually require such high temperatures that pyrolysis of the organometallic compounds occurs and complicates the control of the self-limiting growth conditions [18, 19, 22, 48, 255, 397]. Indeed, a mechanism which would explain the different results obtained under different GaAs growth conditions has been speculated about for a long time. The current opinion is that the two key requirements for the self-limiting growth are an avoidance of complete gas phase decomposition of $Ga(CH_3)_3$ in the boundary layer above the substrate and a high enough methyl radical flux to compensate for the methyl radicals which desorb from the surface [22]. On the other hand, with the aid of laser assistance the growth temperature may be lowered so that the thermal decomposition is significantly decreased, and at the same time the width of the temperature range for the self-limiting film growth is increased [15, 17, 48, 49]. Another consequence of the metal alkyl pyrolysis is carbon residual incorporation causing relatively high p-type carrier concentrations [18, 19]. However, with careful control of the growth conditions, in particular by reducing the flow rate and the exposure time of the metal alkyl and by increasing the corresponding parameters for the group V hydride, low carrier concentrations and even n-type conductivity could have been achieved [19, 93, 253, 254]. In any event, because of these reasons, chloride-based processes emerged as another main route to ALE of III–V compounds [18]. Here the precursors have been either binary chlorides, often formed *in situ*, or alkyl chlorides which pyrolyze in the reactor into the binary chlorides. With the chloride-based processes, the heavy carbon contamination is avoided and the n-type materials are easily obtained.

The early work on the III–V compounds in the late 1980s was focused on compounds of Ga, Al, In, As, and P. Somewhat later, in the early 1990s, ALE of gallium and aluminum nitrides from the trialkyls was examined [242, 243, 259, 260], and later InN was also grown [246–248]. In addition to the III–V compounds, metal alkyl precursors have successfully been used also in the ALD of epitaxial or nonepitaxial II–VI compounds and polycrystalline or amorphous oxides. Here ZnS, CdS, Al_2O_3, and ZnO have been the most thoroughly examined materials (Table IV). Reactions with H_2S and H_2O are facile and thus proceed at low temperatures, occasionally even at room temperature [274, 298–302], where the pyrolysis of the metal alkyls is much weaker than at the temperatures typically used in the III–V processes.

Metal alkoxides offer chlorine-free alternatives to the growth of oxide thin films. The first ALD experiments were made on aluminum alkoxides using water or alcohols as oxygen sources [129], and subsequently titanium, tantalum, and niobium alkoxides (mainly ethoxides) have successfully been used in reactions with water (Table IV). For tantalum and especially for niobium, alkoxides are important precursors because of the etching problems in the chloride processes (Section 5.1.4). Alkoxides decompose thermally at elevated temperatures and therefore the ALD processes are limited to temperatures below 400°C. On the other hand, the decomposition product often is a rather pure oxide and therefore the decomposition may be accepted to a certain extent. All the previously mentioned alkoxide processes produce good quality films, but zirconium tetra-*tert*-butoxide [310] resulted in ZrO_2 films which were clearly of a lower quality than those obtained from $ZrCl_4$. This is unfortunate because the liquid alkoxide was hoped to solve a problem encountered in the $ZrCl_4$-H_2O process where very fine particles from the solid $ZrCl_4$ source are often transported by the carrier gas and are incorporated into the films.

After the success of the ZnS : Mn TFEL phosphor, the strive toward full color displays turned the ALD research on other TFEL phosphors, most of which have alkaline earth metal sulfides as the host materials and rare-earth metals as the dopants (Section 6.1). These electropositive metals have few volatile

compounds, β-diketonates being the well known and the most thoroughly examined exception. Though the β-diketonates, especially those of the alkaline earth metals, suffer somewhat from instability, they have served as reasonably good precursors for the TFEL phosphors (Table IV). For example, the $Sr(thd)_2$-$Ce(thd)_4$-H_2S process has been used in a pilot scale growth of SrS:Ce [338]. On the other hand, while reactive with H_2S, most of the β-diketonates do not react with water at temperatures where they would not decompose already on their own. Here, $Ga(acac)_3$ has been an exception and reacted with water but the Ga_2O_3 films obtained were heavily carbon contaminated [327]. $Mg(thd)_2$, in turn, has been used together with H_2O_2 to grow MgO films but the deposition rate was low, only 0.1–0.2 Å $cycle^{-1}$ [316]. Thus, oxides are best grown from the β-diketonates with ozone as the oxygen source (Table IV). In reactions with ozone, the large β-diketonato ligands are probably burned into smaller molecules and thus these reactions essentially differ from most of the other ALD processes where the ligands are removed more or less intact, either after protonation by the hydrogen containing nonmetal precursor or as a consequence of radical desorption.

Cyclopentadienyl compounds (metallocenes) have been examined as alternatives to alkaline earth and rare-earth metal β-diketonates with a number of promising results (Table IV). The use of cyclopentadienyls in ALD was first demonstrated in the growth of MgO from $Mg(C_5H_5)_2$ and H_2O [241, 353, 354], and subsequently $Mn(C_5H_5)_2$ and $Mn(C_5MeH_4)(CO)_3$ were examined as dopant sources for ZnS:Mn [295] and $Ce(C_5Me_4H)_3$ for SrS:Ce [360]. In any event, so far the greatest progress with the cyclopentadienyls has been made in the growth of $SrTiO_3$ and $BaTiO_3$ [356–358] (Section 6.2.2), because these can be deposited from the β-diketonates only with ozone and then the resulting film is amorphous which requires high temperature annealing to get crystallized [322]. Using $Sr(C_5{}^iPr_3H_2)_2$ together with $Ti(O^iPr)_4$ and H_2O, crystalline $SrTiO_3$ was obtained already at 250°C [356–358]. Despite some decomposition of $Sr(C_5{}^iPr_3H_2)_2$, a good control of film stoichiometry was achieved by varying the pulsing ratio of the two metal compounds. $BaTiO_3$ films were obtained with an analogous process with $Ba(C_5Me_5)_2$ [356, 357] or $Ba(C_5{}^tBu_3H_2)_2$ [357] as the barium precursor. These Sr and Ba compounds also react with hydrogen sulfide forming the corresponding sulfides at remarkably low temperatures: well-crystallized SrS was obtained already at 120°C [359].

Overall, cyclopentadienyl compounds form a large family of potential precursors since these are known for many metals and the ligands can be varied by substitutions in the carbon 5-ring, largening the ring system (indene, fluorene) and by linking two rings together by a bridge. Cyclopentadienyls have often been considered too air sensitive but the foregoing experiences demonstrate that with a reasonably careful handling they can be used without difficulty. The first experiments on these compounds have been promising but the full potential still remains to be explored and may provide interesting findings in the near future.

5.3.2. Nonmetal Precursors

For the nonmetals, the simple hydrides have mostly been used: H_2O, H_2O_2, H_2S, H_2Se, H_2Te, NH_3, N_2H_4, PH_3, AsH_3, SbH_3, and HF. These are all sufficiently reactive but some of them are very poisonous and therefore their alkyl derivatives have been examined as substitutes. Hydrogen peroxide is oxidizing by its nature while most of the others, hydrazine in particular, are reducing. The oxidizing power of H_2O_2 is seldom made use of, however. By contrast, the reducing action is highly needed in the growth of transition metal nitrides where the metals have higher oxidation states in their precursors than in the nitrides. Ammonia is powerful enough to reduce most of the transition metal chlorides to the desired metallic nitrides, though films with better conductivity are usually obtained when elemental zinc is used as an additional reducing agent (Section 5.3.6). However, $TaCl_5$ is not reduced by ammonia and insulating Ta_3N_5 is obtained [113]. A hydrazine derivative $(CH_3)_2NNH_2$ does not reduce tantalum either [114], and TaN is obtained only with zinc as a reducing agent [113].

Molecular oxygen, O_2, is usually too inert to react with the typical metal compounds under reasonable growth temperatures. Instead, ozone O_3 has been used to grow oxides from many β-diketonate compounds (Table IV) which do not react with the most common oxygen sources water and hydrogen peroxide. Other less used oxygen sources include N_2O and alcohols. A new approach applicable to many oxides is to use metal alkoxides as both metal and oxygen sources (Section 5.3.5).

Similarly to oxygen, also molecular nitrogen, N_2, and hydrogen, H_2, are quite inert toward the common metal sources at low temperatures. They are indeed often used as carrier gases, but while nitrogen is in most cases truly inert, hydrogen sometimes participates the surface reactions and removes surface terminating ligands (Section 7.2.1) [18]. Hydrogen has also been used as a reducing agent in ALD but this requires either catalytically active surfaces or high temperatures (Section 5.3.6). On the other hand, when dissociated by thermal cracking or plasma discharge, reactive atomic species are produced from hydrogen and nitrogen [60–62, 64–66, 68–71, 74]. Also oxygen may be dissociated in a plasma discharge but until now atomic-oxygen-based ALD processes have only briefly been demonstrated [75].

For the chalcogens (S, Se, Te), elements can be used as precursors, though usually only when the metal source also is an element (Table IV). It has also been demonstrated that elemental Se replaces sulfur atoms on the surface of the growing ZnS and SrS films. With this replacement reaction, the corresponding sulfoselenides with as much as 90 anion-% Se were deposited from $ZnCl_2$ or $Sr(thd)_2$, H_2S, and Se [108, 109], thereby avoiding the use of the highly toxic H_2Se. Finally, elemental As_4 and P_4 have been employed in the growth of GaAs and GaP from GaCl with hydrogen as a carrier gas [146, 147].

5.3.3. In situ Synthesized Precursors

A majority of the precursors used in ALD are synthesized beforehand but in some cases precursors generated *in situ* have

been used as well. *In situ* synthesis makes it possible to use compounds which are otherwise difficult to handle because of their high reactivity or which easily age when stored for long times.

The most common way for the *in situ* synthesis is to employ gas–solid reactions. As in CVD, also in ALD this has most often been used with chlorides, especially with gallium and indium chlorides, but also strontium and barium β-diketonates and tungsten oxyfluorides have been synthesized *in situ*. Gallium and indium chlorides were synthesized from metallic gallium and indium and hydrogen chloride at around 750°C [18]. For *in situ* synthesis of $[Sr(thd)_2]_n$, reactions between solid Sr, SrO, $Sr(OH)_2$, or $SrCO_3$ and Hthd vapor were examined and the best results were obtained with Sr and SrO [325]. $[Ba(thd)_2]_n$ was synthesized from $Ba(OH)_2$ and Hthd [326], and WO_xF_y from WO_3 and WF_6 [205]. A risk related to the *in situ* precursor synthesis by the gas–solid reactions is the possibility that part of the gaseous reactant passes the source to the reaction chamber and etches the film. Therefore, the souce must be properly designed to ensure complete reactions.

The *in situ* generation of HF differs from the preceding solid–gas reactions in that HF was obtained by decomposing NH_4F thermally [215]. The ammonia liberated in the decomposition apparently had no effect in that study since the fluoride films deposited (ZnF_2, CaF_2, SrF_2) are inert toward ammonia.

In addition, gas–gas reactions have been employed for *in situ* generation of desired precursor compounds too. Chlorides of gallium and indium were formed by mixing $Ga(C_2H_5)_3$ and $In(CH_3)_3$ vapors with HCl in a reaction zone heated around 100°C, thereby avoiding problems related to the low vapor pressures of the binary chlorides and alkyl chlorides [18].

5.3.4. Single Source Precursors

In general, ALD processes employ two or more precursors which each contain one of the film constituent elements (see Section 5.3.5, however). Single source precursors which contain all the film constituents are actively examined in CVD, but in ALD they are not directly applicable because the self-limiting growth mechanism by its nature requires exchange reactions between different precursors and stability against self-decomposition. On the other hand, single source ALD processes can be realized by ramping the temperature repeatedly so that the adsorption takes place at a low temperature and the decomposition takes place at a higher temperature. Simple thermal heating and cooling of the substrate is inevitably too slow to be practical except for very thin films, but heating with laser or lamp or photodissociation with high energy photons makes the process faster. However, so far such processes have not been examined for compound films for which the single source CVD precursors are usually aimed, but only for deposition of elemental silicon [51, 54, 55, 57, 65, 67, 378, 381] and germanium [55, 56, 383]. For example, to deposit germanium, $Ge(C_2H_5)_2H_2$ was adsorbed at 220°C with a release of hydrogen and a formation of a monolayer of $Ge(C_2H_5)_2$, and then the ethyl groups were desorbed by heating above 400°C [383]. Similarly, silicon was deposited in a self-limiting manner at 180–400°C by first adsorbing Si_2H_6 and then by heating the substrate with a UV laser to desorb the surface terminating hydrogen atoms [51, 378].

The combination of using only one precursor and short heating (or dissociating) light pulses also offers an interesting possibility to have the precursor continuously present in the reactor and omit the purging. Within the duration of short light pulses, adsorption of new molecules in place of the decomposed chemisorption monolayer is negligible, and thus self-limiting film growth is achieved. This approach has been used for ALD of silicon and germanium from SiH_4 and GeH_4 by heating with a Xe flash lamp [54–56]. In fact, with these particular precursors the continuous presence is vital because the surface density of the chemisorbed species is determined by the balance between adsorption and desorption; i.e., the chemisorbed species have a high desorption probability and might thus be lost during a purge period.

5.3.5. Combinations of Two Metal Compounds

Quite recently a novel approach to the ALD of oxides was introduced [393]. In this process, two metal compounds, at least one of which is an alkoxide and thus contains a metal–oxygen bond, were used (Table IV). The metal alkoxide serves as both the metal and the oxygen source while the other metal compound, typically a metal chloride, acts as the other metal source:

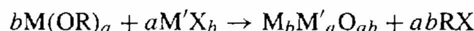

$$bM(OR)_a + aM'X_b \rightarrow M_bM'_aO_{ab} + abRX$$

Depending on whether M and M′ are similar or different, binary or mixed oxides are obtained. The major benefit of not using separate oxygen sources like water or hydrogen peroxide is the less susceptible oxidation of the substrate surface. This is especially important when thin high permittivity dielectric layers are to be deposited directly on silicon without creating an interfacial silicon oxide layer (Section 6.2.2).

5.3.6. Reducing Agents and Other Additional Reagents

Under this heading, reagents which take part in the film formation reactions but do not leave any constituents to the film are considered. The most obvious of these are the reducing agents in the growth of elemental films. For this purpose, both molecular and atomic hydrogen as well as elemental zinc and disilane have been examined. Atomic hydrogen which may be produced by either plasma discharge or thermal cracking is very reactive and facilitates even the deposition of metallic titanium and tantalum from their chlorides [74]. Also $SiCl_2H_2$ [60, 64–66, 170], Si_2Cl_6 [61], $GeCl_4$ [62], and $Ge(CH_3)_2H_2$ [68, 69] have been reduced with atomic hydrogen. Molecular hydrogen, by contrast, is quite inert and reduces CuCl [209, 210] and $Cu(thd)_2$ [210, 343, 344] only on appropriate metal surfaces (Section 6.6). For instance, the $Cu(thd)_2$-H_2 process resulted in a film growth only when the surface was seeded with a predeposited platinum–palladium layer [210, 343, 344], and

even then the copper deposition could not be repeated in a different reactor where high partial pressures of hydrogen could not be used and where the residence time of the precursors was much shorter [186]. The ALD studies on $Ni(acac)_2$, $Cu(acac)_2$, and $Pt(acac)_2$ reduction by H_2 also indicated the low reactivity of molecular hydrogen; metallic deposits seemed to be obtained only through interactions with substrates or as a consequence of thermal decomposition of the metal precursors [342]. Finally, high temperatures of 815–825°C were required to obtain monomolecular layer growth when $SiCl_2H_2$ was reduced by H_2 [373, 374].

Elemental zinc is a powerful reducing agent and has been employed in the ALD of copper [110] and molybdenum [204] but it suffers from its tendency to dissolve into the metallic films. Though the films contain only a few atomic percentages of zinc, the dissolution and subsequent outdiffusion during the process destroy the self-limiting growth mechanism (Section 5.1.5). In the growth of transition metal nitrides, the dissolution of zinc into the films is not a problem [112] and intermediate zinc pulses have been employed in improving the properties of the films deposited from metal chlorides and ammonia (Section 6.5). In addition to acting as a reducing agent, zinc may also assist in removing chlorides from the surface by forming $ZnCl_2$. In the $TaCl_5$-NH_3 process, the use of zinc is vital because otherwise semiconducting Ta_3N_5 is obtained instead of the desired TaN [113], but in the other cases the positive effect of zinc is not necessarily just simply due to a reducing action but also other chemical and structural factors appear to be involved [112]. However, as zinc forms electrically active states in silicon, the concern that zinc could dissolve into a silicon substrate has limited further interest toward these zinc-based ALD nitride processes. The most recently examined reducing agent is disilane Si_2H_6 which was successfully used in the ALD of metallic tungsten from WF_6 [206] (Sections 6.6 and 7.2.2). No silicon or fluorine could be detected in the films by X-ray photoelectron spectroscopy.

Moving to other additional reagents, pyridine [165, 166] and ammonia [167] have been used in catalyzing reactions between the alternately pulsed $SiCl_4$ and H_2O. In this way, the deposition temperature of SiO_2 was decreased remarkably from above 300°C to room temperature and at the same time the reactant exposure required to complete the surface reactions was decreased from 10^9 to 10^4–10^5 L (1 L = 10^{-6} Torr s). Unfortunately, also these catalyzed reactions required tens of seconds to get completed and thus the main problem of SiO_2-ALD, i.e., the long cycle times causing low deposition rates per time unit, still remains. The mechanism proposed for explaining the catalytic effect of pyridine and ammonia involves hydrogen bonding of the nitrogen atom in the catalyst molecule to surface hydroxyl groups (during the $SiCl_4$ pulse) or water molecules (during the H_2O pulse) with a concomitant weakening of the O−H bond and an increase of the nucleophilicity of the oxygen atom. The catalytic effect decreased as the temperature was increased above room temperature which may be related to decreased surface coverages of $SiCl_4$ and, perhaps more importantly, of catalyst molecules. As good film properties were achieved with these catalyzed processes, they are clearly an interesting approach to very low temperature ALD and they deserve further studies to clarify their applicability to other materials.

Additional reagents may also be used for assisting the completion of the reactions. Occasionally, the complete ligand removal from the metal precursors is hard and may thus lead to impurity incorporation. This has been a severe problem in the epitaxial growth of the III–V semiconductors where low impurity levels are required; especially aluminum containing compounds are prone to carbon incorporation. In the growth of AlAs from $Al(CH_3)_2H$ and AsH_3, dimethylamine ($(CH_3)_2NH$) supplied intermediately after $Al(CH_3)_2H$ was used to remove methyl groups from the surface [240]. A mechanism which involves reactions between the methyl groups and amine and hydrogen radicals was suggested to explain the observed decrease of the carbon content from 6×10^{20} to 8×10^{19} cm^{-3} as determined by secondary ion mass spectrometry (SIMS). Nitrogen contents were not reported, however. Anyhow, the idea of using separate reagents for assisting surface ligand removal is evidently worth further consideration.

6. FILM MATERIALS AND APPLICATIONS

Table V summarizes the film materials deposited by ALD thus far. As in Table IV, all the reported materials have been included regardless of how effective the processes actually are. For references, see Table IV. In this section, the most important nonepi-

Table V. Thin Film Materials Deposited by ALD[a]

II–VI compounds	ZnS, ZnSe, ZnTe, $ZnS_{1-x}Se_x$, CaS, SrS, BaS, $SrS_{1-x}Se_x$, CdS, CdTe, MnTe, HgTe, $Hg_{1-x}Cd_xTe$, $Cd_{1-x}Mn_xTe$
II–VI-based TFEL phosphors	ZnS : M (M = Mn, Tb, Tm), CaS : M (M = Eu, Ce, Tb, Pb), SrS : M (M = Ce, Cu, Tb, Pb)
III–V compounds	GaAs, AlAs, AlP, InP, GaP, InAs, $Al_xGa_{1-x}As$, $Ga_xIn_{1-x}As$, $Ga_xIn_{1-x}P$
Nitrides	
semiconductors/dielectric	AlN, GaN, InN, SiN_x, Ta_3N_5
metallic	TiN, Ti-Si-N, TaN, NbN, MoN, W_2N
Oxides	
dielectric	Al_2O_3, TiO_2, ZrO_2, HfO_2, Ta_2O_5, Nb_2O_5, Y_2O_3, MgO, CeO_2, SiO_2, La_2O_3, $SrTiO_3$, $BaTiO_3$, $Bi_xTi_yO_z$
Transparent conductors/ semiconductors	In_2O_3, In_2O_3 : Sn, SnO_2, SnO_2 : Sb, ZnO, ZnO : Al, ZnO : B, ZnO : Ga, Ga_2O_3, WO_3, NiO, Co_3O_4, MnO_x
Ternary oxides	$LaCoO_3$, $LaNiO_3$, $LaMnO_3$
Fluorides	CaF_2, SrF_2, ZnF_2
Elements	Si, Ge, Cu, Mo, Ta, W
Others	La_2S_3, PbS, In_2S_3, $CuGaS_2$, SiC

[a] For references, see Table IV.

taxial thin film materials, grouped according to their applications, are discussed.

As the epitaxial semiconductors were limited outside the main scope of this presentation, they are not dealt with here but rather review articles [19–23] are suggested for the III–V compounds, and [24, 25] for the II–VI compounds. In contrast to the compound semiconductors, little has been published thus far on the material properties of the ALD made Si and Ge films, the focus in these studies has been on the film growth and the related chemistry. Also deposits other than thin films are skipped here; the use of ALD in processing of porous materials [30–33] and in nanotechnology [398] have been reviewed in the references cited.

6.1. Electroluminescent Display Phosphors

As already noted, ALD was originally developed by Suntola and co-workers for making thin film electroluminescent (TFEL) displays [2, 5–9]. In this application, ALD has been very successful and has been used for nearly 20 years in manufacturing [7–11]. In addition, research on using ALD in making thin films for the TFEL displays has been active all the time and has formed a solid basis for the more recent ALD research, particularly that on insulators (Section 6.2). Therefore, it is instructive to first have a closer look at the TFEL display itself.

A schematic of a conventional TFEL display is shown in Figure 12. A more recently developed, so-called inverted structure is otherwise similar but the places of the transparent and metal electrodes have been exchanged. In the conventional structure, glass is used as a substrate because viewing is through the substrate. Also in the inverted structure glass is often used but also opaque ceramics may be applied as substrates because the viewing is on the opposite side. The benefit of glass is its low price whereas ceramics make it possible to use high annealing temperatures for improving the phosphor crystallinity. If soda lime glass is used, it is passivated by an ALD made Al_2O_3 to prevent sodium outdiffusion (Section 6.4). The actual TFEL device structure consists of an electrode-insulator-semiconducting phosphor-insulator-electrode film stack where the electrodes are patterned into stripes perpendicular to each other while the other films are continuous. The electrode on the viewing side must of course be transparent and thus indium–tin oxide (ITO) is usually used. The other electrode is metal; in the conventional structure it is aluminum but in the inverted structure molybdenum or tungsten with better thermal properties must be used. A passivating layer is finally deposited on the top of the structure. At present, ALD is used in industrial scale for all the other films except the electrodes which are sputtered. ZnS : Mn, Al_2O_3 and Al_2O_3/TiO_2(ATO) are the dominant ALD made materials used by the industry. The thickness of the phosphor layer is in the range of 500–1000 nm while the insulators are about 200-nm thick, and the three layers are deposited in one continuous ALD process.

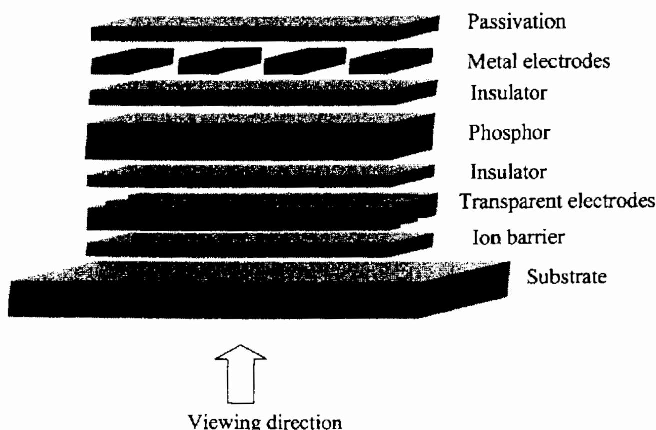

Fig. 12. Schematics of a TFEL display with a conventional structure. In the inverted structure the metal and transparent electrodes have changed places and the viewing is from the film stack side of the substrate.

In the TFEL displays, each crossing point of the bottom and top electrodes defines a picture element (pixel). A pixel is lit by applying an ac (typically 60 Hz) voltage to the two electrodes. At low voltages, the insulator-phosphor-insulator structure acts like three capacitors in series, but when the electric field in the phosphor layer exceeds a certain threshold value, electrons begin to flow through the phosphor from one insulator-phosphor interface to the other. When arriving at the interface, the electrons are trapped in the interface states from which they are emitted when the polarity of the electric field reverses. For an effective operation of the typically used phosphor materials, the threshold field must be in the range of 1 to 2 MV cm^{-1}, so that once released, the electrons are rapidly accelerated to energies high enough to impact excite the luminescent centers which then emit light while returning to the ground state. The phosphor layer must withstand these high fields without destructive breakdown. Likewise, the insulators must possess high breakdown strength and low leakage currents at the operation voltages. Pinhole-freeness over the large-area substrate is a key aspect in meeting these requirements. In the late 1970s, few techniques existed for making high quality insulator-phosphor-insulator structures, and that was the main motivation for developing ALD.

Unlike the other flat panel displays, the TFEL displays have complete solid-state structures which gives them many advantages like wide operating temperature, ruggedness, exceptionally broad viewing angle, and fast response. On the other hand, operation voltages around 200 V are typically needed which means that the driving electronics and thus the whole display is rather expensive as compared to its main competitors, especially liquid crystal displays. Therefore, TFEL displays are not found in laptops but rather they are found in applications like medical, instrumentation, and transportation where their special characteristics are valued.

Quite recently a new kind of TFEL display, active matrix EL (AMEL) display has been developed [399]. Here, the insulator-phosphor-insulator-transparent top electrode film stack is deposited directly on single crystal silicon-on-insulator (SOI) wafers to which all the required driving circuitry has been integrated. This makes it possible to make small high resolution

displays for head mounted applications, for example. On the other hand, the deposition on top of the driving circuitry sets strict demands on the film conformality, thus favoring the use of ALD (Fig. 13).

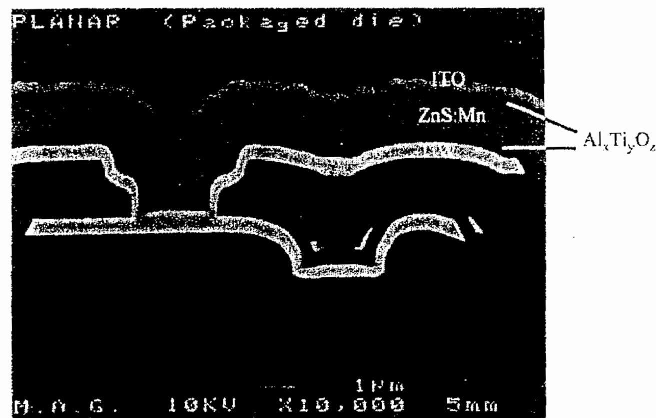

Fig. 13. Cross-sectional image of an AMEL display. Only the films of the TFEL structure are shown, the driving circuitry below is not shown. The ZnS : Mn and $Al_xTi_yO_z$ films are made by ALD. (Courtesy B. Aitchison, Planar Systems Inc.)

Comprehensive review articles on TFEL phosphor materials can be found in Refs. [11, 400, 401], so here they are discussed chiefly from the ALD point of view. A summary of the ALD made TFEL phosphors is presented in Table VI. The most important of the TFEL phosphors is the yellow–orange emitting ZnS : Mn which is made by ALD primarily from $ZnCl_2$, $MnCl_2$, and H_2S [3, 4, 8, 402], though alternatives have been used for both zinc ($Zn(C_2H_5)_2$) and manganese ($Mn(thd)_3$, $Mn(C_5H_5)_2$, $Mn(C_5MeH_4)(CO)_3$) [295, 296, 402]. The concentration of Mn is typically 0.5–2 mol%. In ALD, the doping is realized most simply by replacing a certain number of the zinc precursor pulses with manganese precursor pulses. Though this seems to lead to delta doping depth profiles, concentration quenching has not been found to be a major problem. Apparently, surface roughness and diffusion smooth the doping profile. On the other hand, due to the forbidden transitions in the Mn luminescence the Mn–Mn energy transfer is not very probable. The other option for doping is to supply the dopant simultaneously with the matrix cation but in that approach differences in reactivities may cause nonuniformity over the substrate.

ZnS : Mn is the most efficient TFEL phosphor ever found (3–8 $lm\,W^{-1}$). No major differences in the performance can be found between the ALD films [402, 403] and those made

Table VI. Luminescent Thin Films Made by ALD for TFEL Devices

Phosphor material	Emission color	Luminance $cd\,m^{-2}$ at 60 Hz[a]	CIE coordinates x	CIE coordinates y	Reference
ZnS : Mn^{2+} (chloride-process)	Yellow	440	0.52	0.48	[402]
ZnS : Mn^{2+} (organometallic precursors)	Yellow	430	0.54	0.46	[402, 403]
ZnS : Tb^{3+}	Green	35			[350]
ZnS : Tb^{3+}(O, Cl)	Green	75	0.28	0.64	[351]
ZnS : Tm^{3+}	Blue	<1 (300 Hz)			[345]
CaS : Eu^{2+}	Red	2–6	0.68	0.31	[404, 405]
CaS : Tb^{3+}	Green	20			[319]
CaS : Pb^{2+}	Blue	2.5 (300 Hz)	0.17	0.13	[406]
		80	0.14–0.15	0.07–0.15	[407]
SrS : Ce^{3+}	Bluish-green	130	0.30	0.54	[408]
SrS : Ce^{3+} (filtered)	Blue	8	0.08	0.20	[408]
SrS : Ce^{3+}, Y^{3+}	Bluish-green	100	0.3	0.5	[360]
SrS : Ce^{3+}, Y^{3+} (filtered)	Blue	20	0.21	0.39	[360]
SrS : Pr^{3+}	White	30 (300 Hz)			[345]
SrS : Tb^{3+}	Green	5.5			[347]
SrS : Mn^{2+}	Green	3.5 (300 Hz)	0.37–0.44	0.55–0.61	[409]
SrS : Mn^{2+}, Pb^{2+}	White	7 (300 Hz)	0.28	0.39	[409]
SrS : Cu^{+}	Blue (green)	25	0.17	0.30	[410]
SrS : Pb^{2+}	Bluish-green	17 (300 Hz)	0.26	0.33	[406]
SrS : Pb^{2+} (filtered)	Blue	1.8 (300 Hz)	0.14	0.09	[406]
CaF_2 : Eu^{2+}	Blue (450 nm)	2 (1 kHz)	0.2	0.1	[215]
ZnS : Mn^{2+}/SrS : Ce^{3+}	White	480[b]	0.49	0.48	[338, 402, 408]

[a] Note that the voltages in the luminance measurements vary in different references from 25 to 50 V above the threshold.

[b] Value for one pixel; in patterned full devices values of 21 and 70 $cd\,m^{-2}$ with 60 and 350 Hz, respectively, have been achieved for areal luminance [411, 412].

by other methods, like thermal and electron beam evaporation or sputtering. A clear advantage of ALD is, however, a larger grain size at the beginning of the film growth which ensures that in the ALD made films the dead layers, i.e., layers with no emission due to poor crystallinity, are thinner than in the films made by the other techniques [413, 414]. The emission band of ZnS : Mn is so broad that with proper filters it may also be used as a red or a green phosphor for multi- and full color displays. To avoid parallax, the filters need to be placed close to the film stack and because this is not possible in the conventional structure (Fig. 12) where the substrate would be left in between, the inverted structure was developed by replacing the positions of the metal and the transparent electrodes [10].

ZnS : Tb is the other zinc sulfide-based material which has shown EL properties good enough for applications. In the deposition, $Tb(thd)_3$ has been used as a precursor and good results have been obtained when several subsequent $Tb(thd)_3/H_2S$ cycles have been used instead of one. Thus, the actual structure has been of a TbS_x/ZnS sandwich type [350, 351]. The rare-earth ions (Ln^{3+}) are large as compared to the zinc ion and therefore in practical rare-earth concentrations (few percent) the rare-earth ions when homogeneously distributed cannot locate at the zinc site in ZnS but rather a Ln_2O_2S center is formed [415].

Due to the excellent performance of ZnS : Mn in the long wavelength part of the visible spectrum, quite a lot of the more recent phosphor research has been devoted to the blue phosphors which are needed to complement ZnS : Mn in making a full color display. Here, the most intensively studied material has been bluish-green emitting SrS : Ce for which the basic process uses $Sr(thd)_2$, $Ce(thd)_4$, and H_2S as the precursors [337, 338], but also different fluorinated β-diketonate Ce complexes have been studied as source materials for the Ce dopant [339, 340]. The use of cyclopentadienyl compounds as precursors began with Ce compounds [360] but also the host material SrS has been made from metalorganic precursors, from $Sr(C_5{}^iPr_3H_2)_2$ for instance [359, 416]. Despite all the efforts, the performance of SrS : Ce after blue filtering (10–20 $cd\,m^{-2}$ depending on the filter) is still somewhat lacking the level required (20–30 $cd\,m^{-2}$) for commercializing the full color displays. The total EL brightness of SrS : Ce is good (>100 $cd\,m^{-2}$) but unfortunately the majority of the emission falls in the green region (Table VI). Quite recently, SrS : Cu and CaS : Pb have been taken under study as new potential blue phosphors. Especially for CaS : Pb, deposited from $Ca(thd)_2$, $Pb(C_2H_5)_4$, and H_2S, very promising results have been reported: deep blue emission, CIE (Comission Internationale de l'Eclairage) color coordinates ranging from (0.14, 0.07) to (0.15, 0.15), and luminance of 80 $cd\,m^{-2}$ with low driving voltage but the efficiency is still an issue [407].

In addition to the previously mentioned, many other potential phosphors have been deposited by ALD in the search of materials for full color TFEL displays (Table VI). The materials studied are rare-earth doped zinc and alkaline earth sulfides. The rare-earth ions, besides cerium and terbium, include europium (red), samarium (red), praseodymium (white), and thulium (blue). Most of the materials have been examined already in the 1980s and the EL performance levels reached by ALD are also here quite similar to those obtained by the other film deposition methods. Unfortunately, the EL properties of these materials are far below the level needed in TFEL devices.

6.2. Insulators

6.2.1. Insulators for TFEL Displays

In the TFEL displays (Section 6.1, Fig. 12), the insulator films limit current transport across the TFEL device. Since high electric fields of about 2 $MV\,cm^{-1}$ are typically used, high dielectric field strength (high breakdown field, E_{BD}) and pinhole-freeness over the whole display area is required. Therefore, the insulators seem to be perhaps the most critical part in the preparation of reliable TFEL displays. A detailed discussion on the role of the insulators and their requirements has been presented in Refs. [11, 400, 401], so here we just summarize the most important properties of the insulator films:

(i) high electric field strength,
(ii) high relative permittivity, ε_r,
(iii) pinhole-free structure,
(iv) self-healing breakdown mode,
(v) convenient and stable interface-state distribution from which electrons are emitted into the phosphor at proper electric fields,
(vi) good thickness uniformity and conformality,
(vii) good adhesion and stability with the adjacent electrode and phosphor layers,
(ix) stress-free.

The insulator films should preferably be amorphous because polycrystalline films lead to rough interfaces and they contain grain boundaries through which electrons can flow and ions can migrate. The requirements of high field strength and high permittivity are contradictory since, in general, insulators with high permittivity suffer from low breakdown fields. In addition, their breakdown mechanism is usually propagating rather than self-healing. Therefore, insulators with moderate permittivity but high E_{BD} have usually been preferred. A convenient figure of merit for the insulators is the charge storage factor, $\varepsilon_0\varepsilon_r E_{BD}$, which shows the maximum charge density that can be stored in a capacitor made of a given insulator. Here, it must be noted, however, that while ε_r is usually well defined, E_{BD} is a statistical quantity and depends on the measurement method and the definition of breakdown; i.e., whether the breakdown field is that causing a destructive breakdown or a certain leakage current density, like 1 $\mu A\,cm^{-2}$. Table VII summarizes dielectric properties of ALD made insulators potential for TFEL displays. In addition to those listed in Table VII, several other potential insulator films have also been grown by ALD (Y_2O_3, MgO, CeO_2, AlN, see Tables IV and V) but their dielectric properties have not been reported in enough detail. On the other hand, some of the high permittivity insulators (TiO_2, Nb_2O_5, $SrTiO_3$, $BaTiO_3$) are considered too leaky to be applied in the TFEL

Table VII. Dielectric Properties of ALD Made Insulators Potential for TFEL Displays[a]

Material	ε_r	E_{BD} (MV cm^{-1})	$\varepsilon_0\varepsilon_r E_{BD}$ (nC mm^{-2})	Reference
Al_2O_3	7–9	3–8	16–50	[129, 133, 135, 136, 216, 220, 225, 227, 237]
$Nb_xAl_yO_z$	8	5	42	[136]
Al_2O_3/TiO_2	9–18	5–7	40–80	[107, 417]
Al_2O_3/Ta_2O_5	10–20	2–6.6	20–55	[130, 131, 133, 135]
HfO_2	13–16	1–5	8	[131, 197]
Ta_2O_5/HfO_2	19–23	2.5–5	40–66	[131, 197]
ZrO_2	20	1	20	[133]
Ta_2O_5	23–25	0.5–1.5	5–10	[131, 133, 197]
Ta_2O_5/ZrO_2	25–28	2–2.5	40–60	[133]
$Ta_xTi_yO_z$	27–28	1	33	[418]
$Nb_xTa_yO_z$	25–35	0.5–1	25	[202]
$Nb_xTa_yO_z/ZrO_2$	31–33	3	83	[192]
Ta_2O_5/Nb_2O_5	38	0.5	17	[202]

[a]Typically the best results or a range of the best values are given for each material. The notation of AB/CD refers to a stacked insulator (nanolaminate) with a variable number of layers. Note that the E_{BD} values depend on its definition, and consequently also $\varepsilon_0\varepsilon_r E_{BD}$ depend on the definition of E_{BD}. Most of the results are based on E_{BD} corresponding to a leakage current density of 1 μA cm^{-2}.

displays as such, without a combination with higher resistivity materials, and are therefore not included in Table VII.

In the commercial TFEL displays, the ALD made insulators are Al_2O_3/TiO_2 (ATO) or just Al_2O_3 which are made from the corresponding chlorides and water. For aluminum, $Al(CH_3)_3$ may also be used. The Al_2O_3/TiO_2 insulator [107, 399, 402, 417, 419] is a good representative of composite structures where advantageous characteristics of two or more materials are combined in realizing insulators which are at the same time reliable (high E_{BD}) and efficient (high ε_r). In other words, the $\varepsilon_0\varepsilon_r E_{BD}$ value of the composite exceeds those of its binary constituents (Table VII).

Later, Ta_2O_5 based composite insulators have been examined in great detail (Table VII). Ta_2O_5 has a relatively high permittivity of 25 but in the as-deposited state it is usually quite leaky due to oxygen deficiency. To improve this shortcoming, a concept of nanolaminate was introduced. Nanolaminates consist of alternating layers of two or more insulator materials so that each separate layer has a thickness in a range of 1–20 nm (Fig. 14a) [197]. Due to the sequential film deposition in ALD, the preparation of nanolaminates with accurately varying composition depth profiles is straightforward. The ALD made nanolaminates studied so far have consisted of stacked layers of Ta_2O_5, ZrO_2, HfO_2, Al_2O_3, Nb_2O_5, and their solid solutions deposited from $Ta(OC_2H_5)_5$, $TaCl_5$, $ZrCl_4$, $Zr(OC(CH_3)_3)_4$, $HfCl_4$, $AlCl_3$, $Nb(OC_2H_5)_5$, and H_2O at 325°C and below. Figure 14 compares the dielectric properties of HfO_2-Ta_2O_5 nanolaminates to their binary constituents. The labels describe the nanolaminate configuration as $N \times (d_{HfO_2} + d_{Ta_2O_5})$ where N is the number of the HfO_2-Ta_2O_5 bilayers, and d_{HfO_2} and $d_{Ta_2O_5}$ are the thicknesses of the corresponding single layers in nanometers. A number of conclusions can be drawn:

(i) the leakage current in the nanolaminates is lowered in relation to both constituents and is strongly dependent on the actual nanolaminate configuration (Fig. 14b),

(ii) the permittivity is nearly, though not entirely a linear function of the relative thickness of the binary constituents (Fig. 14c),

(iii) the charge storage factor has a maximum, about 10-fold of that of the binaries, at a certain relative thickness of the constituents (Fig. 14d).

An interesting observation is that in the nanolaminates the leakage current density is lowered not only in relation to the more leaky component, Ta_2O_5, but also in relation to the higher resistivity HfO_2 (Fig. 14b). In other words, the addition of layers of the high leakage current material Ta_2O_5 to HfO_2 has a positive effect on the leakage current properties. This improvement, which at first sight seems somewhat surprising, is attributed to the elimination of grain boundaries extending through the whole insulator from one electrode to the other. Polycrystalline insulator films, like HfO_2 here, usually exhibit extra conductivity along the grain boundaries. In the nanolaminate structure, the continuous grain growth of HfO_2, and thus the continuous grain boundaries, are interrupted by the amorphous Ta_2O_5 layers. Another potential explanation for the improved leakage current properties of the nanolaminates is the trapping of electrons at an interface next to a weak point in one sublayer, thereby decreasing the injecting electric field in the vicinity of this point. Nevertheless, if these two mechanisms were the only ones responsible for the reduced leakage current, the layer thicknesses should not have such a significant effect as observed (Fig. 14b). Therefore, it appears that also some other, layer thickness-dependent factors are involved. Especially the crystal structures and crystallite sizes of the poly-

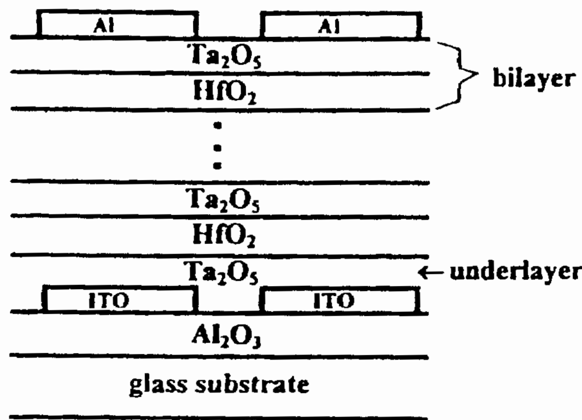

(a)

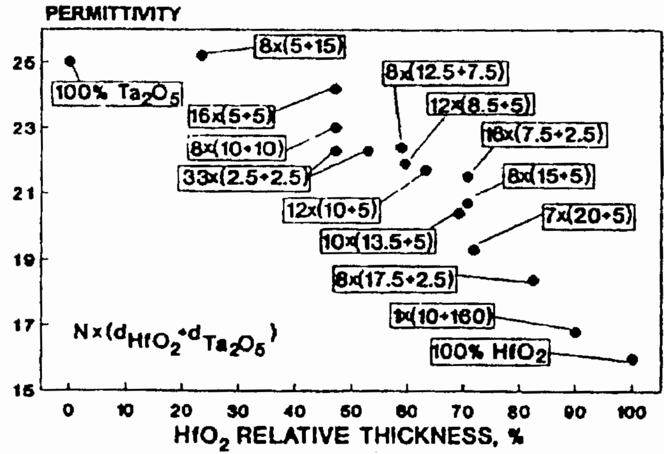

(c)

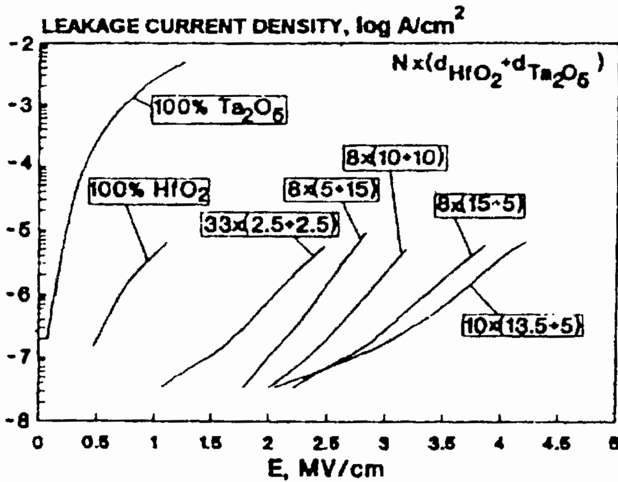

(b)

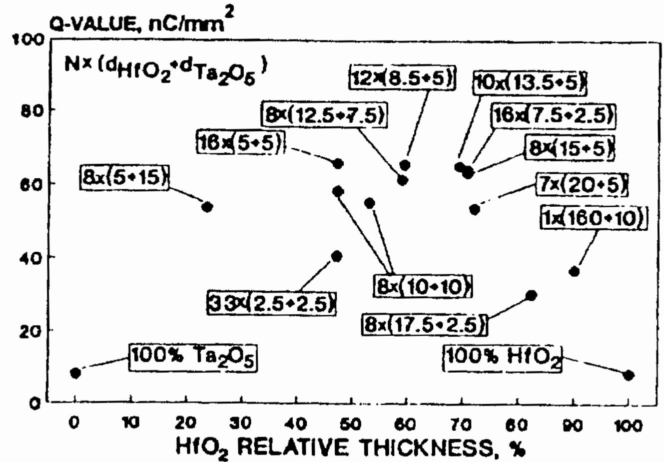

(d)

Fig. 14. (a) Schematic of a HfO_2-Ta_2O_5 nanolaminate insulator between ITO and Al electrodes. (b) Leakage current densities of HfO_2 and Ta_2O_5 films and various HfO_2-Ta_2O_5 nanolaminates, all having a total thickness of about 170 nm. The nanolaminate configurations are described with a notation $N \times (d_{HfO_2} + d_{Ta_2O_5})$ where N is the number of bilayers, and d_{HfO_2} and $d_{Ta_2O_5}$ are thicknesses of the single HfO_2 and Ta_2O_5 layers, expressed in nanometers. (c) Relative permittivities and (d) charge storage factors $Q = \varepsilon_0\varepsilon_r E_{BD}$ of the HfO_2-Ta_2O_5 nanolaminates vs the relative thickness of the HfO_2 layers. E_{BD} is taken as a field which induces a leakage current density of 1 $\mu A\,cm^{-2}$ [197]. Reprinted with permission from K. Kukli et al., Tailoring the dielectric properties of HfO_2-Ta_2O_5 nanolaminates, *Appl. Phys. Lett.* 68, 3737 (1996), © 1996, American Institute of Physics.

crystalline layers seem to affect both leakage current and permittivity [133, 197].

The other nanolaminate structures examined have shown rather similar basic behavior as the HfO_2-Ta_2O_5 nanolaminates, though some interesting differences have been identified as well. In the Al_2O_3-Ta_2O_5 nanolaminates where the both constituents are amorphous, no improvement of the leakage current was observed in comparison with Al_2O_3 which is the component having the better resistivity [133]. This supports the idea that the improvements observed in the HfO_2-Ta_2O_5 nanolaminates are indeed due to the grain boundary interruption. In the ZrO_2-Ta_2O_5 nanolaminates, on the other hand, the permittivity did not decrease smoothly as a function of the increasing ZrO_2 relative thickness but had values (27 to 28) which were higher than those of either of the constituents (25 for Ta_2O_5, 20 for ZrO_2) when as thick (150–200 nm) as the total thickness of the nanolaminate [133]. This was attributed to the dominance of the higher permittivity tetragonal phase of ZrO_2 in the thin layers in the nanolaminates as opposite with the monoclinic phase in the thicker binary films. Such an effect could also possibly explain the observed nonlinearities in the permittivity of the HfO_2-Ta_2O_5 nanolaminates (Fig. 14c) since these films were found to consist of a mixture of monoclinic and tetragonal HfO_2. By contrast, in the completely amorphous Al_2O_3-Ta_2O_5 nanolaminates the permittivity decreased linearly from 25 for Ta_2O_5 to 8 for Al_2O_3 [133].

The highest charge storage factor obtained so far is 84 $nC\,mm^{-2}$ measured for the $Nb_xTa_yO_z$-ZrO_2 nanolaminates where solid solutions were formed from Ta_2O_5 and Nb_2O_5, the latter of which has a high permittivity (about 50) but is very

leaky in the binary form [192]. When mixed with Ta_2O_5, the leakage is decreased to a reasonable level, and even if also the permittivity decreases to 25–35, it remains higher than that of Ta_2O_5. As a consequence, the $Nb_xTa_yO_z$ solid solution shows improved dielectric properties in comparison to both of its constituents, and hence the nanolaminates are also improved by replacing Ta_2O_5 with $Nb_xTa_yO_z$.

6.2.2. Insulators for Microelectronics

The success in the demanding application of the TFEL displays clearly demonstrated the capabilities of ALD in making high quality insulators for large-area applications. This, together with the other beneficial features of ALD, has subsequently encouraged ALD insulator research also in other areas, particularly in microelectronics. While the TFEL insulator research serves as a good starting point for microelectronic applications, there also are some important differences which somewhat limit the direct applicability of the results from the TFEL insulators. First, the insulators in the TFEL displays are usually about 200 nm thick while the present and future integrated circuits require much thinner films down to a few nanometers. Second, the electrodes are quite different: in TFEL displays Al, Mo, and ITO are typically used whereas in the integrated circuits the insulators are combined with Si, Al, Pt, and perhaps with also some other conductors yet to be defined.

In the silicon-based integrated circuits, SiO_2 and SiO_xN_y have been the insulators of choice for decades. Unfortunately, no effective ALD processes for these materials have been found so far. In all the processes reported by now (Table IV), lengthy exposure times are required. On the other hand, an interesting room temperature ALD process for depositing SiO_2 from $SiCl_4$ and H_2O using pyridine [165, 166] or ammonia [167] as a catalyst has been reported, though also there long exposure times were needed (Section 5.3.6).

As is well known, the continuous decrease of the device sizes in the integrated circuits will soon lead to a situation where SiO_2 and SiO_xN_y can no longer be used as the insulators. In both metal-oxide-semiconductor-field-effect transistors (MOSFET) and dynamic random access memory (DRAM) capacitors silicon-based insulators are projected to be scaled so thin in the coming years that direct tunneling currents through them become detrimentally large. Therefore, insulators with higher permittivity and methods for their controlled deposition are urgently looked for. As the new materials are required for replacing SiO_2 in devices where the latter would need to have a thickness of 1.5 nm or below, the substitutes must accordingly have an equivalent thickness ($d_{eq} = (\varepsilon_{SiO_2}/\varepsilon)d = (3.9/\varepsilon)d$) of 1.5 nm or less. Such equivalent thicknesses must be achieved repeatedly over the 200- or 300-mm wafers. Clearly, this is an application to which ALD is ideally suited: very thin films with accurately controlled thickness over large areas. In addition, in DRAM capacitors excellent conformality is also highly appreciated as the memory capacitors will have three-dimensional structures.

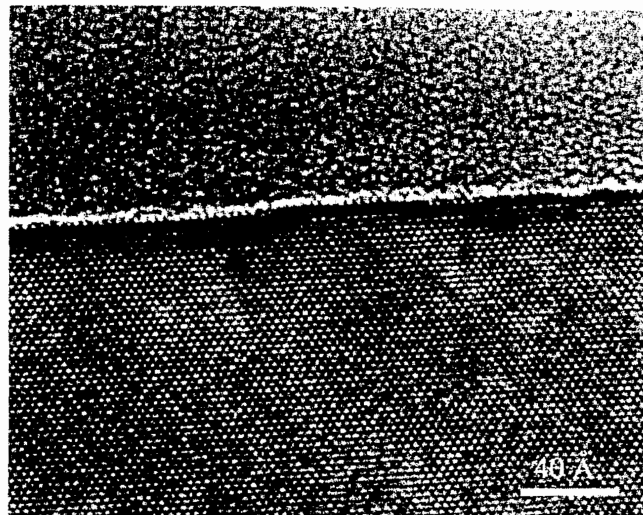

Fig. 15. High resolution TEM image of an Al_2O_3-Si interface where the Al_2O_3 film was deposited from $AlCl_3$ and $Al(OCH(CH_3)_2)_3$.

In MOSFETs, the gate insulator is deposited directly on silicon. An achievement of an equivalent thickness of 1.5 nm and below requires that the high permittivity insulator is deposited on silicon so that only very thin, preferably only a one-to-two monolayers thick silicon oxide layer forms at the interface. If the interface oxide becomes of a considerable thickness, it will start to dominate the overall capacitance of the resulting insulator stack which may be understood to consist of two capacitors in a series giving a total equivalent thickness $d_{eq,\,tot} = d_{SiO_2} + d_{eq}$. A very thin interface layer is preferred, however, as it is beneficial for good interface characteristics, i.e., low interface trap density. The interfacial SiO_2 layer may form by two mechanisms: by a reaction between silicon and the high permittivity oxide, and by oxidation of the silicon surface during the oxide deposition. To avoid the first mechanism, oxides which appear to be thermodynamically stable in contact with silicon should be chosen, such as Al_2O_3, ZrO_2, and HfO_2 and their silicates. ALD processes have been reported for all these oxides (Table IV).

Amorphous Al_2O_3 films have already been grown directly on HF etched silicon without creating an interfacial layer by both $Al(CH_3)_3$-H_2O [194, 222] and $AlCl_3$-$Al(OCH(CH_3)_2)_3$ (Fig. 15) [393] ALD processes. The latter belongs to the new group of ALD oxide processes where no separate oxygen sources are used (Section 5.3.5). These were developed to eliminate the possibility that the conventional oxygen sources used in the ALD processes, like water and hydrogen peroxide, could oxidize the silicon surface and thereby create the interfacial oxide layer. Detailed electrical characterization of these films are still in progress, however. The absence of the interface layer below the films deposited by the $Al(CH_3)_3$-H_2O process is somewhat surprising as water might be expected to oxidize the silicon surface (see the following). Perhaps this is counterbalanced by the reducing nature of $Al(CH_3)_3$. These Al_2O_3 films have shown low leakage currents, and C–V measurements have indi-

cated relatively low midgap interface-state densities (one estimate being 10^{11} states eV^{-1} cm^{-2} [216]) but have at the same time given indications of some mobile and fixed charges, especially when large bias voltages have been applied [216, 220, 222].

Ultrathin ZrO_2 films have been deposited by ALD from $ZrCl_4$ and H_2O at 300°C on differently treated silicon surfaces [193, 194, 420, 421]. Contrary to the previously mentioned Al_2O_3 films, on native oxide-free (HF etched) silicon the ZrO_2 films exhibited rather poor morphology with islands of crystalline ZrO_2 dispersed in an amorphous matrix and roughened interfaces [193, 194]. In addition, an interfacial SiO_2 layer was also formed. On thermally oxidized silicon, the crystallites were better developed and interfaces were abrupt, and more ZrO_2 was deposited than on the HF stripped silicon. These findings suggest that the initial nucleation of ZrO_2 on oxide-free, hydrogen terminated silicon is suppressed, but the possibility of detrimental reactions between $ZrCl_4$ and silicon must be kept in mind as well. The ZrO_2 films on thermal SiO_2 were stable against intermixing and interfacial reactions up to approximately 900°C but higher temperature annealing in vacuum resulted in a formation of $ZrSi_2$ islands.

On chemically oxidized silicon, $ZrCl_4$ interacted with the oxide layer resulting in a Zr-Si-O interface layer with a permittivity twice as high as that of SiO_2 [420]. This difference in comparison with the thermal oxide was attributed to the presence of silicon suboxides in the chemical oxide. The resulting Zr-Si-O interface layer was not very stable, however, and decomposed into ZrO_2 and SiO_2 at 500°C. Electrical characterization of SiO_x/ZrO_2 dielectric stacks obtained by depositing 5 to 10-nm ZrO_2 on a chemical oxide indicated both a presence of fixed negative charge (effective density of 5.2×10^{12} cm^{-2}) and an electron trapping (1.5×10^{12} cm^{-2}) [421]. Leakage through such a stack was concluded to proceed by a direct tunneling of electrons through SiO_x and trap-assisted tunneling through ZrO_2. A similar mechanism was also observed for an analogous SiO_x/Ta_2O_5 dielectric stack [421].

A good quality ZrO_2 was obtained on an ammonia treated (nitrided) silicon. A 4.0-nm thick ZrO_2 film on a 1.3-nm interface layer resulted in an equivalent thickness $d_{eq} = 1.4$ nm and a low leakage current of 10^{-8} A cm^{-2} [420].

On a bare silicon substrate, the $TaCl_5$-H_2O process caused a formation of a 1.5-nm SiO_2 interface layer at 300°C [195]. When the silicon was passivated with 2.8-nm silicon nitride, no oxide layer was observed at the interface.

A common observation on many thin ALD oxide films on silicon is that their permittivity decreases considerably as the thicknesses are scaled down. Such a decrease cannot be explained solely in terms of a lower permittivity interface layer but is also observed when the contribution of the interface is taken into account. For example, in the study of the SiO_x/ZrO_2 dielectric stacks a permittivity of 15 was evaluated for the 5- to 10-nm ZrO_2 layers after subtracting the contribution of SiO_x [421] while values around 20 have usually been obtained for thicker films (Table VII). A similarly decreased permittivity of 15 was also obtained for 10-nm ZrO_2 in another study where, in addition, parallel decreases were observed with Ta_2O_5 (from 27 to 15 for a 16-nm film) and HfO_2 (from 16 to 11 for an 11-nm film) [195]. On the other hand, rapid thermal annealing at 700°C increased the permittivity of Ta_2O_5 to 21, obviously due to a densification of the films. In fact, studies on the effects of postdeposition treatments on the dielectric properties of ALD made oxide films have so far remained in their infancy and should be explored in detail in the future.

In the DRAM capacitors, the insulator film is deposited on three-dimensional electrodes. For the near future DRAMs, $Ba_{1-x}Sr_xTiO_3$ is the most extensively examined insulator. Recently ALD processes were developed for both $SrTiO_3$ and $BaTiO_3$ using novel Sr and Ba cyclopentadienyl compounds as precursors together with $Ti(OCH(CH_3)_2)_4$ and H_2O [356–358]. The use of these new precursors was crucial because the β-diketonates $Sr(thd)_2$ and $Ba(thd)_2$ that have been widely used in CVD, and that have also been used in the ALD of sulfides (cf. Table IV), do not react with water at temperatures which would be low enough so that they or $Ti(OCH(CH_3)_2)_4$ would not decompose thermally. The β-diketonates do react with ozone, e.g., $Sr(thd)_2$ reacts with ozone at around 300°C but the resulting film contains $SrCO_3$, or when combined with titanium, an amorphous mixture which needs to be annealed at 700°C to get $SrTiO_3$ crystallized [322]. By contrast, using strontium bis(tri-isopropylcyclopentadienyl) ($Sr(C_5{}^iPr_3H_2)_2$), crystalline $SrTiO_3$ films with excellent conformality were obtained at 250–325°C (Fig. 16a and b) [356–358]. The Sr/Ti ratio in the films was well correlated to the pulsing ratio of the metal precursors (Fig. 16c), and after annealing at 500°C in air, the films with the optimized composition had permittivities up to 180 (Fig. 16c) as measured in a capacitor structure ITO/$SrTiO_3$/Al. However, because the leakage of $SrTiO_3$ is largely governed by the Schottky emission, large leakage current densities were measured with this electrode configuration. Recent studies have indeed verified that the application of Pt electrodes significantly reduces the leakage current level [357]. On the other hand, as common to these materials, a decrease of permittivity with film thickness was observed: for a 50-nm $SrTiO_3$ a permittivity of only 100 was measured [356]. Clearly, high temperature annealings will be needed to increase the permittivity of the thinnest films. Likewise, solid solutions of $Ba_{1-x}Sr_xTiO_3$ are to be examined.

Though clearly beneficial in the case of thicker insulators (Section 6.2.1), the nanolaminate concept is quite problematic to apply in MOSFETs and DRAMs where the insulators are much thinner. Note, for example, that in Figure 14 the lowest leakage current was achieved with a configuration of $10 \times (13.5 + 5$ nm), for which the permittivity was 20. Thus, for an equivalent thickness of, e.g., 2 nm, a single layer pair would already be too thick. On the other hand, taking a thickness of 2.5 nm for each layer, the permittivity is 22 (Fig. 14), and thus a configuration of $2 \times (2.5 + 2.5$ nm) should give an equivalent thickness of 1.8 nm. However, in an attempt to make thin Ta_2O_5-ZrO_2 nanolaminates consisting of either 2.5- or 1.0-nm sublayers, it was observed that although permittivities of 22 (on Si) and 24 (on ITO) were achieved with 100-nm films, the per-

(a)

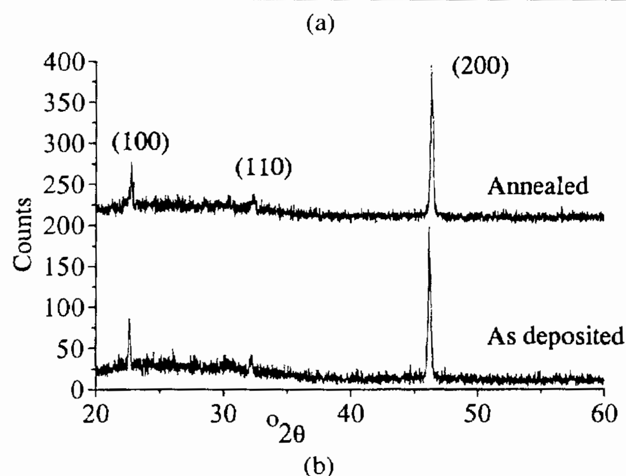

(b)

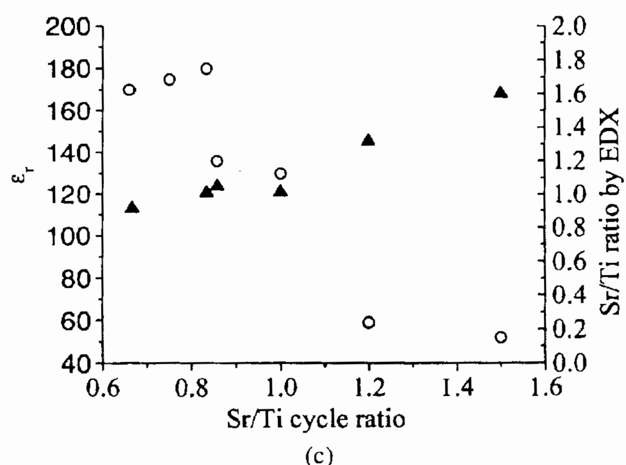

(c)

Fig. 16. (a) SEM image of a cross section of an ALD made $SrTiO_3$ film on a substrate with trenches. (b) X-ray diffraction patterns of a $SrTiO_3$ film as deposited at 325°C and after annealing in air at 500°C. (c) Sr/Ti ratio (▲) and permittivity (o), the latter being measured after the 500°C postdeposition annealing in air, as a function of the $Sr(C_5{}^iPr_3H_2)_2$-H_2O to $Ti(OCH(CH_3)_2)_4$-H_2O cycle ratio for $SrTiO_3$ thin films deposited at 325°C [356]. Reprinted with permission from M. Vehkamäki et al., Growth of $SrTiO_3$ and $BaTiO_3$ thin films by atomic layer deposition, *Electrochem. Solid-State Lett.* 2, 504 (1999), © 1999, The Electrochemical Society Inc.

mittivities decreased substantially when the films were made thinner, 7- to 10-nm thick [357]. The decrease was more severe on silicon ($\varepsilon = 12$ for 2.5 nm and $\varepsilon = 8$ for 1.0-nm sublayers) than on ITO ($\varepsilon = 15$ for 2.5 nm and $\varepsilon = 10$ for 1.0-nm sublayers), but as in both cases a decrease was observed, also other factors than the interfacial SiO_x layer must be involved. These films were in their as-deposited state, however, and hence a further decrease of the obtained equivalent thicknesses of about 3.5 nm may be expected after postannealing treatments. Similar permittivities of 12–14 have also been obtained in another study where thin (10–12 nm, including the underlying 2.8-nm Si_3N_4) Ta_2O_5-HfO_2, Ta_2O_5-ZrO_2, and ZrO_2-HfO_2 nanolaminates were examined, and the resulting equivalent thicknesses were accordingly from 3.0 to 3.3 nm [195].

Another concern in applying nanolaminates in microelectronic applications is charge trapping at the internal interfaces, especially when one of the components shows significant leakage like Ta_2O_5. Such a trapping may manifest itself as hysteresis in the C–V characteristics, for example. In any event, the possibility offered by ALD to straightforward preparation of accurately controlled multilayer insulator structures is clearly an opportunity worth further studies.

Ta_2O_5-HfO_2 nanolaminates have also been examined in integrated passive capacitors [422, 423]. A 48-nm thick film made up of 3-nm layers exhibited a permittivity of 23, so the capacitance density was 4 to 5 nF mm^{-2}. The breakdown strength was high, 6.5 MV cm^{-1}, but the defect density was relatively high because of particles from the $HfCl_4$ source.

In the integrated circuit metallization schemes the situation is the reverse of that in MOSFETs and DRAMs. The intermetal and interlevel SiO_2 insulators have shrunken so narrow and thin that capacitances between the adjacent conductors have become large enough to be the limiting factor for the overall speed of the circuit. In addition, crosstalk between the closely spaced conductor lines has become a concern. To minimize these problems, insulators with permittivity lower than that of SiO_2, such as fluorinated SiO_2 and polymers, are actively examined. Until now, no studies on the ALD of these materials have been reported, however.

6.3. Transparent Conductors

Transparent conducting oxides (TCO) are used in many large-area applications like flat panel displays, solar cells, windows, and antistatic coatings. A good ALD TCO process would be especially important in the TFEL display manufacturing where it could be combined with the preceding ALD process, namely, ion barrier deposition in the conventional structure (cf. Fig. 12) or insulator-phosphor-insulator process in the inverted structure. Nevertheless, though ALD processes have been developed and examined for many TCO films (Table VIII), none of them has so far replaced the well-established sputtered indium–tin oxide (In_2O_3 : Sn, ITO) in commercial TFEL displays.

In general, the properties of the ALD made TCO films (Table VIII) are rather similar to those obtained by other methods. The lowest resistivity (2.4×10^{-4} Ω cm) has been achieved

Table VIII. Electrical Properties of Transparent Conducting Oxide Thin Films Prepared by ALD[a]

Material	ρ (10^{-4} Ω cm)	μ ($cm^2 V^{-1} s^{-1}$)	n ($10^{19} cm^{-3}$)	Reference
In_2O_3	35	72	2.5	[115, 159]
$In_2O_3:Sn$	2.4	34	78	[159, 160]
SnO_2	1400	20	0.2	[173, 175]
	120			[271]
$SnO_2:Sb$	9	12	58	[175]
$SnO_2:F$	3.3			[271]
ZnO	45	33	4.3	[272, 284, 289, 292]
ZnO with UV irradiation	6.9	20	39	[52]
ZnO : Al	8.0	30	26	[272]
ZnO : Ga	8.0	40	20	[293]
ZnO : B	5.0	26	49	[289, 292]

[a] ρ is resistivity, μ is electron mobility, and n is electron concentration.

with ITO deposited from $InCl_3$, $SnCl_4$, and H_2O or H_2O_2. The ITO process suffers, however, from a relatively low deposition rate of 0.2–0.4 Å $cycle^{-1}$ so that the effective growth rate is at best only 2 nm min^{-1} [159]. Attempts to find indium precursors more reactive than $InCl_3$ have all failed so far [424]. Also the $SnCl_4$-$SbCl_5$-H_2O process used for depositing $SnO_2:Sb$ is rather slow (0.35 Å $cycle^{-1}$) [173]. By contrast, ZnO doped with boron, aluminum, or gallium can be deposited from the corresponding metal alkyls, diborane, and water with high rates from 0.5 to 2.8 Å $cycle^{-1}$, and effective growth rates up to 13 nm min^{-1} are achievable [424]. However, the resistivities are remarkably higher than in ITO (Table VIII), and thus a sheet resistance of 5 $\Omega \square^{-1}$ which is typically required in the TFEL displays could be achieved only with about 1600 nm thick ZnO : Al films as compared to the presently used 300- to 500-nm ITO films. An interesting observation on nondoped ZnO films was that their electron concentration could be increased 10-fold by UV irradiation during the growth, thereby resulting in a resistivity of 6.9×10^{-4} Ω cm [52].

As compared to the other ALD TCO processes, the zinc alkyl-based processes have a major benefit in that they may be run well below 200°C. This has been utilized in making front contacts to the temperature sensitive CdS/$CuInSe_2$ solar cell absorber structures: an efficiency of 14.3% was achieved using ZnO : Al made by ALD at 150°C [425]. ZnO : B, in turn, has been examined as a transparent conductor in amorphous-silicon (a-Si) solar cells. Because the ALD made ZnO : B films are only weakly textured, their light scattering properties are poor for the a-Si solar cells. Therefore, a bilayer structure combining a texture of a metal organic chemical vapor deposited (MOCVD) ZnO : B and the low resistivity and good stability of the ALD ZnO : B was developed resulting in an efficiency of 8.2% in a 1.0-cm^2 single p–i–n junction a-Si solar cell [292].

Though not an actual conductor, TiO_2 is often so oxygen deficient that its conductivity may reach 1 $(\Omega\, cm)^{-1}$. The utilization of this moderate conductivity and the good chemical stability of TiO_2 has been examined in a-Si solar cells in protecting ITO from a hydrogen plasma used for depositing the a-Si layer [426]. A 30-nm TiO_2 layer made by ALD from $TiCl_4$ and H_2O increased the cell efficiency from 4.9 to 6.6%. In addition to its protecting action, TiO_2 also served as an antireflection layer for the blue light.

6.4. Passivating and Protecting Layers

The pinhole-free and dense structure of the ALD made films make them interesting also for many passivating and protecting applications. The first one of these is the use of ALD Al_2O_3 as an ion barrier layer in the TFEL displays (Fig. 12). Usually, the sodium out-diffusion from soda lime glass prevents this inexpensive glass from being used as a substrate for the TFEL and other devices sensitive to sodium. It has been proved, however, that the ALD made Al_2O_3 films effectively prevent the sodium migration [427], thus facilitating the use of soda lime glass instead of the more expensive near-zero alkali glasses. ALD made Al_2O_3 is also used as a final passivation layer on top of the TFEL thin film stack (Fig. 12). The excellent conformality and the amorphous structure with no grain boundaries are clearly the key benefits of the ALD Al_2O_3 in blocking the migration of ions and moisture.

Yet another use where the protecting properties of the ALD Al_2O_3 have been examined in the TFEL displays is an etch stop for patterning the phosphor layers [428]. This was needed when a stacked dual substrate structure was examined for multicolor displays. In this structure, one substrate had the blue phosphor as a continuous layer while the other substrate incorporated the red and green phosphors, ZnS : Mn and ZnS : Tb, respectively, patterned to separate pixels. After depositing and patterning ZnS : Tb, that was covered by an Al_2O_3 etch stop layer and ZnS : Mn so that during the wet etching of the latter, the etch stop protected the ZnS : Tb layer. Remarkably, an as thin as 60-nm Al_2O_3 etch stop layer was effective for this purpose. However, because of the complexity of the stacked dual substrate TFEL structure, it was subsequently rejected as a commercial display.

A key aspect in corrosion protection is a prevention of material transportation across the metal-electrolyte interface. Therefore, the good barrier properties discussed earlier clearly point the potential of the ALD made films in corrosion protection. Preliminary studies have indicated that the metal surface has a crucial effect on the film density: dense films were obtained on stainless steel but ordinary steel was much more difficult to protect [429]. The best results were achieved with Ta_2O_5 which at the same time is amorphous and chemically stable. Al_2O_3 is also amorphous and thus free of grain boundaries, but being amphoteric it dissolves to strong acids and bases. TiO_2, in turn, is chemically stable but because it is polycrystalline, it contains grain boundaries along which ions can migrate, though slowly. Similar to the nanolaminate insulators (Section 6.2.1), better results were achieved also in this case by using Al_2O_3-TiO_2 multilayers where the grain boundaries extending through the

whole film were interrupted. Nevertheless, as erosion is usually strongly involved in corrosion, it is doubtful if it is economic to make ALD films thick enough. Rather, it may be envisioned that ALD films could be used as underlayers below thicker but less dense layers made by faster methods. In such a structure, the thicker overlayer would take the erosion load whereas the ALD made layer would give the chemical protection at the interface.

6.5. Transition Metal Nitride Diffusion Barriers

Transition metal nitride layers are used in the integrated circuits as barriers in preventing interdiffusion and reactions between metals and silicon or insulators. As the device dimensions have been aggressively scaled down, the cross sections of metal lines have decreased accordingly. Consequently, the importance to be able to fill the available space with metal as fully as possible has continuously increased. At the same time, the aspect ratios of trenches and vias have increased. These trends have led to such requirements for the future diffusion barriers that will clearly favor the use of ALD: the barriers should be thin, a few nanometers only, uniformly all around the deep trenches and vias, and still have dense and void-free structure to effectively prevent the detrimental interactions. Low resistivity is also required but the thinner the films can be made, the less stringent this requirement apparently becomes. Finally, as the future low permittivity intermetal insulators may be polymers with limited thermal stability, 400°C is often cited as the maximum deposition temperature.

A majority of the ALD transition metal nitride processes examined so far are based on the metal chloride–ammonia precursor combinations (Table IX). In general, these nitrides have acceptably low resistivities which are comparable to those reported for CVD nitrides. The highest quality films have been obtained using zinc as an additional reducing agent, but because of concerns related to zinc these processes hardly become accepted to the semiconductor applications. Nonetheless, also without zinc reasonable film properties have been obtained, tantalum nitride being an exception because without zinc the insulating Ta_3N_5 was obtained even when dimethyl hydrazine was used as the nitrogen source [114]. Excellent film conformality extending down to the sharp corners at the trench bottoms has been verified (Fig. 17), and trench filling as an ultimate conformality test has also been proved [88]. Preliminary barrier studies on TiN between Cu and Si were encouraging as well, the failure temperatures were around 650°C as judged on the basis of surface silicon content and etch pit tests [186]. Grain boundary diffusion was concluded to be the dominant mechanism for the barrier failure.

One concern of the metal chloride–ammonia processes, also shared by the only metal iodide (TiI_4)-ammonia process examined so far and the dimethyl hydrazine-based processes, is the low deposition rate which has typically been only about 0.2 Å $cycle^{-1}$, thereby implying low saturation coverage of the metal precursor. It still remains open whether this is due to a small number of reactive $-NH_x$ groups left on the surface after the ammonia pulse or the adsorption site blockage by a readsorbed reaction byproduct HCl. For instance, the stability

Table IX. Properties of ALD Made Transition Metal Nitrides

Material	Precursors	Growth temperature (°C)	Resistivity ($\mu\Omega$ cm)	Reference
TiN	$TiCl_4 + NH_3$	500	250	[111, 112, 185]
	$TiCl_4 + Zn + NH_3$	500	50	[111, 112]
		400	200	[111]
	$TiI_4 + NH_3$	500	70	[191]
		450	150	[191]
		400	380	[191]
	$TiCl_4 + (CH_3)_2NNH_2$	350	500	[114]
	$Ti(N(CH_3)_2)_4 + NH_3$	180	5000	[384]
$Ti_xSi_yN_z$	$Ti(N(CH_3)_2)_4 + SiH_4 + NH_3$	180	3×10^4	[384]
NbN	$NbCl_5 + NH_3$	500	200, 550	[103, 112, 185]
	$NbCl_5 + Zn + NH_3$	500	200	[103, 112]
	$NbCl_5 + (CH_3)_2NNH_2$	400	2900	[114]
TaN	$TaCl_5 + Zn + NH_3$	400–500	900	[113]
Ta_3N_5	$TaCl_5 + NH_3$	400–500	4.1×10^4, 5×10^5	[113, 185]
	$TaCl_5 + (CH_3)_2NNH_2$	400	NM[a]	[114]
MoN_x	$MoCl_5 + NH_3$	500	100, 260	[114, 185]
	$MoCl_5 + Zn + NH_3$	500	500	[114]
		400	3600	[114]
	$MoCl_5 + (CH_3)_2NNH_2$	400	930	[114]
W_2N	$WF_6 + NH_3$	330–530	4500	[207]

[a] Not measurable.

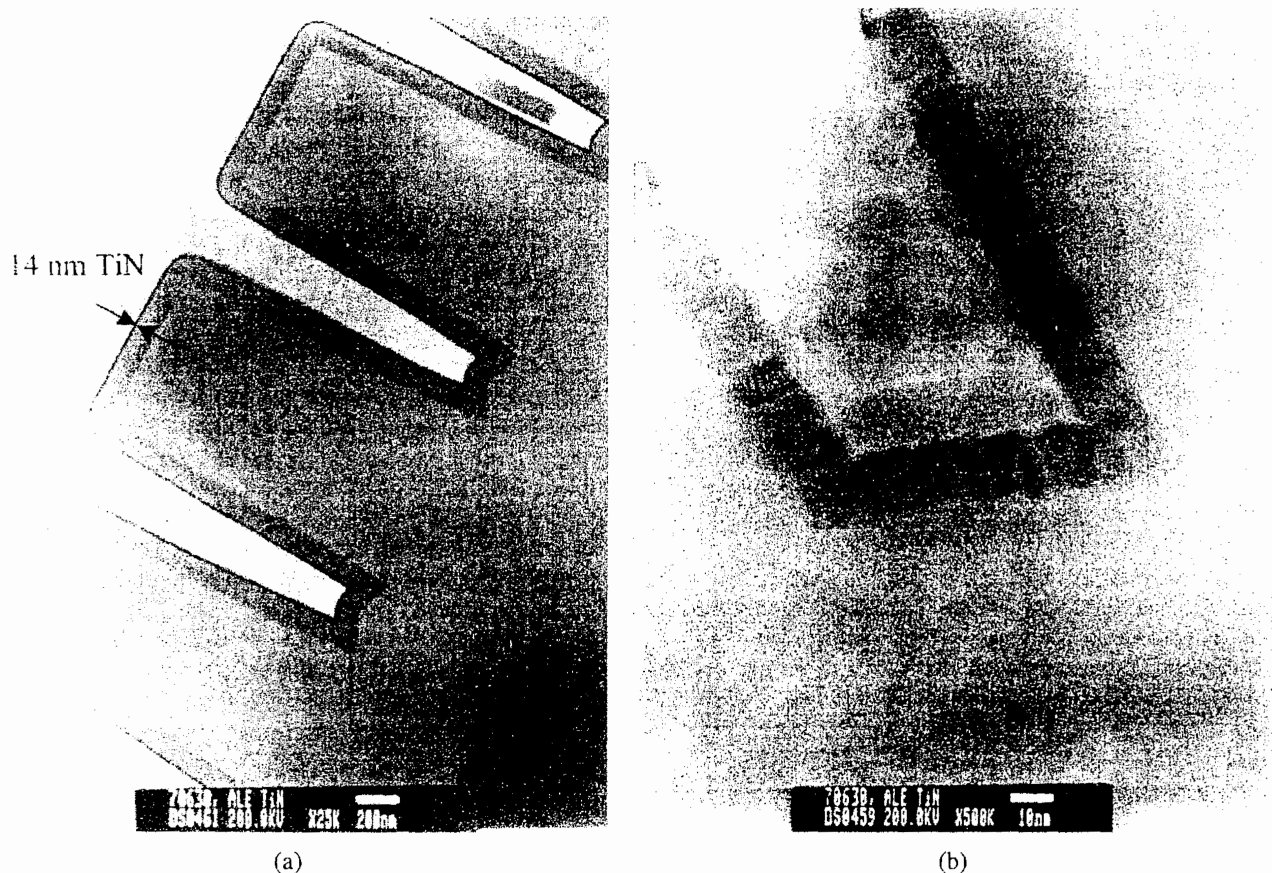

Fig. 17. (a) Cross-sectional TEM image of a 14-nm TiN film deposited on deep trenches. (b) Detail from the bottom of a trench.

of species formed on a TiN surface in an exposure to NH_3 is known to be low [430] at temperatures which are required to get the ALD nitride deposition reactions to proceed. The readsorption of HCl is also well possible because most of these processes have been examined in the traveling-wave reactors (Fig. 7) where the byproduct readsorption probability is especially high because these travel in front of the precursor pulse (cf. Fig. 9). Indeed, a related WF_6-NH_3 process examined at similar temperatures in a more open reaction chamber resulted in a remarkably higher deposition rate of 2.55 Å $cycle^{-1}$ [207]. In any event, still a direct comparison with one process examined in two different reactors is lacking. Other concerns include halide contamination and possible incompatibility problems with metal surfaces due to the reactions between metals and metal chlorides or HCl. The halide contents are strongly dependent on the deposition temperature increasing with decreasing temperature. At 500°C, they are typically well below 1 at.% but at 400°C a few at.% chlorine may be found which is just at the acceptance limit for the microelectronic applications. On the other hand, the iodine content in the TiN films deposited from TiI_4 was 2 at.% already at 350°C. Here, it must be noted that until now no postdeposition treatments have been applied to these films. On basis of the CVD literature, it may be expected that both contamination levels and resistivities could be decreased by, for example, N_2-H_2 plasma treatments.

Metal alkyl amides have been extensively examined as CVD precursors in an effort to decrease nitride deposition temperatures. In ALD, however, these compounds have been only scarcely examined. According to our experiences [431], $Ti(N(C_2H_5)_2)_4$ starts to decompose below temperatures which would be needed for effective reactions with ammonia, and thus films with unacceptably high resistivities were obtained. Nevertheless, in the $Ti(N(C_2H_5)(CH_3))_4$-NH_3 process a self-limiting growth was observed at 170–210°C by using high NH_3 doses with a flow rate of 250 sccm and 10 s or longer exposure times [386]. The deposition rate was high, 5 to 6 Å $cycle^{-1}$, more than twice the distance (2.45 Å) between the subsequent Ti layers in the [111] direction of TiN, thereby implying a complicated reaction mechanism. The films were amorphous and contained 4 at.% carbon and 6 at.% hydrogen but resistivities were not reported. A high deposition rate of 4.4 Å $cycle^{-1}$ was also reported for the $Ti(N(CH_3)_2)_4$-NH_3 process at 180°C [384, 385]. With the addition of silane, either as a separate pulse between $Ti(N(CH_3)_2)_4$ and NH_3 or simultaneously with ammonia, $Ti_xSi_yN_z$ films with up to 23 at.% Si were deposited with a rate which decreased with increasing silicon content from 2.4 Å $cycle^{-1}$ (18 at.% Si) to 1 Å $cycle^{-1}$ (23 at.% Si) [384, 385]. A 10-nm $Ti_{0.32}Si_{0.18}N_{0.50}$ film prevented a diffusion of copper in a barrier test where a metal-oxide-semiconductor (MOS) structure $Cu/Ti_{0.32}Si_{0.18}N_{0.50}/SiO_2/Si$

was annealed at 800°C for 60 min in H_2(10%)-Ar(90%) [385]. These films showed excellent conformality but they suffered from high resistivities of 5000 $\mu\Omega$ cm (TiN) and 30,000 $\mu\Omega$ cm ($Ti_{0.32}Si_{0.18}N_{0.50}$) [384]. Also here the effects of postdeposition treatments remain to be examined.

6.6. Metals

Effective ALD metal processes could find use in many applications. A copper ALD process would offer an interesting alternative for the integrated circuit metallizations. Even if the entire copper layer was not made by ALD, a uniform seed layer for electrochemical copper deposition would already be of interest, especially if directly combined to a diffusion barrier ALD nitride process (see the previous section). Similar to the barriers, also here excellent conformality in high aspect ratio structures is required. On the other hand, some metals like Ta and Ti are considered as potential barriers for copper. For the TFEL displays, a metal ALD process might be interesting because it could be combined with the preceding ALD process step, i.e., deposition of the insulator-phosphor-insulator multilayer in the conventional device (Fig. 12) or the ion barrier in the inverted structure.

ALD of metals is, however, a chemically challenging task with only limited success so far. An effective reducing agent must be found and the metal precursor must be chosen so that it does not etch the metal film by forming volatile lower oxidation state compounds, and while being easily reduced, the metal precursor must be stable against decomposition and disproportionation. Yet another question is the mechanism by means of which the metal precursor can adsorb on the film surface, especially if the surface is free of functional groups.

The WF_6-Si_2H_6 process [206] addresses the previous issues elegantly as the growth involves exchange reactions during both the WF_6 and Si_2H_6 exposures (Section 7.2.2). Tungsten films were deposited at 150–330°C with a high rate per cycle, about 2.5 Å cycle^{-1}, but the cycle time was not specified. No silicon or fluorine could be detected in the films with X-ray photoelectron spectroscopy (XPS). The films were nearly amorphous and thus had smooth surfaces and a relatively high resistivity of 120 $\mu\Omega$ cm.

Cu films have been deposited by ALD using hydrogen as a reducing agent both for CuCl [209, 210] and for $Cu(thd)_2$ [210, 343, 344]. However, both processes seem to be quite specific about the substrate material which suggests that the substrate actively participates or catalyzes the film growth reactions, especially at the beginning of the growth. The CuCl-H_2 process was studied only on tantalum substrates which reduced CuCl causing an initial film thickness of about 30 nm. The $Cu(thd)_2$-H_2 process was examined on many surfaces (Pt/Pd seeded glass, bare glass, Ta, Fe, TiN, Ni, $In_2O_3:Sn$) but film deposition occurred only on the glass surface seeded with a few angstroms thick layer of sputtered Pt/Pd alloy. A self-limiting growth with a rate of 0.3 Å cycle^{-1} was observed within a temperature range of 190–260°C. The catalytic effect of the Pt/Pd seed was explained in terms of a more complete dissociative adsorption of $Cu(thd)_2$ on an oxide-free metal surface as compared with hydroxyl terminated oxide and oxidized metal surfaces where one of the thd ligands remains bound with the adsorbing Cu atom and blocks further reactions. However, even more probably the Pt/Pd seed assists in dissociating the otherwise quite inert molecular hydrogen into reactive hydrogen atoms. In any event, even with the seed layer the process did not result in a film growth in another kind of ALD reactor with lower hydrogen partial pressure and shorter residence times [186].

The Cu films deposited from CuCl and H_2 around 400°C consisted of large grains, typically 1–4 μm in a lateral diameter, some even 10 μm, and showed good adhesion to the tantalum substrate [209]. They contained only 0.5–1.0 at.% chlorine as determined by XPS. No resistivity was reported, however. With $Cu(thd)_2$, a smaller grain size of 0.1 to 0.3 μm was obtained, possibly because of lower deposition temperatures below 350°C [343, 344]. No carbon could be detected with XPS in the highest purity films which had been cooled under hydrogen atmosphere but, interestingly, those cooled under nitrogen contained about 12 at.% carbon. Oxygen concentration was low in all the films, and below 3 at.% hydrogen was detected with nuclear reaction analysis. A resistivity of 8 $\mu\Omega$ cm was measured for a 60-nm film but this high value was attributed to the small thickness. Indeed, lower resistivities down to 3.5 $\mu\Omega$ cm were obtained later with 80- to 120-nm thick films [210].

As already noted in Sections 5.1.5 and 5.3.6, the CuCl-Zn [110] and $MoCl_5$-Zn [204] processes suffered from a reversible dissolution-outdiffusion of zinc into the Cu and Mo films. Further complications to the latter process arose from an etching of the Mo film by $MoCl_5$ through a formation of lower molybdenum chlorides $MoCl_{5-x}$. As a consequence, self-limiting growth conditions were hard to achieve and reproducibility was quite poor. Especially Cu was deposited with a high rate of above 5 Å cycle^{-1} (500°C). The Cu films consisted of large grains which stayed isolated so long that after a formation of a continuous film the sheet resistance was too low for a reliable measurement. About 3 at.% zinc was left in the films while no chlorine could be detected with energy dispersive X-ray spectroscopy (EDX). When Mo films were deposited at 420°C, the growth rate and the zinc residual content decreased from 0.8 to 0.4 Å cycle^{-1} and 2.5 to 0.5 at.%, respectively, with increasing purge time after the zinc pulse. Above 460°C the film growth practically stopped, obviously because of the etching reactions. The lowest resistivites of about 15 $\mu\Omega$ cm were obtained with the films with the lowest zinc contents.

Metallic Ta and Ti films with a conformality approaching 100% have been deposited at 25–400°C using a plasma enhanced ALD process where $TaCl_5$ and $TiCl_4$ were reduced by atomic hydrogen generated upstream with an inductively coupled RF plasma discharge [74]. Ta was deposited with a rate varying from 0.16 Å cycle^{-1} at 25°C to 1.67 Å cycle^{-1} at 250–400°C, and Ti was deposited with a rate of 1.5 to 1.7 Å cycle^{-1}. Because of oxidation during air exposure after the film growth, no meaningful analysis of the Ti films could be done and the Ta

films also appeared to be strongly oxidized since the measured oxygen levels were high, from a few percent up to 26 at.%. On the other hand, chlorine residues were below 3 at.%. At deposition temperatures of 250°C and below, no crystallinity could be observed in the Ta films up to thicknesses of about 40 nm, but at higher temperatures crystalline Ta was obtained. These preliminary results on obtaining metallic films of the highly electropositive elements of titanium and tantalum are strongly encouraging and motivate further studies on atomic hydrogen-based ALD metal processes.

Another approach toward utilization of the advantages of ALD in depositing metal films involves a two step process where an oxide film is first made by ALD and then reduced by hydrogen. As a first example of this approach, a 135-nm NiO film deposited from $Ni(acac)_2$ and ozone at 250°C was converted to a metallic, well-adherent nickel at 260°C in a 5% H_2–95% Ar atmosphere (1 atm) [342]. Though in this case the reduction caused pinholes to the originally dense films, this approach is evidently worth further examination, perhaps with thinner films or by dividing the process into several deposition-reduction steps.

6.7. Solar Cell Absorbers

Studies on ALD deposition of thin film solar cell absorbers have been quite scarce but some promising results have been obtained. An efficiency of 14.0% was achieved using a CdS/CdTe heterojunction made by ALD from elemental sources in a flow-type reactor [432–434] but because of the general concerns related to CdTe solar cells; i.e., the stability of the contacts and the environmental issues, the interest to this ALD application has subsequently turned down.

For $CuInSe_2$-based solar cells, ALD has been examined in depositing not only the transparent front contacts (Section 6.3) but also the buffer layers between $CuInSe_2$ and TCO. As a standard, chemical bath deposited CdS is used as this buffer but for environmental reasons cadmium-free substitutes are actively looked for. With ALD made nondoped ZnO, efficiencies of 11.4–13.2% have been obtained using $Cu(In,Ga)Se_2$ as an absorber [285, 286, 288] while In_2S_3 gave an even higher efficiency of 13.5% [288]. Importantly, both processes were carried out at 160–165°C. A 10-nm ZnSe buffer layer deposited on $Cu(In,Ga)Se_2$ from elemental sources at 250°C by an MBE system operated in an ALD mode resulted in an efficency of 11.6% [119].

Also epitaxial solar cell absorbers have been made by ALD. With an $Al_{1-x}Ga_xAs$/GaAs tandem solar cell structure, an open circuit voltage of 1.945 V and a fill factor of 0.812 were achieved under 10 suns-AM 1.5 conditions [236].

6.8. Optical Coatings

The accurate film thickness control and good uniformity over large-area substrates offered by ALD are valuable characteristics also in making multilayer structures for optics. Due to the wide variety of dielectric materials made by ALD, refractive indexes from 1.43 to 2.6 are available [435]. In addition, a suitable mixing of pulsing sequences of binaries with different refractive indexes should make it rather straightforward to create films with graded refractive index profiles. On the other hand, the slowness of the method is a limiting factor especially when thick structures with tens of layers are needed for sophisticated visible range components.

Optical multilayers have been made by ALD for both visible [435] and soft X-ray [184, 239] wavelength ranges. The visible range components consisted of polycrystalline ZnS ($ZnCl_2$-H_2S) and amorphous Al_2O_3 ($AlCl_3$-H_2O) layers with thicknesses of 62 and 86 nm, respectively. Various structures ranging from simple two- or three-layer antireflection coatings and neutral beam splitters to 19-layer Fabry–Perot filters were made. They all accurately reproduced the spectral responses calculated for the designed multilayer structures, thus evidencing that both the thicknesses and optical properties of the films were well controlled.

In the soft X-ray range, the layers are only a few nanometers thick, thus setting rigorous requirements to the film thickness accuracy and interface smoothness, but at the same time making the deposition rate of less concern as compared to the visible range components. In good agreement with the model calculations, a high reflectance of over 30% at a wavelength of 2.734 nm and an incidence angle of 71.8°C from the surface normal was achieved with an ALD made multilayer consisting of 20 pairs of amorphous Al_2O_3 ($Al(CH_3)_3$-H_2O_2) and TiO_2 ($TiCl_4$-H_2O_2) layers which had a layer-pair thickness of 4.43 nm [184]. Soft X-ray multilayer mirrors have also been made by depositing AlP ($Al(CH_3)_2H$-PH_3) and GaP ($Ga(CH_3)_3$-PH_3) layers on a GaP substrate with a rate of an exact one monolayer per cycle. A structure with 50 bilayers of $(AlP)_{22ML}(GaP)_{13ML}$ gave a maximum reflectance in excess of 10% at a wavelength of about 17 nm and an incidence angle of 35° from the surface normal [239].

7. CHARACTERIZATION OF ALD PROCESSES

ALD processes may be examined by many different ways as summarized in Table X. Among these, the film growth experiments are the most common as they focus on the final goal, i.e., the films themselves, but they give only a limited chemical information. Therefore, other methods are required to get a better understanding of the chemistry involved.

As discussed in Section 4, the most important ALD reactors are the flow-type ones operating at pressures above 1 Torr. In addition, the reaction chambers are often of a traveling-wave design with tightly packed substrates (Figs. 7 and 8). Only a few *in situ* characterization methods may be added to these kinds of reactors, and therefore many alternative approaches have been taken for examining the chemistry relevant to ALD (Table X). A general trend is, however, that the more detailed chemical information the method gives, the farther are the experimental conditions from the flow-type reactors, thus arising an issue of the representativeness of the results for the actual

Table X. Summary of Methods Used to Characterize ALD Processes

Method	Advantages	Limitations
Film growth experiments	Focus on the overall goal, the optimization of the film growth process	Limited chemical information, interpretation requires additional data
In situ measurements under real growth conditions:	Relevancy to the actual film growth processes	Difficulties in sampling
• Microgravimetry	Direct measurement of (relative) surface mass changes	Interpretation requires certain assumptions of the surface species
• Mass spectrometry	Identification of volatile byproducts at various stages of an ALD cycle	Cracking and reactions during ionization complicate the interpretation
• Optical methods	Sensitive observation of changes in surface termination	Chemical interpretation is difficult
Measurements after an inert transfer from the growth conditions to the analysis chamber	A large number of surface analytical techniques applicable ensures thorough characterization	Possible changes during the sample transfer
Reactions under high-vacuum conditions	A large number of surface analytical techniques applicable ensures thorough characterization	Representativity is questionable because of differences in pressures (pressure gap) and reaction times
Reactions on high surface area substrates	The large amount of products makes it possible to use routine chemical techniques, like IR, NMR, and elemental analysis	Representativity is questionable because of very long reaction times Possible changes during the sample transfer

growth processes. The most important differences lie usually in reaction times and operation pressures. Therefore, to attain the most comprehensive understanding of the chemistry in the flow-type ALD reactors, one should combine detailed surface chemistry studies under specifically optimized conditions and *in situ* studies under the real growth conditions—or conditions as close to them as possible. The latter either verify that the reaction mechanisms observed in the surface chemistry studies also prevail under the actual growth conditions or, if not, point out the differences.

In this section, the most common approaches for characterizing the ALD processes are introduced and discussed. The main emphasis is put on the methods which lead to a thorough understanding of the chemistry in the flow-type reactors.

7.1. Film Growth Experiments

The aim of the film growth experiments is of course to find the best conditions for growing high quality films. These studies involve the examination of the effects of the experimental parameters (precursor fluxes (vapor pressures), growth temperatures, pulse and purge times) on the growth rate and film properties, like composition, structure, and uniformity. In addition to revealing the best growth conditions, the observed interdependencies provide a great deal of information about the growth reactions as discussed in this section.

7.1.1. Examination of Growth Rate

ALD growth rate is usually expressed in terms of thickness increment per cycle, e.g., nanometers per cycle or angstroms per cycle. Normally, the growth rate is determined after the film growth by dividing the measured film thickness by the number of deposition cycles applied, but sometimes optical *in situ* measurements are used for real time growth rate measurements (see Section 7.2.1).

7.1.1.1. Pulse Times

The effects of pulse times are usually examined by keeping the other parameters constant and by varying the exposure time of one precursor at the time. As the pulse time is increased, the density of the chemisorbed species on the surface increases toward the saturation level. The fulfilling of the chemisorption sites is basically governed by three factors:

- the number of precursor molecules arriving on the substrate, being determined by the precursor flux and the exposure time,
- the rate of the chemisorption reactions, whether true chemisorption or exchange reactions,
- the rate of further reactions on the surface which reopen chemisorption sites that may have become temporarily blocked by the nearby chemisorbed species, e.g., bulky ligands of a chemisorbed precursor molecule may impose steric hindrances until reordered or desorbed.

If the pulse time is so short that not enough precursor molecules are transported to the reaction chamber, severe thickness nonuniformities result. Especially in the traveling-wave reactors (Section 4.2.4) the precursor is consumed at the substrate area closest to the inlet while the areas further away receive only few molecules, if any. Therefore, a certain delay period

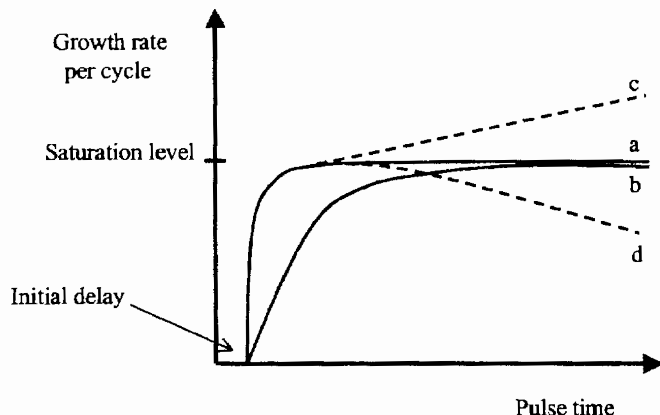

Fig. 18. Different growth rate vs pulse time curves observable in ALD processes: (a) fast and (b) slow chemisorption reactions with no decomposition or etching, (c) chemisorption reactions followed by precursor decomposition, and (d) chemisorption reactions followed by etching reactions. The initial delay period is due to the limited rate of precursor transportation and its length is dependent on the measurement position in the reactor.

is observed in the growth rate vs exposure time curve (Fig. 18). The length of this delay depends on the distance of the measurement point from the reactant inlet and on the precursor flux (see what follows). With increasing pulse time, the whole substrate becomes covered and different kinds of growth rate vs pulse time curves are observed depending on the chemistry (Fig. 18). As the self-limiting film growth mechanism is the characteristic feature of ALD, the growth rate is expected to saturate with long enough exposure times. Ideally, the reactions are fast and thus the saturation level is rapidly achieved (curve a in Fig. 18) but sometimes; e.g., at lower temperatures or with less reactive precursors, the reactions proceed slower (curve b in Fig. 18).

If the precursor is decomposing thermally, the growth rate does not saturate but increases quite linearly with increasing pulse time (Fig. 18, curve c). If the decomposition rate is only modest, the growth rate increases first more rapidly corresponding to the desired surface reactions, and only after that the decomposition dominated region with a smaller slope begins. Naturally, the higher the temperature, the faster the decomposition, and thus the steeper the slope in the decomposition region.

Occasionally, it is observed that the growth rate first increases but then starts to decrease as the pulse time is increased further (Fig. 18, curve d). This may be taken as an indication of an etching reaction which begins after the growth reactions have been completed; i.e., at first the incoming metal precursor reacts with the surface species (e.g., —OH groups) left from the previous pulse, but when they are consumed, the precursor starts to react with the film material itself.

Curve b in Figure 18 also points out why it may often be more effective not to strive for the fully saturated growth rate but instead to satisfy with 90% or so of it. Reaching the last 10% may require significant elongation of the pulse time and thereby decrease the productivity, i.e., deposition rate per time unit. In fact, in the most cases the highest productivities are achieved with the shortest exposure times, the minimum being set by the time required to get the whole substrate covered. Quite often also film properties, such as uniformity, conformality, and purity are acceptable even if the growth rate is not fully saturated, and thus the slightly undersaturated growth conditions may be chosen to maximize the productivity.

7.1.1.2. Precursor Fluxes

The precursor fluxes are usually controlled by either the source temperatures (solids and liquids) or the mass flow controllers (gases). As the first approximation, the precursor flux may be assumed to have a similar effect as the pulse time because the precursor dose is a product of the two. Thus, with insufficiently small fluxes thickness nonuniformities result, and with increasing flux the growth rate behaves quite similarly as with increasing pulse time (Fig. 18). Therefore, a need for long exposure times, causing long cycle times and thereby slow deposition rates, may be circumvented, at least to some extent (see below), by increasing the precursor flux.

However, the relation between exposure time and precursor flux is not that trivial that only their product would determine the growth rate. There are many examples that the growth rate per cycle may be increased only by increasing the exposure time, but not by increasing the precursor flux [19, 269, 270, 307]. This has been attributed to the slowness of the surface reactions which lead to the reopening of the temporarily blocked chemisorption sites. On the other hand, studies on ALD of oxide films showed that the growth rate could be increased by increasing the water flux more than by increasing the water exposure time, though in both cases a saturation was observed [224]. This was explained by an increased surface hydroxylation under high water flux: because of the increased surface hydroxyl group density, more reactive sites were available for the subsequently pulsed metal precursor. Though one might expect that with increased densities the hydroxyl groups could become unstable against dehydroxylation and thereby make the growth dependent on the purge time following the water pulse, this was not observed. Apparently, if dehydroxylation occurred, it was fast enough to reach saturation in less than 0.2 s.

7.1.1.3. Purge Length

Insufficient purging causes overlapping of the precursor pulses and thereby CVD-like growth which manifests itself as increased growth rate and thickness nonuniformity. With increasing purge time, the overlapping is reduced and the growth rate decreases and finally saturates to the constant level. However, if desorption of the chemisorbed precursor molecules occurs, the growth rate continues to decrease even if the pulses are well separated.

In practice, surface species are usually stable and no desorption related behavior can be observed at temperatures used. This is especially true when the chemisorption involves exchange reactions between the incoming precursor and the surface species (Fig. 1a) because by nature these reactions are irreversible as

part of the precursor molecule ligands are immediately released and purged away. On the other hand, desorption may occur if the precursor is molecularly or dissociatively chemisorbed (Fig. 1b), or if the surface species formed in the exchange reactions can combine with each other. In ALD of oxides, for example, hydroxyl groups are produced on the surface in the exchange reactions between the chemisorbed metal compounds and water, and also dissociative adsorption of water may add them. Subsequently, the hydroxyl groups may combine with each other and thereby dehydroxylate the surface, and if this occurs reasonably slowly, it may cause a decrease of the growth rate with increasing purge time after the water pulse [83]. Yet another possibility for desorption at high temperatures is that the film constituents themselves have reasonable equilibrium pressures.

In general, the purge times required to separate the precursor pulses are very much reactor dependent but do not depend that much on the precursors, water with a highly polar molecule perhaps being an exception. Thus, once appropriate purge times are determined for a given reactor with one process, they are usually applicable to also other processes in the same reactor. As discussed in Section 4, the minimization of purge times is one of the key aspects in a design of a productive ALD reactor.

7.1.1.4. Temperature

Different kinds of growth rate vs temperature dependencies which may be observed in ALD processes are schematically depicted in Figure 19. The key temperature range is the one in the middle where the growth proceeds in the self-limiting manner. Depending on if the surface density of the chemisorbed species is temperature dependent or not, the growth rate is also temperature dependent or constant. In the former case, the growth rate usually decreases with increasing temperature because of a decreased density of reactive surface species, a typical example being the dehydroxylation of oxide surfaces (e.g., [436]). In any event, the temperature dependency is usually so weak that small variations in the growth temperature have only minor effects. Temperature-independent growth rates are often observed in the growth of II–VI compounds, for example, [38].

In the low temperature side of the self-limiting region, the growth rate may either decrease or increase with decreasing temperature (Fig. 19). The decrease appears to be much more often observed and may be related to kinetic reasons; i.e., the growth reactions become so slow that they are not completed within the given pulse time. In principle, they might be completed if the pulse times were increased but that would increase the cycle time substantially. The increase of the growth rate with decreasing temperature may occur due to a multilayer adsorption and the condensation of low vapor pressure precursors.

Also at the high temperature side of the self-limiting region the growth rate may either decrease or increase (Fig. 19). The decrease of the growth rate with increasing temperature is related to a desorption of the precursors while the increase is due to a decomposition.

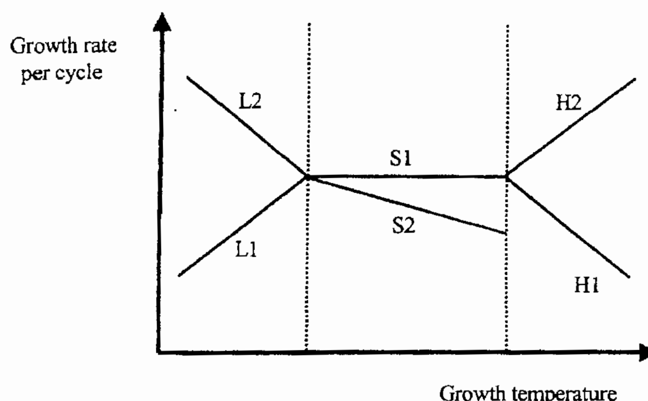

Fig. 19. Various growth rate vs temperature curves observable in ALD processes:
S1: self-limiting growth with temperature-independent rate,
S2: self-limiting growth with temperature-dependent rate,
L1: self-limitation not reached because of slow reactions,
L2: self-limiting growth rate exceeded because of multilayer adsorption or condensation,
H1: self-limitation not maintained because of precursor desorption,
H2: self-limiting growth rate exceeded because of precursor decomposition.

7.1.2. Examination of Film Properties

7.1.2.1. Film Composition

Film compositions, especially impurities, give indications of incomplete reactions or precursor decomposition. At low temperatures, the growth reactions are often somewhat incomplete and thus constituent elements of the precursor molecules may be found as impurities in the films. With increasing temperature, the reactions become more complete and thus the impurity contents decrease (Fig. 20a). This is also reflected in other film properties, like refractive index and dielectric permittivity of insulators (Fig. 20b), or conductivity in the case of conducting materials. On the other hand, if the temperature is increased too much, precursor decomposition may begin and cause an increase of the impurity contents.

7.1.2.2. Uniformity and Conformality

In the ideal ALD process, both uniformity and conformality are excellent. However, as noted earlier, the real processes may differ from the ideal one in two ways: the growth reactions are not entirely saturated or some precursor decomposition occurs in addition to the exchange reactions. The extent to which these nonidealities may be accepted is largely determined by how they affect the uniformity and conformality; i.e., if these two properties are not deteriorated, the reactions responsible for the nonideal behavior may be concluded to proceed in a surface reaction limited manner. For the incomplete saturation, this means that the increase of the surface density of the chemisorbed precursor molecules toward the saturation value is restricted by the rate of surface reactions, i.e., either the chemisorption reaction itself or the further reactions which reopen the momentarily blocked adsorption sites. For the decom-

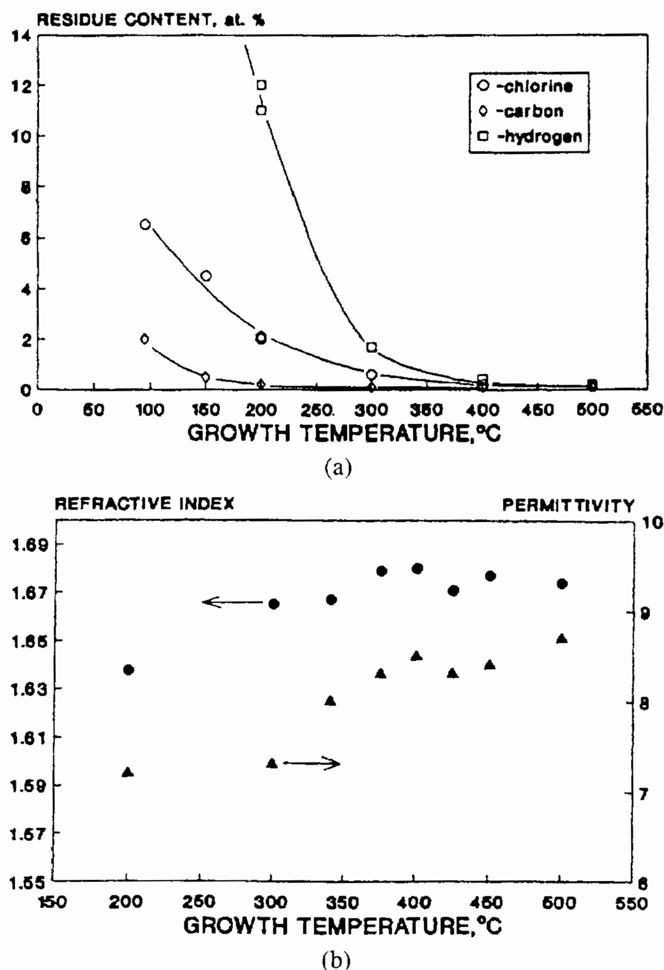

Fig. 20. The effect of growth temperature on (a) impurity contents and (b) refractive index and permittivity of Al_2O_3 films deposited from $Al(CH_3)_2Cl$ and water [237]. Reprinted with permission from K. Kukli et al., Atomic layer epitaxy growth of aluminium oxide thin films from a novel $Al(CH_3)_2Cl$ precursor and H_2O, *J. Vac. Sci. Technol. A* 15, 2214 (1997), © 1997, American Vacuum Society.

position, surface control means that the decomposition reaction rate is slow in comparison to the rate at which new precursors are adsorbed on the sites which are opened in the place of the decomposed molecules.

Thickness nonuniformity and nonconformality may also result because of insufficient purging. In deep and narrow trenches and holes, material transportation and thus also purging is slower than on planar surfaces and therefore purge periods that are too short should first be observed as reduced conformality. In practice, however, 0.5-s purging periods have already resulted in excellent conformality and complete filling of trenches with dimensions comparable to microelectronic devices [88].

Yet another potential reason for thickness nonuniformity is readsorption of reaction byproducts (cf. Section 4.2.4). If this happens, the largest disturbance in the thickness uniformity occurs at the areas closest to the merging point of the precursor flow channels because there the amount of the reaction byproducts varies the most. The surface at the point where the film growth begins receives only the precursor molecules, so the chemisorption density is the highest there. At the same time, this surface and any surface downstream produce the reaction byproducts, the concentration of which thereby increases in the carrier gas until a steady state is reached. As a consequence, the film thickness decreases over the range where this concentration develops [96, 97].

7.1.2.3. *Crystallinity and Morphology*

Film crystallinity is not related that much to the growth reactions but rather reflects the mobility of the film material and is thus strongly affected by the growth temperature—not to forget the possible crystallization promoting effect of the substrate, however. In general, the temperature limit between amorphous and crystalline deposits and the overall crystallinity are in the first place material dependent, and not largely affected by the precursors. There are some exceptions, however. For example, the crystallinity of TiO_2 films appears to be better when deposited from titanium alkoxides than when deposited from $TiCl_4$. This has been explained by an ordering effect of bridging alkoxide groups on the surface of the growing film [304, 307]. In contrast, Ta_2O_5 films obtained from $Ta(OC_2H_5)_5$ at around 300°C are completely amorphous [312] whereas the films obtained from $TaCl_5$ show some crystallinity [106, 200] which is ascribable to the rather exceptional formation of tantalum oxychlorides which, on the one hand, appear to favor crystallization by increasing mobility but, on the other hand, being volatile lead to etching of Ta_2O_5 above 300°C [104–106].

The formation of a polycrystalline film is accompanied by surface roughening which increases with increasing film thickness [82–87]. In this respect, the polycrystalline deposits made by ALD differ from the amorphous and epitaxial films which usually preserve rather well the morphology of the substrate surface. In any case, even if within the dimensions of the crystallites the film does not grow uniformly, in larger scale, like that of microelectronic device structures (Figs. 2 and 16) or on macroscopic level, the uniformity is still excellent.

Ex situ AFM studies on polycrystalline films have revealed that during the early stages of the growth agglomerates are formed on the surface (Fig. 21). As more ALD cycles are applied, the agglomerates grow both laterally and vertically, and once they grow into contact with each other, a continuous film is formed but with a roughened surface as compared with the substrate surface (Fig. 21). The roughness of a film with a given thickness is largely determined by the areal density of the agglomerates formed in the beginning of the growth.

Basically, agglomeration might be explained either as a process by means of which the system tries to minimize the substrate-film interface energy, or as a consequence of a limited number of reactive sites on the starting surface. However, though it has indeed been suggested that roughening would be an inherent consequence of a less than a monolayer per cycle growth, the growth rate is hardly the determining factor because rough films are obtained also with a full monolayer per

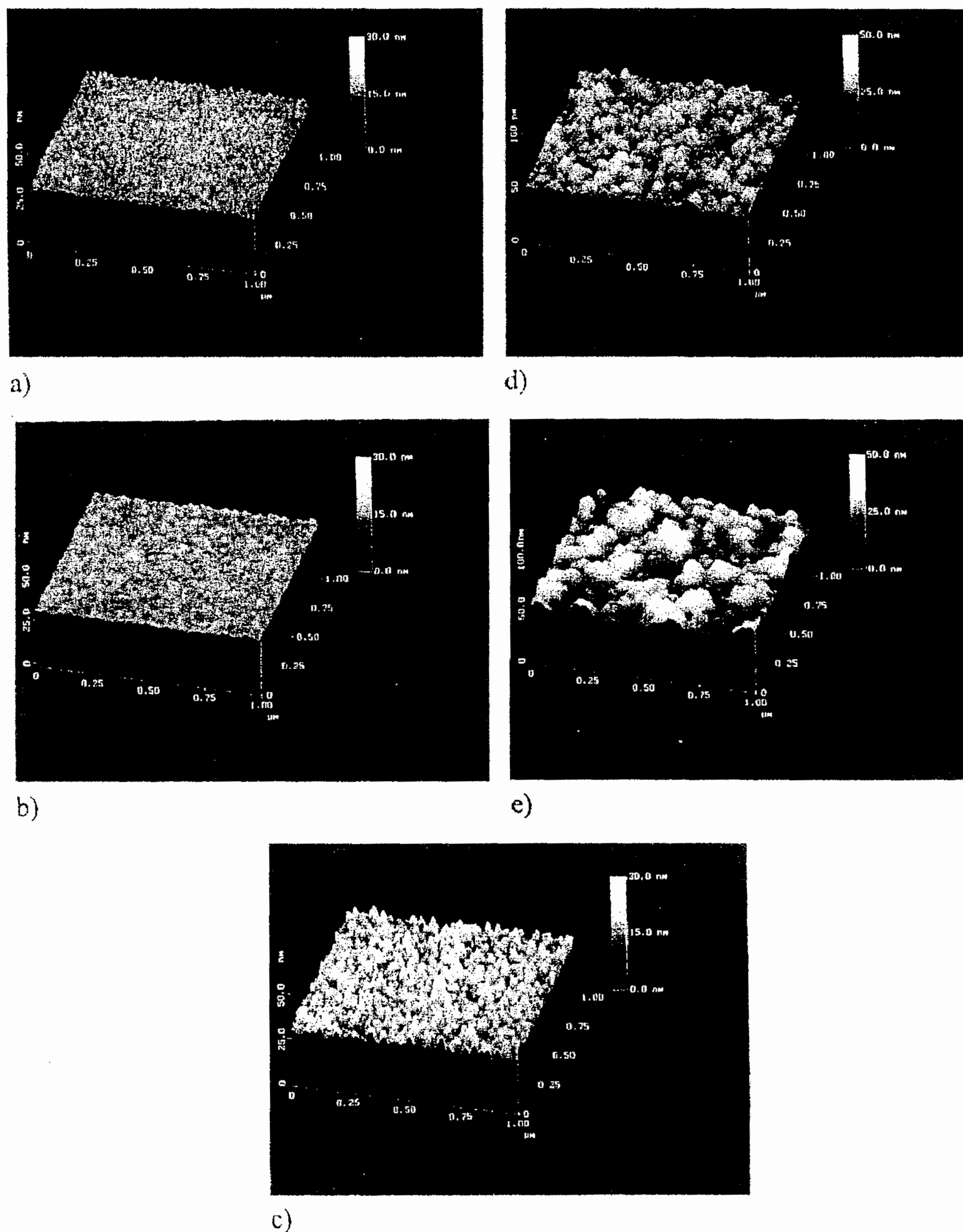

Fig. 21. Development of surface roughness of ZnS films grown on glass from $ZnCl_2$ and H_2S at 500°C with (a) 8, (b) 50, (c) 200, (d) 800, and (e) 3000 deposition cycles [85]. Reprinted with permission from J. Ihanus et al., AFM studies on ZnS thin films grown by atomic layer epitaxy, *Appl. Surf. Sci.* 120, 43 (1997), © 1997, Elsevier Science.

cycle growth rates [52, 284] and smooth films with lower rates [132]. Therefore, the interface energy minimization appears to be a more valid explanation. Evidently, in the case of epitaxial films, the driving force for the agglomeration is much lower because of the well-matched crystal structures of the film and the substrate.

Since polycrystalline structure and roughening are nearly always observed together, a connection between them appears evident. Crystallization and the interface energy driven agglomeration are both thermodynamically favored processes which, however, require sufficient mobility to occur. At low temperatures, the mobility is low, and amorphous and smooth films are obtained, but as the temperature is increased, the mobility increases and agglomeration and crystallization occur. Most probably, the agglomerates are preferably formed at certain special surface sites which on one substrate may be more numerous

than on the other. For example, on mica the initial ZnS agglomerate density was much lower than on glass [85].

The final and apparently the hardest question is the atomic mechanism which at the same time can explain the agglomeration and maintain the self-limitation of the film growth. By now, the identity of the migrating species can mainly be just speculated about. The simplest possibility is that the agglomerates are formed as a consequence of a migration and the nucleation of the film material itself. Once an ALD cycle has been completed and a layer or a sublayer of the film material has been deposited, the material may be mobile enough to nucleate, i.e., to form agglomerates with a crystalline structure. To estimate if this is possible, one can try to look for a similar film-substrate combination made by reactive evaporation at the same substrate temperature: if a deposit formed in such a process has sufficient mobility for crystallization and agglomeration, the ALD made material should have that too. In other words, there should not be any reason why the nucleation would be restricted in ALD.

Another mechanistic explanation for the agglomeration is that one or several of the species formed as intermediates in the ALD reactions are able to migrate on the surface or in the gas phase. Such species are hard to identify, but in the $TiCl_4$-H_2O process, for example, $Ti(OH)_xCl_y$ and $TiOCl_2$ have been suggested [27, 28, 82]. Importantly, the possible formation of such species does not hurt the self-limitation of the film growth, since that would occur through reactions which passivate the reaction or chemisorption sites against further interaction with $TiCl_4$, for example:

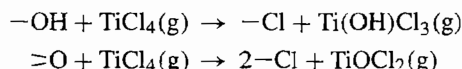

$$-OH + TiCl_4(g) \rightarrow -Cl + Ti(OH)Cl_3(g)$$
$$=O + TiCl_4(g) \rightarrow 2{-}Cl + TiOCl_2(g)$$

7.2. Reaction Mechanism Studies

ALD reaction mechanisms may be investigated by analyzing either the surface or the gas phase, preferably both. The ultimate goal is to specify the species existing on the surface at each phase of an ALD cycle and to identify the volatile byproducts and the time of their release. From this information, the prevailing reaction mechanism can be determined. Obviously, the most definite conclusions would be obtained via a detailed chemical characterization of the surface but such studies are often hard to realize and, instead, less direct methods need to be applied. For example, the two alternative reaction mechanisms suggested in Figure 1 for the deposition of TiO_2 may be distinguished by observing whether gaseous HCl is released during both $TiCl_4$ and H_2O pulses (Fig. 1a) or only during the latter (Fig. 1b). Alternatively, or complementary, these mechanisms also may be distinguished by measuring surface mass changes during the various steps of an ALD cycle, the ratio of which is characteristic for each suggested mechanism (Section 7.2.1).

7.2.1. Flow-type Reactor Conditions

The reaction mechanism studies discussed here are those that have been carried out under conditions which are the most representative for the practical flow-type ALD thin film reactors in what comes to the pressure (a few Torrs), the exposure time (a few seconds in maximum), and the surface area of the substrates. For these studies, a differentially pumped quadrupole mass spectrometer (QMS) has been the choice for analyzing the gas phase whereas microgravimetry and optical techniques have been used for the surface characterization. Even these techniques are quite hard to integrate to the compact traveling-wave reactor geometries, and therefore certain modifications have been needed for their implementation. Nevertheless, the required modifications are after all quite straightforward, and because all these measurements are done in real time, they might also be applicable for process control in industry.

7.2.1.1. Analysis of the Gas Phase

For the gas phase analysis, it is important to note that the amount of byproducts released is directly related to the reactive surface area: an order of magnitude estimation is 10^{14} molecules released per 1 cm^2. In addition, the reactions are often fast and completed in fractions of a second. Therefore, the analysis method, also including the sampling arrangement, and the reactive surface area must be carefully designed and adjusted in accordance with each other to ensure meaningful and time-resolved detection of the byproducts. Until now, only QMS with differentially pumped sampling has been used [211, 223, 437–439].

Because mass spectrometers need to be operated below 10^{-4} Torr, a pressure reduction of at least 4 orders of magnitude is needed from the flow-type ALD reactor conditions. This has been realized by sampling with either a capillary [211, 223, 437] or an orifice [438, 439]. To minimize the contributions of reactions in the sampling setup, there must be as small a surface area as possible and therefore an orifice is the best choice, though capillaries can also be made small enough, e.g., 0.2 mm in diameter and 2 mm in length [223, 437]. As many of the precursors used in ALD are solids, the sampling setup must be heated; most preferably it is held at the reaction temperature. To keep the detector and the associated electronics close to room temperature, the QMS is inserted into a temperature gradient so that only the sampling setup and the ionizer are at the reaction chamber temperature. An ALD-QMS setup, also incorporating a quartz crystal microbalance (QCM, see the following) [439] is shown in Figure 22.

Figure 23 shows an example of data acquired with the instrument shown in Figure 22 on the $TiCl_4$-D_2O process. The dominant reaction byproduct is DCl which is followed as $D^{37}Cl^+$ ($m/z = 39$). The ratio of DCl liberated during the $TiCl_4$ pulse to that liberated during the D_2O pulse is about 1/3 which implies that each chemisorbing $TiCl_4$ molecule reacts with one surface $-OD$ group releasing one of its Cl ligands. The other three Cl ligands are released during the D_2O pulse. The simultaneously measured QCM data supports this conclusion (see the following).

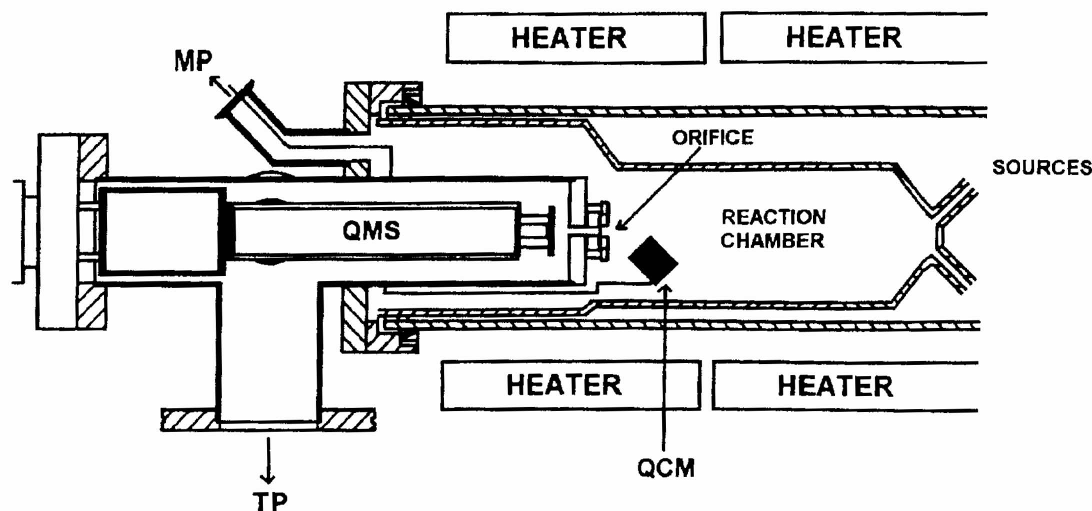

Fig. 22. Schematics of an ALD-QMS-QCM setup (after [438]). The precursors are transported by a carrier gas from their sources at right (not shown) through the reaction chamber to the mechanical pump (MP). The reaction chamber is quite tightly packed with glass substrates to have enough surface area (about 3500 cm^2) for producing detectable amounts of reaction byproducts. A small fraction of the total flow is pumped through the sampling orifice and the QMS chamber by the turbomolecular pump (TP). The pressure drop across the orifice is from about 2 Torr in the reaction chamber to below 10^{-6} Torr in the QMS chamber. The QCM is located in the vicinity of the orifice so that they both are at the reaction chamber temperature.

7.2.1.2. Analysis of the Surface

As the detailed identification of surface species is difficult under the flow-type reactor conditions, the surface studies have focused quite a lot on observing changes in surface termination during each ALD process step. Rates of exchange reactions, chemisorption, desorption, and decomposition, and their effects on self-limitation have been of interest. Because all these processes affect the mass of the film-substrate system, they may be followed by real time mass measurements. In addition, when only well-defined exchange reactions occur, the relative mass changes provide information of the average species terminating the surface at each stage of an ALD cycle.

Real time mass measurements may be done with either a quartz crystal microbalance (QCM) [96, 104, 105, 128, 179, 188, 198, 305, 308, 313, 438, 439] (Fig. 22) or with a sensitive electrobalance [144, 151, 152]. An example of the latter is shown in Figure 24. The electrobalance itself is outside the reaction chamber and is protected with a carrier gas flow. The substrate is connected to the electrobalance with a fused quartz fiber. The sensitivity of the microbalance is better than 0.025 μg, so with a 2.6-cm^2 substrate the smallest detectable mass change corresponds to less than 0.05 ML of GaAs or GaN, for example. The main problem of this system appears to be its sensitivity to flow rate changes associated with pulsing of the precursors [151]. In addition, a reactor specially designed for a connection to the electrobalance is evidently needed.

Quartz crystal microbalances are routinely used as real time film thickness monitors in evaporation, for example. The operation of QCM is based on the relation between the resonance oscillation frequency of the piezoelectric quartz crystal and its mass, also including the film mass. QCM is rather easily integrated to any ALD reactor into a space of a few cubic centimeters, but its sensitivity to temperature variations may cause problems. Therefore, during the measurements the temperature of the crystal must either stay constant or vary with a constant rate so that its contribution can be subtracted from the measured frequency changes. Any temperature variations due to the precursor pulsing must be eliminated. In any case, above 300–350°C noise in the QCM signal becomes largely disturbing. The primary data of QCM, i.e., the changes in crystal oscillation frequency, directly give the relative surface mass changes which are usually enough for examining the ALD reaction mechanisms. For this reason and because of uncertainties related to the absolute mass measurements, the latter are rarely done.

Figure 23 shows QCM data measured on the $TiCl_4$-D_2O process [439] with the ALD-QMS-QCM setup shown in Figure 22. Basically, similar data are also obtained with electromicrobalances. During each precursor pulse, a fast mass change followed by a saturation is observed as expected for an effective and self-limiting ALD process. Any decomposition or etching reactions causing deviations from the self-limiting growth conditions could easily be distinguished as continuous mass increase or decrease, respectively, [104, 105, 313]. During the $TiCl_4$ pulse, the mass increases by m_1 as adsorbates $-TiCl_x$ are formed, and during the D_2O pulse the mass decreases as Cl ligands are replaced by $-OD$ groups or oxide ions. The mass increase m_0 brought about by the complete cycle corresponds to TiO_2. The ratio m_1/m_0 can be calculated for any suggested reaction mechanism, and thereby the correct mechanism may be distinguished from the measured ratio. In Figure 23, the m_1/m_0 ratio is about 1.9 which, in good agreement with the QMS results (see the foregoing text), points to the following reaction

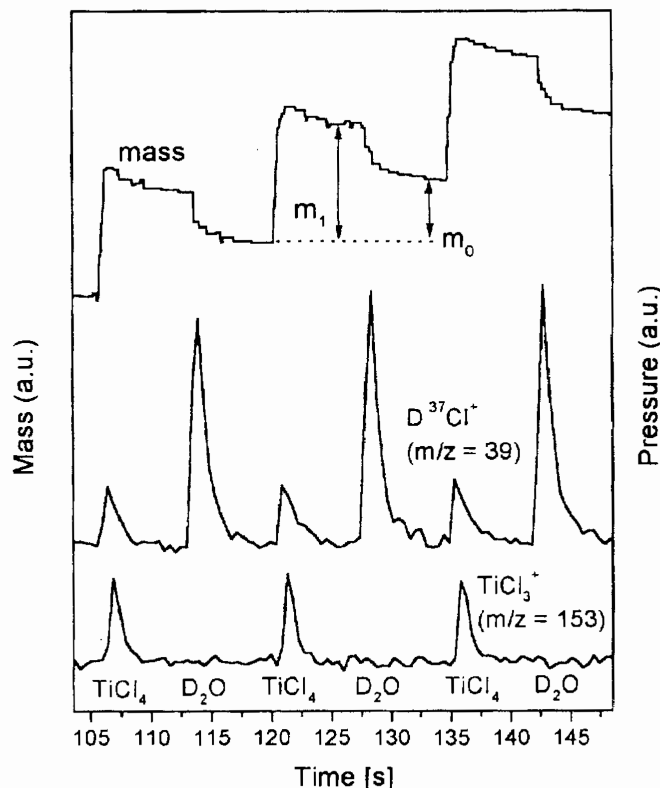

Fig. 23. QMS and QCM measurements on a $TiCl_4$-D_2O process done with the ALD-QMS-QCM setup shown in Figure 22. The pulse times are 0.5 s for both precursors and purge periods are 6.0 s. The reaction temperature is 200°C [439]. The QMS data shows the time variation of the ions $TiCl_3^+$ ($m/z = 153$) and $D^{37}Cl^+$ ($m/z = 39$). From the $D^{37}Cl^+$ signal the background observed during subsequent reference D_2O pulses applied after the ALD cycles has been subtracted. The mass signal was obtained from the negative resonance oscillation frequency change, $-\Delta f$, which is in a direct relationship to the surface mass load. m_1 and m_0 denote the mass changes during the $TiCl_4$ pulse and during one completed ALD cycle, respectively, and they are related to the intermediate surface species $-TiCl_x$ and TiO_2, respectively.

mechanism:

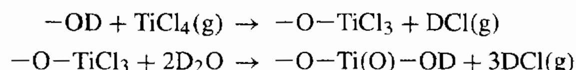

$$-\mathrm{OD} + \mathrm{TiCl_4(g)} \rightarrow -\mathrm{O{-}TiCl_3} + \mathrm{DCl(g)}$$

$$-\mathrm{O{-}TiCl_3} + 2\mathrm{D_2O} \rightarrow -\mathrm{O{-}Ti(O){-}OD} + 3\mathrm{DCl(g)}$$

$$m_1 \propto M(-\mathrm{TiCl_3}) - M(\mathrm{D}) = (154 - 2)\,\mathrm{g\,mol^{-1}} = 152\,\mathrm{g\,mol^{-1}}$$

$$m_0 \propto M(\mathrm{TiO_2}) = 80\,\mathrm{g\,mol^{-1}}$$

$$\frac{m_1}{m_0} = 1.9$$

Note that the surface species formed in the latter reaction is $-O-Ti(O)-OD$ rather than $-O-Ti(-OD)_3$ because otherwise the $-OD$ group density would be threefold in the beginning of the next cycle whereas the cycle-to-cycle repeatability (Fig. 23) indicates that such variation does not exist. On the other hand, the reaction mechanism was found to be clearly temperature dependent: the higher the temperature, the lower the amount of DCl released during the $TiCl_4$ pulse. This behavior can be correlated to the density of hydroxyl groups on the TiO_2 surface which decreases with increasing temperature [436]. Obviously, as the reaction temperature is increased, few hydroxyl groups are left on the surface after the water pulse and the dominating mechanism become that shown in Figure 1b; i.e., $TiCl_4$ chemisorbs without exchange reactions and all the Cl ligands are released during the water pulse. It must be emphasized, however, that both QMS and QCM give information of only the net reactions during each pulse, and the actual mechanism may consist of several elementary reactions. For example, even if $-OD$ groups existed on the surface in significant amounts and reacted with $TiCl_4$, a release of DCl would not necessarily be observed during the $TiCl_4$ pulse as DCl might readsorb on the surface and stay there until the next water pulse.

Optical techniques form another group of methods which are applicable for analyzing surface processes in the flow-type ALD reactors. In fact, these techniques have been applied over the entire pressure range from UHV to atmospheric. Only one or two windows and an open light path to the sample surface are needed. If film growth on the window constitutes a problem, it may be prevented with proper inert gas flow curtains. Optical methods are well suited for following changes in surface termination and for examining dynamics of these changes. However, the chemical interpretation of the data is difficult without supplementary methods.

Surface photoabsorption (SPA) [18, 149–152, 156, 266, 397, 440–444] and reflectance difference spectroscopy (RDS) [244, 257, 258, 270, 445] have been the most extensively used optical techniques in the characterization of ALD processes. In SPA, the reflectivity of p-polarized light incident on the surface at the Brewster angle is measured [446]. With this geometry, the bulk contribution is minimized, enabling sensitive detection of the reflectivity changes caused by surface reactions. Under the self-limiting ALD growth conditions, the reflectivity varies periodically between two constant levels corresponding to the two differently terminated surfaces. Deviations from these reflectivity levels give indications of other kinds of surface terminations caused by, for example, incomplete reactions, decomposition, or desorption. For instance, SPA measurements have indicated that the GaCl-AsH_3 process proceeds differently in hydrogen and helium carrier gases, and it was suggested that in H_2 chlorides are removed from the surface as HCl already during the purge following the GaCl pulse whereas in the inert carrier the chlorides are removed during the AsH_3 pulse [150]. The suggested mechanism in H_2 was later verified by gravimetric studies [151] whereas further SPA investigations revealed that part of the Ga atoms left on the surface after the chloride removal in H_2 are covered with hydrogen atoms [443]. Additionally, arsenic desorption during elongated purge times after the AsH_3 pulse was revealed and kinetically measured by both SPA and microgravimetry [444].

In RDS, nearly normal incident light polarized along two certain crystallographic axes of the substrate is used, and the difference in their reflectivity is measured [447]. The alternate pulsing in ALD causes changes in the RDS signal similar to the SPA. Because the RDS signal is derived from the anisotropy between two crystallographic directions in the surface plane,

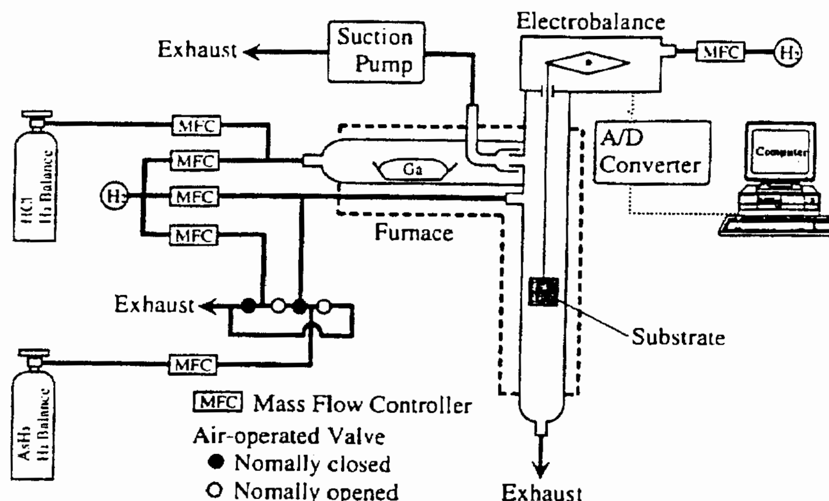

Fig. 24. Schematic of an *in situ* gravimetric monitoring system used to examine ALD processes in which GaCl was formed in situ from a metallic gallium and HCl vapor [151]. Reprinted with permission from A. Koukitu, N. Takahashi, and H. Seki, *In situ* monitoring of the growth process in GaAs atomic layer epitaxy by gravimetric and optical methods, *J. Cryst. Growth* 146, 467 (1995), © 1995, Elsevier Science.

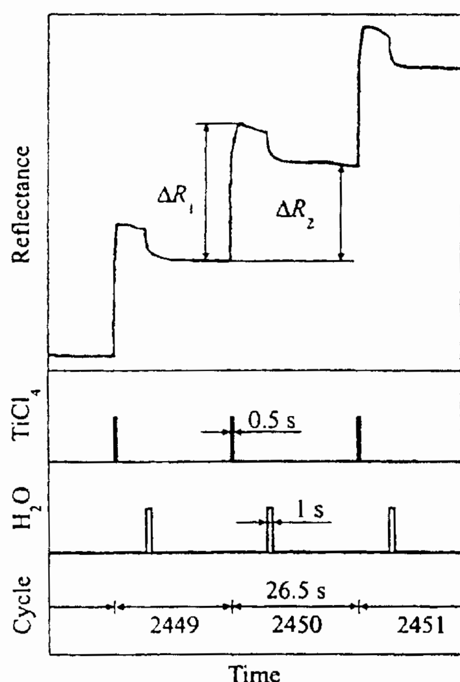

Fig. 25. Reflectance transients measured by the incremental dielectric reflection technique during three subsequent TiO_2 growth cycles with $TiCl_4$ and H_2O as precursors [182]. Reprinted with permission from A. Rosental et al., Surface of TiO_2 during atomic layer deposition as determined by incremental dielectric reflection, *Appl. Surf. Sci.* 142, 204 (1999), © 1999, Elsevier Science.

RDS is applicable only to epitaxial growth. SPA has also mainly been used in epitaxy processes, though in principle it is also applicable to nonepitaxial cases. In fact, a similar technique, called incremental dielectric reflection (IDR) [182, 448, 449] was applied for following the ALD growth of TiO_2 on glass (Fig. 25). As in SPA, also in IDR the reflection of p-polarized light incident at the Brewster angle is measured but here the reflectivity variations originate from interference effects rather than from absorption. If not only the film but also the substrate is transparent to the probing light, the substrate may be used as the window for the light [182, 449]. This makes it possible to apply IDR also to the traveling-wave reactor geometrics. Another technique similarly based on the effects of the surface layer on light interference, named as surface photointerference (SPI), has been applied for the *in situ* characterization of ALD growth of epitaxial ZnSe and CdSe on GaAs [279]. As compared with the methods based on light absorption, IDR and SPI have a benefit in that they employ lower energy photons which apparently have less effect on the growth reactions.

Ellipsometer is a common tool for *in situ* characterization of thicknesses and optical properties of thin films. Its suitability to the analysis of the separate ALD reaction steps has been quite scarcely examined, however. A spectroscopic ellipsometer has been used for following the $Al(CH_3)_3$-H_2O_2 ALD process [229]. Using predetermined optical properties and a single layer model for the film, thickness increments of 0.17 nm cycle^{-1} were resolved during the $Al(CH_3)_3$ pulse though the data was quite noisy, peak-to-peak variations in the thickness were at best 0.1 nm.

7.2.2. High Surface Area Substrates

High surface area substrates have been a subject of an ALD research both because of their practical importance, like in heterogeneous catalysts, and because they offer plenty of material for detailed chemical characterization. Nanoporous silica and alumina powders have high specific surface areas of several hundred square meters per gram, silica even up to 1000 m^2 g^{-1}, which ensures that already a monolayer of reaction products or intermediates is enough for routine chemical analysis tech-

niques, such as IR, NMR, and elemental analysis. For example, if 1 cm^2 planar substrate holds about 10^{14} surface species, 100-mg nanoporous powder with a surface area of 300 $m^2\,g^{-1}$ contains 3×10^{19} of them.

The major difference of reactions on porous powders in comparison with thin film growth comes from the slow transportation into and out of the porous particles and from the need to deliver much larger quantities of precursors in each pulse. Therefore, the exposure and purge times must be much longer than on planar substrates, typical values being a few hours. As a consequence, the reactions may proceed quite differently than during the second and subsecond range exposures in thin film growth. Slower reactions may become dominating when more time is given, especially decomposition is observed at much lower temperatures than on planar surfaces. In addition, because only a few cycles are applied, the reactions often represent more an interface formation than a steady-state film growth, though sometimes this may be taken as an advantage as well. From a practical point of view, it is important to note that prior to and during the analysis the sample must be kept under an inert atmosphere, hence requiring appropriate means for transferring the sample powder from the reactor to the analysis.

Studies on porous powders have clearly pointed out the importance of the surface terminating groups with respect to the metal precursor chemisorption density [30–33]. For example, when the hydroxyl group density on silica is decreased by preheating it at increasing temperatures, the number of metal atoms bound to silica decreases accordingly. At the same time, a consumption of the hydroxyl groups in reactions with the metal precursor may be verified with IR and NMR measurements. These observations imply that the chemisorption mainly occurs via a reaction with the hydroxyl groups.

The chemisorption density is also affected by steric factors: the larger the precursor molecule of a given metal, the lower the number of metal atoms chemisorbed. For example, $Ni(acac)_2$ results in a saturation density of 2.5 Ni nm^{-2} whereas the more bulky $Ni(thd)_2$ gives only 0.92 Ni nm^{-2} [30, 33]. If the precursors are significantly different in their character, their binding modes to the surface may differ. For instance, $Al(CH_3)_3$ has a high affinity toward oxygen and thus reacts on silica not only with the $-OH$ groups but also with siloxane bridges ($Si-O-Si$), whereas $Al(acac)_3$ reacts only with the $-OH$ groups and, unlike $Al(CH_3)_3$, is not able to consume them all because of its larger size [33]. On the other hand, the chemical nature of the powder may also have significant effects. Alumina, for example, catalyzes the decomposition of $Ti(OCH(CH_3)_2)_4$ already above 100°C whereas on silica self-limiting adsorption occurs at least up to 200°C (Fig. 26a) [32]. The elemental C/Ti ratios measured after the $Ti(OCH(CH_3)_2)_4$ exposure (Fig. 26b) imply that on silica two ligands are consumed in reactions with the surface $-OH$ groups and the surface is terminated with $(-Si-O-)_2Ti(-OCH(CH_3)_2)_2$ species.

An intermediate case between loose beds of porous powders and planar substrates is formed by thinner porous objects, such as porous silicon surface layers, high surface area membranes, and powders pressed into thin grids or in the form of thin pellets. These resemble powders in that IR characterization is possible but the required exposure times are shorter, tens of seconds, and thus closer to thin film growth, though still the difference is notable, 1 to 2 orders of magnitude. In any event, the reactions are fast enough so that several deposition cycles may be repeated for observing the cyclic changes in surface termination. Also these studies have supported the view that surface terminating groups play a decisive role in each chemisorption step in ALD of oxides [36, 42, 162, 163, 219, 264] and nitrides [168, 207, 231, 232]. The same also applies to the novel tungsten process where WF_6 and Si_2H_6 are used as precursors [206]. The increase and the decrease, respectively, in the $Si-H$ and $W-F$ absorption bands in the IR spectra after the Si_2H_6 exposure im-

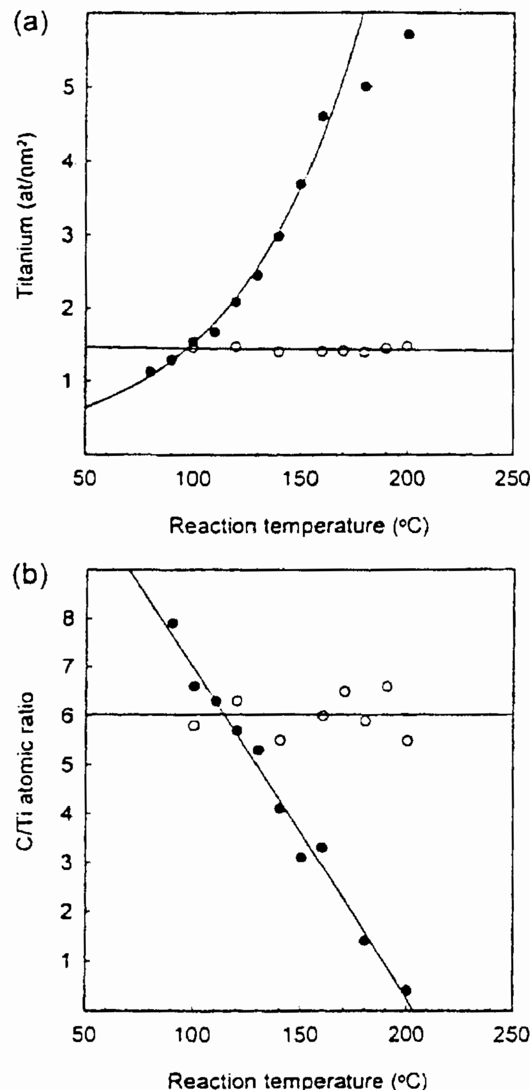

Fig. 26. (a) Titanium surface density and (b) C/Ti atomic ratio on high surface area alumina (•) and silica (o) powders after $Ti(OCH(CH_3)_2)_4$ exposure at different temperatures [32]. Reprinted with permission from M. Lindblad et al., Processing of catalysts by atomic layer epitaxy: Modification of supports, *Appl. Surf. Sci.* 121–122, 286 (1997), © 1997, Elsevier Science.

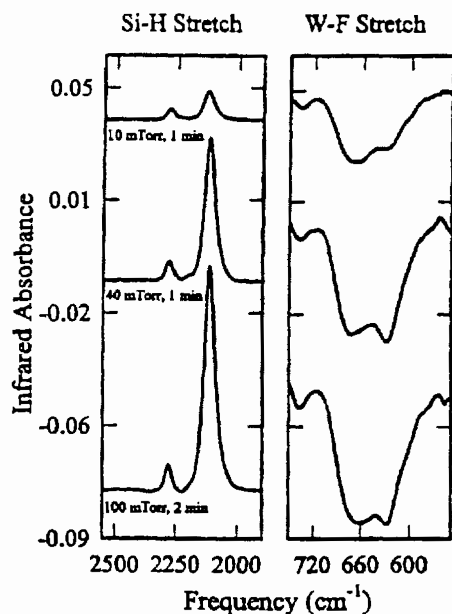

(a)

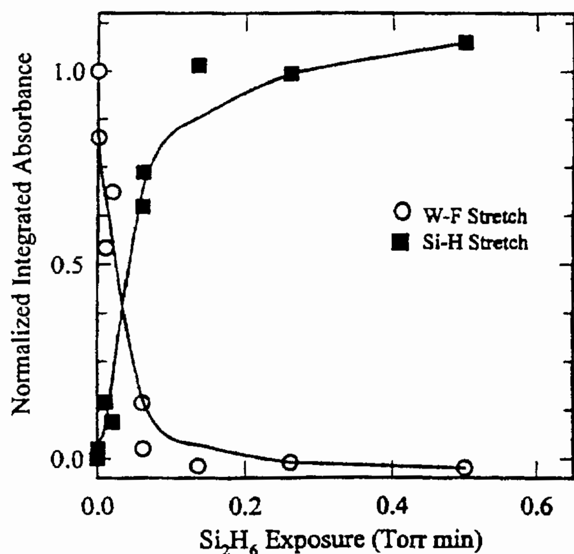

(b)

Fig. 27. (a) Fourier transform infrared (FTIR) difference spectra recorded in the tungsten ALD process after various Si_2H_6 exposures on a surface previously saturated with WF_6. Each spectrum is referenced to the initial surface left after the WF_6 pulse. The reaction temperature is 150°C. (b) The Si_2H_6 exposure dependence of the normalized integrated absorbances of the W$-$F stretching vibration at $\sim$680 cm^{-1} and the Si$-$H stretching vibrations at 2115 and 2275 cm^{-1} [206]. Reprinted with permission from J. W. Klaus, S. J. Ferro, and S. M. George, Atomic layer deposition of tungsten using sequential surface chemistry with a sacrificial stripping reaction, *Thin Solid Films* 360, 145 (2000), © 2000, Elsevier Science.

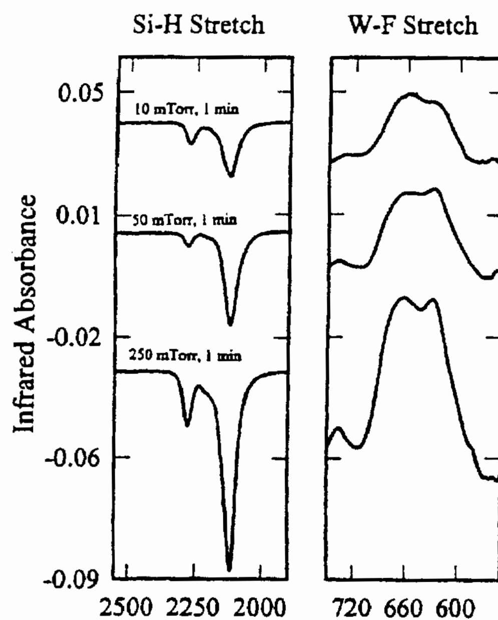

(a)

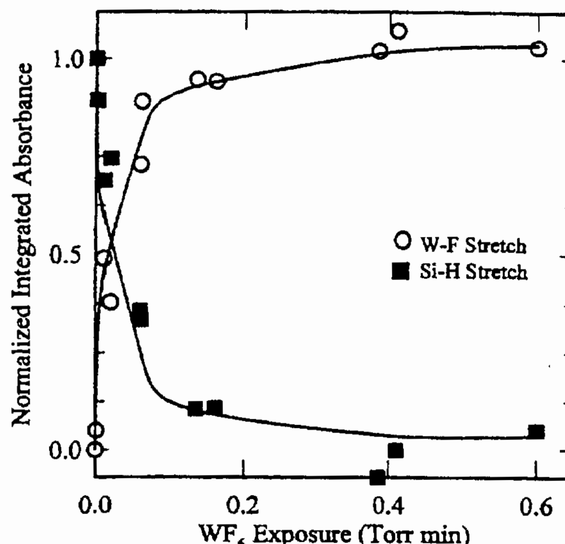

(b)

Fig. 28. (a) FTIR difference spectra recorded in the WF_6-Si_2H_6 ALD process vs WF_6 exposure at 150°C. Each spectrum is referenced to the initial, Si_2H_6 saturated surface. (b) Normalized integrated absorbances of the W$-$F (680 cm^{-1}) and Si$-$H (2115 and 2275 cm^{-1}) stretching vibrations vs the WF_6 exposure at 150°C [206]. Reprinted with permission from J. W. Klaus, S. J. Ferro, and S. M. George, Atomic layer deposition of tungsten using sequential surface chemistry with a sacrificial stripping reaction, *Thin Solid Films* 360, 145 (2000), © 2000, Elsevier Science.

ply that disilane reduces $-WF_x$ surface species into metallic tungsten and forms $-SiH_xF_y$ species instead (Fig. 27). Subsequently, WF_6 reacts with the $-SiH_xF_y$ surface groups and regenerates the $-WF_x$ terminated surface (Fig. 28). Since the films deposited with this process contained no silicon or fluorine detectable with XPS, it could be concluded that the intermediate SiH_xF_y groups were removed as volatile SiH_aF_b species. Both reactions appear self-limiting, as the absorbances saturate above certain exposure levels (Figs. 27b and 28 b).

7.2.3. *High Vacuum Conditions*

As ALD processes proceed via saturating surface reactions, it is evident that techniques having the highest surface sensitivity should be applied for their characterization. Among these techniques the most valuable are perhaps XPS which provides information of not only the elements present on the surface but also of their chemical environment, and low energy ion scattering (LEIS) which probes only the topmost layer of atoms. Other applicable surface analysis techniques include the well-known Auger electron spectroscopy (AES), SIMS, reflection high energy electron diffraction (RHEED), and low energy electron diffraction (LEED), for example. However, the ultrahigh-vacuum conditions required by these techniques are in a clear contradiction with the practical ALD reactors. Therefore, either sample transfer or reactions performed in high vacuum are needed.

Sample transfer from a higher pressure reactor to the UHV analysis chamber may be realized in several ways. If the two are separate, a transfer container with inert atmosphere or vacuum must be used. More conveniently, a reaction chamber is connected directly to the analysis chamber through a gate valve. The reaction chamber may be just another high-vacuum chamber which during the reactions is filled alternately to certain pressures of the precursors and then evacuated to a similar level as the analysis chamber. Such systems are well suited for reasonably volatile precursors but low vapor pressure sources may constitute problems because of condensation. To avoid these problems, a special mini-ALD reactor built in connection to a UHV surface analysis chamber is apparently advantageous [450]. It is also possible to build inside the analysis chamber a small high pressure reaction chamber which after evacuation is opened for the surface studies [163]. Occasionally, the reactions have been carried out in the analysis chamber itself.

These kinds of high-vacuum studies are not unique to ALD but they have also been performed in an attempt to deepen the understanding of CVD chemistry. There also alternate dosing is often used to better identify the potential surface intermediates. No matter what the original aim of the studies, their eventual outcome is obvious: the elemental composition of the surface intermediates terminating the surface after each reaction step (Fig. 29). Light elements, especially hydrogen, are unfortunately difficult to detect with most of the methods. On the other hand, as XPS shows information of the chemical environment of the elements, it can indirectly reveal also the presence of hydrogen. RHEED and LEED, in turn, give structural information and are usually used in connection with epitaxial growth processes on single crystal substrates.

It must be recognized, however, that both sample transfer and different reaction conditions may effect the chemistry in comparison with the practical ALD processes. Sample transfer obviously takes time and involves cooling of the sample, thus raising a question if the surface intermediates stay unchanged. Likewise, reactions often behave quite differently under high-vacuum conditions as compared with higher pressures. In fact, sometimes reactions known from higher pressure conditions appear not to proceed at all in high vacuum. This effect is well

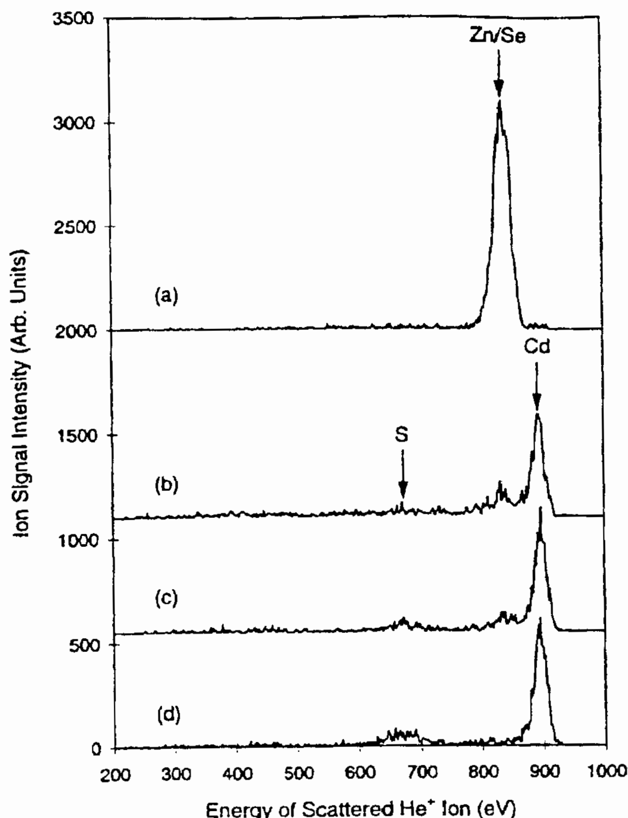

Fig. 29. Low energy ion scattering (LEIS) spectra from (a) a clean ZnSe surface, and after (b) one, (c) two, and (d) four CdS deposition cycles [299]. The energy of the incident He^+ ions was 1000 eV and the peaks at 679, 840, and 896 eV correspond to He^+ ions scattered off S, Zn or Se, and Cd, respectively. Reprinted with permission from Y. Luo et al., *Langmuir* 14, 1493 (1998). © 1998, American Chemical Society.

known in heterogeneous catalyst studies, for instance, and is often called a pressure gap. To explain the pressure gap, both a too small number of molecules having enough thermal energy to overcome the reaction barrier and a lack of collision-induced chemistry have been suggested [451]. In any case, application of conclusions drawn from the high-vacuum experiments to practical, higher pressure ALD reactors clearly requires critical evaluation and, preferably, comparison with film growth and/or reaction mechanism studies under the reactor conditions.

Temperature programmed desorption (TPD, also called thermal desorption spectroscopy, TDS) [18, 299–301, 375, 382, 383, 442] may also be considered as a high-vacuum method though high vacuum is not necessarily required but often used to obtain supplementary information with the surface analysis techniques. TPD is an effective method for examining the identity, relative quantity, and thermal stability of surface species. In TPD, the sample is first prepared at a chosen temperature by exposing the surface to the compound being studied and then, after evacuation, the temperature is steadily increased and the desorbed species are monitored with a mass spectrometer. When applied to ALD studies, a number of alternate precursor exposures may be given before starting the heating.

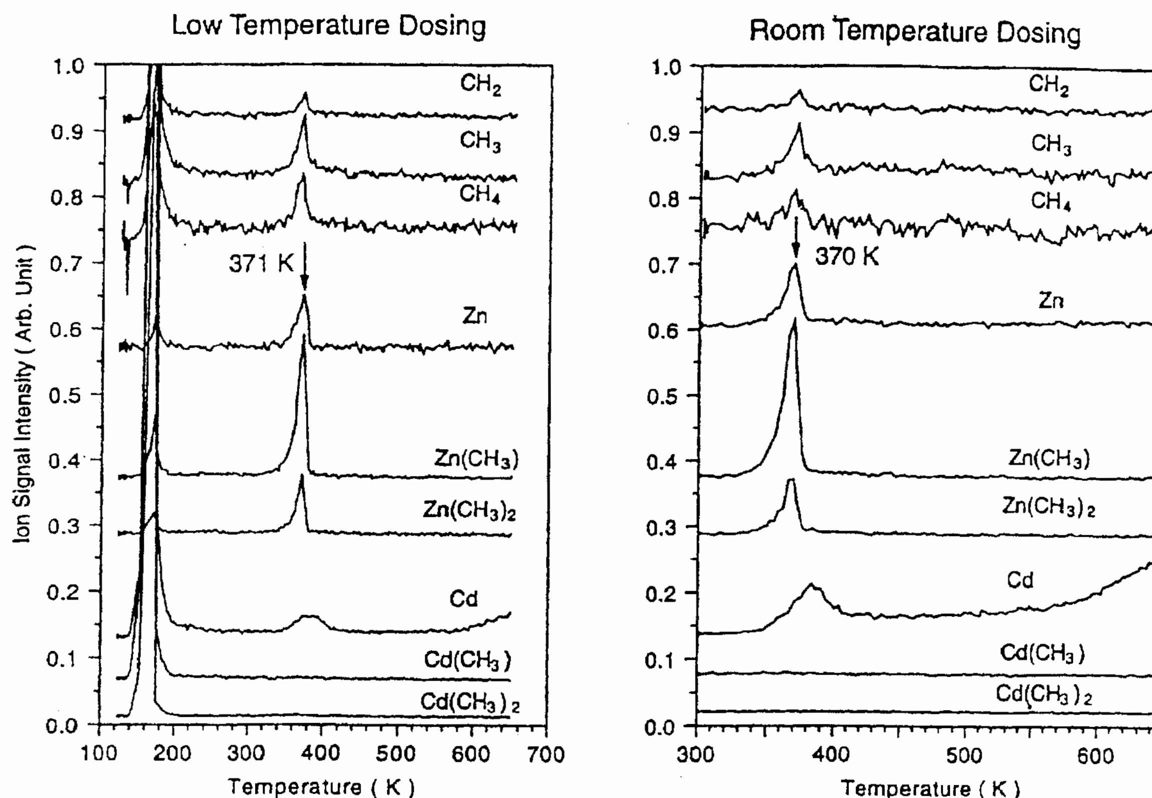

Fig. 30. Temperature programmed desorption (TPD) spectra measured after dosing of $Cd(CH_3)_2$ on to ZnSe at 100 K (low temperature dosing) and room temperature [299]. Reprinted with permission from Y. Luo et al., *Langmuir* 14, 1493 (1998), © 1998, American Chemical Society.

An illustrative example of TPD studies on ALD processes is the examination of CdS deposition from $Cd(CH_3)_2$ and H_2S on a ZnSe substrate [299–301]. Figure 30 shows two TPD spectra measured after dosing $Cd(CH_3)_2$ onto ZnSe at 100 K (low temperature dosing) and room temperature [299]. In the case of the low temperature dosing, desorption of physisorbed $Cd(CH_3)_2$ multilayer is observed at 160 K, otherwise the two spectra are essentially similar. At 370 K, desorption of $Zn(CH_3)_2$ is observed (the lower mass species come from cracking of $Zn(CH_3)_2$) which indicates that $Cd(CH_3)_2$ was dissociatively adsorbed on ZnSe, and upon heating the surface terminating methyl groups combined preferably with zinc, thereby causing zinc to cadmium replacement in the surface layer. Remarkably, the dissociative adsorption occurred also during the low temperature dosing before the desorption of the physisorbed species.

When H_2S was dosed at 100 K upon the methyl terminated surface, left from the preceding exposure of $Cd(CH_3)_2$ onto ZnSe, no reaction occurred and the physisorbed H_2S desorbed at 150 K and the methyl groups at 370 K (Fig. 31). By contrast, when dosed at room temperature, H_2S reacted completely with the $-CH_3$ groups which were not detected in TPD anymore (Fig. 31). After this reaction, the surface was terminated with $-SH$ groups which were stable up to 485 K where they combined and desorbed as H_2S. LEIS measurements showed that already after the first deposition cycle the ZnSe substrate was nearly completely covered by CdS (Fig. 29). As a consequence, the desorption of $Zn(CH_3)_2$ ceased rapidly with an increasing number of deposition cycles [301]. However, at this phase no substantial $Cd(CH_3)_2$ desorption was observed either, but rather the $-CH_3$ groups desorbed in the form of radicals [301].

The $Cd(CH_3)_2$-H_2S precursor combination is apparently an exceptionally efficient one since the reactions go into completion already at room temperature. In any case, procedures similar to that outlined above are applicable for analyzing other ALD processes as well but the dosing temperatures must be carefully chosen according to the kinetic limitations of the chemistry under study. A serious concern is that the surface species forming during the low temperature exposure are different from those which form at higher temperatures in an ALD process. Likewise, if the initial surface in TPD differs from that in an ALD process, different kinds of surface species are likely to form. For example, if an oxide surface is carefully cleaned under high vacuum prior to a TPD experiment, it most probably has no $-OH$ groups and therefore no exchange reactions are possible in an adsorption of a metal compound. By contrast, as discussed before, in ALD oxide processes surface $-OH$ groups are often present and thus some of the metal precursor ligands may become lost in reactions with them. The surface species formed in these two alternative cases apparently exhibit different decomposition and desorption behavior in TPD. For

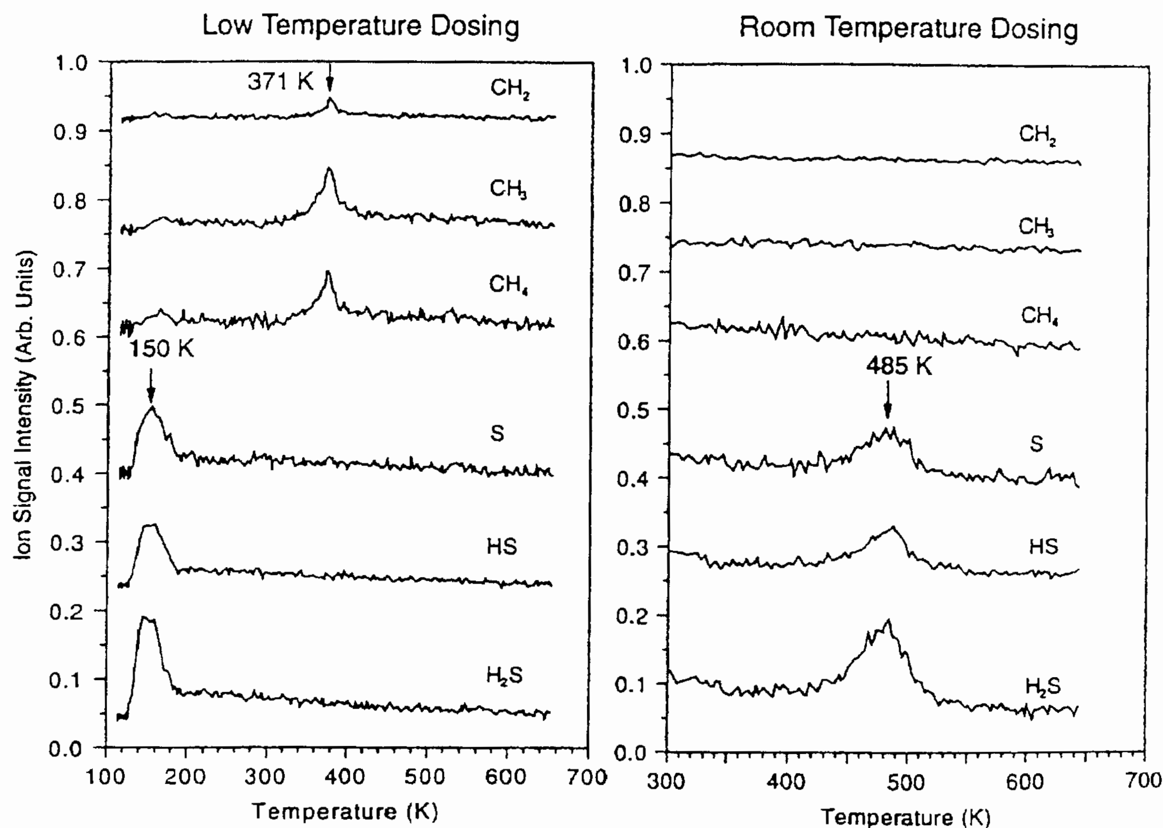

Fig. 31. TPD spectra after dosing of H_2S at 100 K (low temperature dosing) and room temperature on a ZnSe surface which was previously exposed to $Cd(CH_3)_2$ and was thus methyl terminated [299]. Reprinted with permission from Y. Luo et al., *Langmuir* 14, 1493 (1998), © 1998, American Chemical Society.

these reasons, the sample preparation in TPD must be carefully planned to be the most representative for the ALD process conditions. It might also be valuable to compare TPD spectra of surfaces prepared at various temperatures.

8. SUMMARY

ALD is a unique process based on alternate surface reactions which are accomplished by dosing the gaseous precursors on the substrate alternately. Under the ideal conditions, these reactions are saturative ensuring many advantageous features like excellent conformality, large-area uniformity, accurate, and simple film thickness control, repeatability, and large-batch processing capability. As these advantages can often be achieved also under growth conditions which are not fully saturated, in many cases it is beneficial to employ short exposure times to maximize the effective growth rate even if the process is not then strictly self-limited.

While ALD has been employed in TFEL display manufacturing for many years, its broader utilization has been limited by its slowness as evaluated in terms of thickness increment per time unit. At the same time, the high productivity achievable through large-batch processing has perhaps not gained enough attention. In the near term future, the conformality demands and film thicknesses in the integrated circuits are approaching levels which favor ALD as a highly potential manufacturing method, provided of course that proper processes can be developed for the materials needed. As a consequence, the main focus of the ALD research is foreseen to change from the thus far dominated epitaxial semiconductors to oxides, nitrides, and metals.

Among the various reactor types used for ALD, the flow-type traveling-wave geometry has been the most common one, at least in industry. It has a number of benefits, like fast pulsing and purging, effective precursor utilization and scalability to large batches. The major limitation is a difficulty to implement extra energy sources. Methods for *in situ* process control should also be developed.

Precursor chemistry is definitely the key issue in developing effective ALD processes. Aggressively reacting precursor combinations should be looked for to ensure fast completion of the reactions and effective precursor utilization. Solid sources are otherwise well applicable but they are quite laborious, and if in the form of a fine powder, may cause particle defects into the films. Therefore, high vapor pressure compounds, preferably liquids, should be looked for in the first place but often such choices are not available. By now, development of precursors specifically tailored for ALD has been quite limited but also in this area increasing efforts may be expected.

ALD processes activated by light or radicals have been demonstrated, but so far this has remained quite an unexplored area and will certainly open up new possibilities for ALD. Lowered deposition temperatures and higher purity films may be expected, and metal precursors which have so far been quite inert toward the common nonmetal sources may turn reactive. In addition, completely new film materials like metals are likely to appear in the ALD material selection. On the other hand, while suitable for single substrate processing, the activated processes may be hard to scale-up to large batches which are often required to make ALD productive enough.

Many approaches have been taken toward a better understanding of the ALD chemistry. The reaction mechanism studies all point out the importance of surface groups as intermediates in ALD processes.

REFERENCES

1. T. Suntola and J. Antson, U.S. Patent 4,058,430, 1977.
2. T. Suntola, J. Antson, A. Pakkala, and S. Lindfors, *SID 80 Dig.* 11, 108 (1980).
3. T. S. Suntola, A. J. Pakkala, and S. G. Lindfors, U.S. Patent 4,389,973, 1983.
4. T. S. Suntola, A. J. Pakkala, and S. G. Lindfors, U.S. Patent 4,413, 022, 1983.
5. T. Suntola and J. Hyvärinen, *Annu. Rev. Mater. Sci.* 15, 177 (1985).
6. C. H. L. Goodman and M. V. Pessa, *J. Appl. Phys.* 60, R65 (1986).
7. T. Suntola, *Mater. Sci. Rep.* 4, 261 (1989).
8. M. Leskelä and L. Niinistö, in "Atomic Layer Epitaxy" (T. Suntola and M. Simpson, Eds.), p. 1. Blackie, Glasgow, 1990.
9. T. Suntola, *Thin Solid Films* 216, 84 (1992).
10. R. Törnqvist, *Displays* 13, 81 (1992).
11. Y. A. Ono, "Electroluminescent Displays." World Scientific, Singapore, 1995.
12. J. Nishizawa, H. Abe, and T. Kurabayashi, *J. Electrochem. Soc.* 132, 1197 (1985).
13. S. M. Bedair, M. A. Tischler, T. Katsuyama, and N. A. El-Masry, *Appl. Phys. Lett.* 47, 51 (1985).
14. A. Usui and H. Sunakawa, *Japan. J. Appl. Phys.* 25, L212 (1986).
15. A. Doi, Y. Aoyagi, and S. Namba, *Appl. Phys. Lett.* 49, 785 (1986).
16. M. A. Tischler and S. M. Bedair, in "Atomic Layer Epitaxy" (T. Suntola and M. Simpson, Eds.), p. 110. Blackie, Glasgow, 1990.
17. Y. Aoyagi, T. Meguro, S. Iwai, and A. Doi, *Mater. Sci. Eng. B* 10, 121 (1991).
18. A. Usui, *Proc. IEEE* 80, 1641 (1992).
19. M. Ozeki, *Mater. Sci. Rep.* 8, 97 (1992).
20. S. M. Bedair and N. A. El-Masry, *Appl. Surf. Sci.* 82–83, 7 (1994).
21. Y. Sakuma, M. Ozeki, N. Ohtsuka, Y. Matsumiya, H. Shigematsu, O. Ueda, S. Muto, K. Nakajima, and N. Yokoyama, *Appl. Surf. Sci.* 82–83, 46 (1994).
22. S. M. Bedair, *J. Vac. Sci. Technol. B* 12, 179 (1994).
23. J. Nishizawa and T. Kurabayashi, *Thin Solid Films* 367, 13 (2000).
24. T. Yao, in "Atomic Layer Epitaxy" (T. Suntola and M. Simpson, Eds.), p. 155. Blackie, Glasgow, 1990.
25. M. Konagai, Y. Takemura, H. Nakanishi, and K. Takahashi, *Mater. Res. Soc. Symp. Proc.* 222, 233 (1991).
26. E.-L. Lakomaa, S. Haukka, and T. Suntola, *Appl. Surf. Sci.* 60–61, 742 (1992).
27. S. Haukka, E.-L. Lakomaa, and A. Root, *J. Phys. Chem.* 97, 5085 (1993).
28. S. Haukka, E.-L. Lakomaa, O. Jylhä, J. Vilhunen, and S. Hornytzkyj, *Langmuir* 9, 3497 (1993).
29. A. Kytökivi, E.-L. Lakomaa, A. Root, H. Österholm, J.-P. Jacobs, and H. H. Brongersma, *Langmuir* 13, 2717.
30. E.-L. Lakomaa, *Appl. Surf. Sci.* 75, 185 (1994).
31. S. Haukka and T. Suntola, *Interface Sci.* 5, 119 (1997).
32. M. Lindblad, S. Haukka, A. Kytökivi, E.-L. Lakomaa, A. Rautiainen, and T. Suntola, *Appl. Surf. Sci.* 121–122, 286 (1997).
33. S. Haukka, E.-L. Lakomaa, and T. Suntola, *Stud. Surf. Sci. Catal.* 120, 715 (1998).
34. C. Dücsö, N. Q. Khanh, Z. Horváth, I. Bársony, M. Utriainen, S. Lehto, M. Nieminen, and L. Niinistö, *J. Electrochem. Soc.* 143, 683 (1996).
35. M. Utriainen, S. Lehto, L. Niinistö, C. Dücsö, N. Q. Khanh, Z. E. Horváth, I. Bársony, and B. Pécz, *Thin Solid Films* 297, 39 (1997).
36. A. W. Ott, J. W. Klaus, J. M. Johnson, S. M. George, K. C. McCarley, and J. D. Way, *Chem. Mater.* 9, 707 (1997).
37. B. S. Berland, I. P. Gartland, A. W. Ott, and S. M. George, *Chem. Mater.* 10, 3941 (1998).
38. T. Suntola, in "Handbook of Crystal Growth" (D. T. J. Hurle, Ed.), Vol. 3b, p. 601. Elsevier, Amsterdam, 1994.
39. M. Leskelä and M. Ritala, *J. Phys. IV* 5, C5-937 (1995).
40. L. Niinistö, M. Ritala, and M. Leskelä, *Mater. Sci. Eng. B* 41, 23 (1996).
41. M. Ritala, *Appl. Surf. Sci.* 112, 223 (1997).
42. S. M. George, A. W. Ott, and J. W. Klaus, *J. Phys. Chem.* 100, 13,121 (1996).
43. L. Niinistö, Ed., *Acta Polytechnol. Scand., Ser. Chem. Technol. Metall.* 195 (1990).
44. S. M. Bedair, Ed., *Thin Solid Films* 225 (1993).
45. M. Ozeki, A. Usui, Y. Aoyagi, and J. Nishizawa, Eds., *Appl. Surf. Sci.* 82–83 (1994).
46. H. Sitter and H. Heinrich, Eds., *Appl. Surf. Sci.* 112 (1997).
47. T. Meguro, S. Iwai, Y. Aoyagi, K. Ozaki, Y. Yamamoto, T. Suzuki, Y. Okano, and A. Hirata, *J. Cryst. Growth* 99, 540 (1990).
48. P. D. Dapkus, S. P. DenBaars, Q. Chen, W. G. Jeong, and B. Y. Maa, *Prog. Cryst. Growth Charact.* 19, 137 (1989).
49. M. Yoshimoto, A. Kajimoto, and H. Matsunami, *Thin Solid Films* 225, 70 (1993).
50. Q. Chen and P. D. Dapkus, *Thin Solid Films* 225, 115 (1993).
51. D. Lubben, R. Tsu, T. R. Bramblett, and J. E. Greene, *J. Vac. Sci. Technol. A* 9, 3003 (1991).
52. K. Saito, Y. Watanabe, K. Takahashi, T. Matsuzawa, B. Sang, and M. Konagai, *Solar Energy Mater. Solar Cells* 49, 187 (1997).
53. R. M. Emerson, J. L. Hoyt, and J. F. Gibbons, *Appl. Phys. Lett.* 65, 1103 (1994).
54. J. Murota, M. Sakubara, and S. Ono, *Appl. Phys. Lett.* 62, 2353 (1993).
55. M. Sakuraba, J. Murota, T. Watanabe, Y. Sawada, and S. Ono, *Appl. Surf. Sci.* 82–83, 354 (1994).
56. M. Sakuraba, J. Murota, N. Mikoshiba, and S. Ono, *J. Cryst. Growth* 115, 79 (1991).
57. J. Nishizawa, A. Murai, T. Ohizumi, T. Kurabayashi, K. Ohtsuka and T. Yoshida, *J. Cryst. Growth* 209, 327 (2000).
58. H. Yokoyama, M. Shinohara, and N. Inoue, *Appl. Phys. Lett.* 60, 377 (1992).
59. S. Yokoyama, N. Ikeda, K. Kajikawa, and Y. Nakashima, *Appl. Surf. Sci.* 130–132, 352 (1998).
60. D. D. Koleske and S. M. Gates, *J. Appl. Phys.* 76, 1615 (1994).
61. D. D. Koleske and S. M. Gates, *Appl. Phys. Lett.* 64, 884 (1994).
62. S. Sugahara, Y. Uchida, T. Kitamura, T. Nagai, M. Matsuyama, T. Hattori, and M. Matsumura, *Jpn. J. Appl. Phys.* 36, 1609 (1997).
63. J. Sumakeris, Z. Sitar, K. S. Ailey-Trent, K. L. More, and R. F. Davis, *Thin Solid Films* 225, 244 (1993).
64. S. Imai, T. Iizuka, O. Sugiura, and M. Matsumura, *Thin Solid Films* 225, 168 (1993).
65. S. Imai and M. Matsumura, *Appl. Surf. Sci.* 82–83, 322 (1994).
66. E. Hasunuma, S. Sugahara, S. Hoshino, S. Imai, K. Ikeda, and M. Matsumura, *J. Vac. Sci. Technol. A* 16, 679 (1998).
67. Y. Suda, Y. Misato, and D. Shiratori, *Jpn. J. Appl. Phys.* 38, 2390 (1999).
68. S. Sugahara, T. Kitamura, S. Imai, and M. Matsumura, *Appl. Surf. Sci.* 82–83, 380 (1994).
69. S. Sugahara, M. Kadoshima, T. Kitamura, S. Imai, and M. Matsumura, *Appl. Surf. Sci.* 90, 349 (1995).

70. M. de Keijser and C. van Opdorp, *Appl. Phys. Lett.* 58, 1187 (1991).
71. C.-Y. Hwang, P. Lu, W. E. Mayo, Y. Lu, and H. Liu, *Mater. Res. Soc. Symp. Proc.* 326, 347 (1994).
72. H. Goto, K. Shibahara, and S. Yokoyama, *Appl. Phys. Lett.* 68, 3257 (1996).
73. S. Yokoyama, H. Goto, T. Miyamoto, N. Ikeda, and K. Shibahara, *Appl. Surf. Sci.* 112, 75 (1997).
74. S. M. Rossnagel, A. Sherman, and F. Turner, *J. Vac. Sci. Technol. B* 18, 2016 (2000).
75. A. Sherman, private communication.
76. M. Ylilammi, *Thin Solid Films* 279, 124 (1996).
77. T. Suntola, *Thin Solid Films* 225, 96 (1993).
78. K. Kodama, M. Ozeki, Y. Sakuma, K. Mochizuki, and N. Ohtsuka, *J. Cryst. Growth* 99, 535 (1990).
79. M. Ishizaki, N. Kano, J. Yoshino, and H. Kukimoto, *Thin Solid Films* 225, 74 (1993).
80. M. Ozeki and N. Ohtsuka, *Appl. Surf. Sci.* 82–83, 233 (1994).
81. S. Hirose, M. Yamaura, A. Yoshida, H. Ibuka, K. Hara, and H. Munekata, *J. Cryst. Growth* 194, 16 (1998).
82. M. Ritala, M. Leskelä, L.-S. Johansson, and L. Niinistö, *Thin Solid Films* 228, 32 (1993).
83. M. Ritala and M. Leskelä, *Appl. Surf. Sci.* 75, 333 (1994).
84. M. Ritala, M. Leskelä, L. Niinistö, T. Prohaska, G. Friedbacher, and M. Grasserbauer, *Thin Solid Films* 250, 72 (1994).
85. J. Ihanus, M. Ritala, M. Leskelä, T. Prohaska, R. Resch, G. Friedbacher, and M. Grasserbauer, *Appl. Surf. Sci.* 120, 43 (1997).
86. T. Asikainen, M. Ritala, M. Leskelä, T. Prohaska, G. Friedbacher, and M. Grasserbauer, *Appl. Surf. Sci.* 99, 91 (1996).
87. S. Dey and S. J. Yun, *Appl. Surf. Sci.* 143, 191 (1999).
88. M. Ritala, M. Leskelä, J.-P. Dekker, C. Mutsaers, P. J. Soininen, and J. Skarp, *Chem. Vapor Deposition* 5, 7 (1999).
89. J. I. Skarp, P. J. Soininen, and P. T. Soininen, *Appl. Surf. Sci.* 112, 251 (1997).
90. *Eur. Semicond.* April 1999, p. 69.
91. B. T. McDermott, N. A. El-Masry, M. A. Tischler, and S. M. Bedair, *Appl. Phys. Lett.* 51, 1830 (1987).
92. K. Mori, S. Sugou, Y. Katol, and A. Usui, *Appl. Phys. Lett.* 60, 1717 (1992).
93. A. Dip, G. M. Eldallal, P. C. Colter, N. Hayafuji, and S. M. Bedair, *Appl. Phys. Lett.* 62, 2378 (1993).
94. M. Ylilammi, *J. Electrochem. Soc.* 142, 2474 (1995).
95. J. Aarik and H. Siimon, *Appl. Surf. Sci.* 81, 281 (1994).
96. H. Siimon, J. Aarik, and T. Uustare, *Electrochem. Soc. Proc.* 97-25, 131 (1997).
97. H. Siimon and J. Aarik, *J. Phys. D: Appl. Phys.* 30, 1725 (1997).
98. M. A. Tischler and S. M. Bedair, *Appl. Phys. Lett.* 48, 1681 (1986).
99. H. Liu, P. A. Zawadski, and P. E. Norris, *Thin Solid Films* 225, 105 (1993).
100. J. J. Sumakeris, L. B. Rowland, R. S. Kern, S. Tanaka, and R. F. Davis, *Thin Solid Films* 225, 219 (1993).
101. T. Ozawa, *Thermochim. Acta* 174, 185 (1991).
102. A. Niskanen, T. Hatanpää, M. Ritala, and M. Leskelä, *J. Thermal. Anal. Calorim.* 64, 955 (2001).
103. K.-E. Elers, M. Ritala, M. Leskelä, and E. Rauhala, *Appl. Surf. Sci.* 82–83, 468 (1994).
104. J. Aarik, A. Aidla, K. Kukli, and T. Uustare, *J. Cryst. Growth* 144, 116 (1994).
105. J. Aarik, K. Kukli, A. Aidla, and L. Pung, *Appl. Surf. Sci.* 103, 331 (1996).
106. K. Kukli, M. Ritala, R. Matero, and M. Leskelä, *J. Cryst. Growth* 212, 459 (2000).
107. J. Skarp, U.S. Patent 4,486,487, 1984.
108. J. Ihanus, M. Ritala, M. Leskelä, and E. Rauhala, *Appl. Surf. Sci.* 112, 154 (1997).
109. J. Ihanus, M. Ritala, and M. Leskelä, *Electrochem. Soc. Proc.* 97-25, 1423 (1997).
110. M. Juppo, M. Ritala, and M. Leskelä, *J. Vac. Sci. Technol. A* 15, 2330 (1997).
111. M. Ritala, M. Leskelä, E. Rauhala, and P. Haussalo, *J. Electrochem. Soc.* 142, 2731 (1995).
112. M. Ritala, T. Asikainen, M. Leskelä, J. Jokinen, R. Lappalainen, M. Utriainen, L. Niinistö, and E. Ristolainen, *Appl. Surf. Sci.* 120, 199 (1997).
113. M. Ritala, P. Kalsi, D. Riihelä, K. Kukli, M. Leskelä, and J. Jokinen, *Chem. Mater.* 11, 1712 (1999).
114. M. Juppo, M. Ritala, and M. Leskelä, *J. Electrochem. Soc.* 147, 3377 (2001).
115. T. Asikainen, M. Ritala, and M. Leskelä, *J. Electrochem. Soc.* 141, 3210 (1994).
116. W. Faschinger, P. Juza, S. Ferreira, H. Zajicek, A. Pesek, H. Sitter, and K. Lischka, *Thin Solid Films* 225, 270 (1993).
117. Y. Takemura, M. Konagai, K. Yamasaki, C. H. Lee, and K. Takahashi, *J. Electron. Mater.* 22, 437 (1993).
118. M. Konagai, Y. Takemura, K. Yamasaki, and K. Takahashi, *Thin Solid Films* 225, 256 (1993).
119. M. Konagai, Y. Ohtake, and T. Okamoto, *Mater. Res. Soc. Symp. Proc.* 426, 153 (1996).
120. A. Szczerbakow, E. Dynowska, K. Swiatek, and M. Godlewski, *J. Cryst. Growth* 207, 148 (1999).
121. R. Kimura, M. Konagai, and K. Takahashi, *J. Cryst. Growth* 116, 283 (1992).
122. F. Hauzenberger, W. Faschinger, P. Juza, A. Pesek, K. Lischka, and H. Sitter, *Thin Solid Films* 225, 265 (1993).
123. A. Rautiainen, Y. Koskinen, J. Skarp, and S. Lindfors, *Mater. Res. Soc. Symp. Proc.* 222, 263 (1991).
124. M. Ahonen, M. Pessa, and T. Suntola, *Thin Solid Films* 65, 301 (1980).
125. M. Pessa, P. Huttunen, and A. Herman, *J. Appl. Phys.* 54, 6047 (1983).
126. A. Kytökivi, Y. Koskinen, A. Rautiainen, and J. Skarp, *Mater. Res. Soc. Symp. Proc.* 222, 269 (1991).
127. H. Sitter and W. Faschinger, *Thin Solid Films* 225, 250 (1993).
128. J. Aarik, A. Aidla, A. Jaek, A.-A. Kiisler, and A.-A. Tammik, *Acta Polytechnol. Scand., Ser. Chem. Technol. Metall.* 195, 201 (1990).
129. L. Hiltunen, H. Kattelus, M. Leskelä, M. Mäkelä, L. Niinistö, E. Nykänen, P. Soininen, and M. Tiitta, *Mater. Chem. Phys.* 28, 379 (1991).
130. H. Kattelus, M. Ylilammi, J. Saarilahti, J. Antson, and S. Lindfors, *Thin Solid Films* 225, 296 (1993).
131. H. Kattelus, M. Ylilammi, J. Salmi, T. Ranta-aho, E. Nykänen, and I. Suni, *Mater. Res. Soc. Symp. Proc.* 284, 511 (1993).
132. M. Ritala, H. Saloniemi, M. Leskelä, T. Prohaska, G. Friedbacher, and M. Grasserbauer, *Thin Solid Films* 286, 54 (1996).
133. K. Kukli, M. Ritala, and M. Leskelä, *J. Electrochem. Soc.* 144, 300 (1997)
134. S. J. Yun, K.-H. Lee, J. Skarp, H. R. Kim, and K.-S. Nam, *J. Vac. Sci. Technol. A* 15, 2993 (1997).
135. Y. S. Kim, K.-L. Cho, and S. J. Yun, "5th International Conference on the Science and Technology of Display Phosphors," San Diego, 1999, p. 97, Extended Abstracts.
136. K. Kukli, M. Ritala, and M. Leskelä, *J. Electrochem. Soc.* 148, F35 (2001).
137. G. Oya, M. Yoshida, and Y. Sawada, *Appl. Phys. Lett.* 51, 1143 (1987).
138. G. Oya and Y. Sawada, *J. Cryst. Growth* 99, 572 (1990).
139. M. Leskelä, L. Niinistö, E. Nykänen, P. Soininen, and M. Tiitta, *Acta Polytechnol. Scand., Ser. Chem. Technol. Metall.* 195, 193 (1990).
140. M. Nieminen, L. Niinistö, and R. Lappalainen, *Mikrochim. Acta* 119, 13 (1995).
141. M. Tiitta, E. Nykänen, P. Soininen, L. Niinistö, M. Leskelä, and R. Lappalainen, *Mater. Res. Bull.* 33, 1315 (1998).
142. K.-E. Elers, M. Ritala, M. Leskelä, and L.-S. Johansson, *J. Phys. IV* 5, C5-1021 (1995).
143. M. Akamutsu, S. Narahara, T. Kobayashi, and F. Hagesawa, *Appl. Surf. Sci.* 82–83, 228 (1994).
144. A. Koukitu, Y. Kumagai, T. Taki, and H. Seki, *Japan. J. Appl. Phys.* 38, 4980 (1999).
145. A. Usui, H. Sunakawa, F. J. Stützler, and K. Ishida, *Appl. Phys. Lett.* 56, 289 (1990).
146. H. Ikeda, Y. Miura, N. Takahashi, A. Koukitu, and H. Seki, *Appl. Surf. Sci.* 82–83, 257 (1994).

147. T. Taki, T. Nakajima, A. Koukitu, and H. Seki, *J. Cryst. Growth* 183, 75 (1998).
148. J. Ahopelto, H. P. Kattelus, J. Saarilahti, and I. Suni, *J. Cryst. Growth* 99, 550 (1990).
149. K. Nishi, A. Usui, and H. Sakaki, *Thin Solid Films* 225, 47 (1993).
150. N. Takahashi, M. Yagi, A. Koukitu, and H. Seki, *Japan. J. Appl. Phys.* 32, L1277 (1993).
151. A. Koukitu, N. Takahashi, and H. Seki, *J. Cryst. Growth* 146, 467 (1995).
152. A. Koukitu, T. Taki, K. Norita, and H. Seki, *J. Cryst. Growth* 198–199, 1111 (1999).
153. A. Koukitu, H. Nakai, A. Saegusa, T. Suzuki, O. Nomura, and H. Seki, *Japan. J. Appl. Phys.* 27, L744 (1988).
154. H. Tsuchiya, M. Akamutsu, M. Ishida, and F. Hagesawa, *Japan. J. Appl. Phys.* 35, L748 (1996).
155. R. Kobayashi, K. Ishikawa, S. Narahara, and F. Hagesawa, *Japan. J. Appl. Phys.* 31, L1730 (1992).
156. R. Kobayashi, S. Narahara, K. Ishikawa, and F. Hagesawa, *Japan. J. Appl. Phys.* 32, L164 (1992).
157. N. Tsuboi, T. Isu, N. Kakuda, T. Terasako, and S. Iida, *Japan. J. Appl. Phys.* 33, L244 (1994).
158. T. Taki and A. Koukitu, *Appl. Surf. Sci.* 112, 127 (1997).
159. M. Ritala, T. Asikainen, and M. Leskelä, *Electrochem. Solid-State Lett.* 1, 156 (1998).
160. T. Asikainen, M. Ritala, and M. Leskelä, *J. Electrochem. Soc.* 142, 3538 (1995).
161. T. Asikainen, M. Ritala, and M. Leskelä, *Appl. Surf. Sci.* 82–83, 122 (1994).
162. S. M. George, O. Sneh, A. C. Dillon, M. L. Wise, A. W. Ott, L. A. Okada, and J. D. Way, *Appl. Surf. Sci.* 82–83, 460 (1994).
163. O. Sneh, M. L. Wise, A. W. Ott, L. A. Okada, and S. M. George, *Surf. Sci.* 334, 135 (1995).
164. J. W. Klaus, A. W. Ott, J. M. Johnson, and S. M. George, *Appl. Phys. Lett.* 70, 1092 (1997).
165. J. W. Klaus, O. Sneh, and S. M. George, *Science* 278, 1934 (1997).
166. J. W. Klaus, O. Sneh, A. W. Ott, and S. M. George, *Surf. Rev. Lett.* 6, 435 (1999).
167. J. W. Klaus and S. M. George, *Surf. Sci.* 447, 81 (2000).
168. J. W. Klaus, A. W. Ott, A. C. Dillon, and S. M. George, *Surf. Sci.* 418, L14 (1998).
169. P. Soininen, L. Niinistö, E. Nykänen, and M. Leskelä, *Appl. Surf. Sci.* 75, 99 (1994).
170. D. D. Koleske and S. M. Gates, *Appl. Surf. Sci.* 82–83, 344 (1994).
171. S. Morishita, S. Sugahara, and M. Matsumura, *Appl. Surf. Sci.* 112, 198 (1997).
172. M. Ylilammi, M.Sc. Thesis, Helsinki University of Technology, 1979.
173. H. Viirola and L. Niinistö, *Thin Solid Films* 249, 144 (1994).
174. M. Utriainen, K. Kovács, J. M. Campbell, L. Niinistö, and F. Réti, *J. Electrochem. Soc.* 146, 189 (1999).
175. H. Viirola and L. Niinistö, *Thin Solid Films* 251, 127 (1994).
176. S. B. Desu, *Mater. Sci. Eng. B* 13, 299 (1992).
177. M. Ritala, M. Leskelä, E. Nykänen, P. Soininen, and L. Niinistö, *Thin Solid Films* 225, 288 (1993).
178. J. Aarik, A. Aidla, T. Uustare, and V. Sammelselg, *J. Cryst. Growth* 148, 268 (1995).
179. J. Aarik, A. Aidla, V. Sammelselg, H. Siimon, and T. Uustare, *J. Cryst. Growth* 169, 496 (1996).
180. J. Aarik, A. Aidla, A.-A. Kiisler, T. Uustare, and V. Sammelselg, *Thin Solid Films* 305, 270 (1997).
181. V. Sammelselg, A. Rosental, A. Tarre, L. Niinistö, K. Heiskanen, K. Ilmonen, L.-S. Johansson, and T. Uustare, *Appl. Surf. Sci.* 134, 78 (1998).
182. A. Rosental, A. Tarre, P. Adamson, A. Gerst, A. Kasikov, and A. Niilisk, *Appl. Surf. Sci.* 142, 204 (1999).
183. H. Kumagai, M. Matsumoto, K. Toyoda, M. Obara, and M. Suzuki, *Thin Solid Films* 263, 47 (1995).
184. H. Kumagai, K. Toyoda, K. Kobayashi, M. Obara, and Y. Iimura, *Appl. Phys. Lett.* 70, 2338 (1997).
185. L. Hiltunen, M. Leskelä, M. Mäkelä, L. Niinistö, E. Nykänen, and P. Soininen, *Thin Solid Films* 166, 149 (1988).
186. P. Mårtensson, M. Juppo, M. Ritala, M. Leskelä, and J.-O. Carlsson, *J. Vac. Sci. Technol. B* 17, 2122 (1999).
187. K. Kukli, M. Ritala, M. Schuisky, M. Leskelä, T. Sajavaara, J. Keinonen, T. Uustare, and A. Hårsta, *Chem. Vapor Deposition* 6, 297 (2000).
188. K. Kukli, A. Aidla, J. Aarik, M. Schuisky, A. Hårsta, M. Ritala, and M. Leskelä, *Langmuir* 16, 8122 (2000).
189. M. Schuisky, A. Hårsta, A. Aidla, K. Kukli, A.-A. Kiisler, and J. Aarik, *J. Electrochem. Soc.* 147, 3319 (2000).
190. M. Schuisky, K. Kukli, A. Aidla, J. Aarik, M. Ludvigsson, and A. Hårsta. *Electrochem. Soc. Proc.* 2000-13, 637 (2000).
191. M. Ritala, M. Leskelä, E. Rauhala, and J. Jokinen, *J. Electrochem. Soc.* 145, 2914 (1998).
192. K. Kukli, M. Ritala, and M. Leskelä, *Nanostruct. Mater.* 8, 785 (1997).
193. M. Copel, M. Gibelyuk, and E. Gusev, *Appl. Phys. Lett.* 76, 436 (2000).
194. E. P. Gusev, M. Copel, E. Cartier, D. Buchanan, H. Okorn-Schmidt, M. Gribelyuk, D. Falcon, R. Murphy, S. Molis, I. J. R. Baumvol, C. Krug, M. Jussila, M. Tuominen, and S. Haukka, *Electrochem. Soc. Proc.* 2000-2, 477 (2000).
195. H. Zhang, R. Solanki, B. Roberds, G. Bai, and I. Banerjee, *J. Appl. Phys.* 87, 1921 (2000).
196. K. Kukli, K. Forsgren, J. Aarik, T. Uustare, A. Aidla, A. Niskanen, M. Ritala, M. Leskelä, and A. Hårsta, to be published.
197. K. Kukli, J. Ihanus, M. Ritala, and M. Leskelä, *Appl. Phys. Lett.* 68, 3737 (1996).
198. J. Aarik, A. Aidla, A.-A. Kiisler, T. Uustare, and V. Sammelselg, *Thin Solid Films* 340, 110 (1999).
199. M. Pessa, R. Mäkelä, and T. Suntola, *Appl. Phys. Lett.* 38, 131 (1981).
200. K. Kukli, J. Aarik, A. Aidla, O. Kohan, T. Uustare, and V. Sammelselg, *Thin Solid Films* 260, 135 (1995).
201. H. Siimon and J. Aarik, *J. Phys. IV* 5, C5-277 (1995).
202. K. Kukli, M. Ritala, and M. Leskelä, *J. Appl. Phys.* 86, 5656 (1999).
203. K. Forsggren, J. Sundqvist, A. Hårsta, K. Kukli, J. Aarik, and A. Aidla, *Electrochem. Soc. Proc.* 2000-13, 645 (2000).
204. M. Juppo, M. Vehkamäki, M. Ritala, and M. Leskelä, *J. Vac. Sci. Technol. A* 16, 2845 (1998).
205. P. Tägtsröm, P. Mårtensson, U. Jansson, and J.-O. Carlsson, *J. Electrochem. Soc.* 146, 3139 (1999).
206. J. W. Klaus, S. J. Ferro, and S. M. George, *Thin Solid Films* 360, 145 (2000).
207. J. W. Klaus, S. J. Ferro, and S. M. George, *J. Electrochem. Soc.* 147, 1175 (2000).
208. M. Tammenmaa, M.Sc. Thesis, Helsinki University of Technology, 1983.
209. P. Mårtensson and J.-O. Carlsson, *Chem. Vapor Deposition* 3, 45 (1997).
210. P. Mårtensson, "Acta Universitatis Upsaliensis, Comprehensive Summaries of Uppsala Dissertations from the Faculty of Science and Technology," Vol. 421, 1999.
211. J. Hyvärinen, M. Sonninen, and R. Törnqvist, *J. Cryst. Growth* 86, 695 (1988).
212. M. Oikkonen, *Mater. Res. Bull.* 23, 133 (1988).
213. A. Szczerbakow, M. Godlewski, E. Dynowska, V. Yu. Ivanov, K. Swiatek, E. M. Goldys, and M. R. Phillips, *Acta Phys. Pol. A* 94, 579 (1998).
214. C. D. Lee, B. K. Kim, J. W. Kim, H. L. Park, C. H. Chung, S. K. Chang, J. I. Lee, and S. K. Noh, *J. Cryst. Growth* 138, 136 (1994).
215. M. Ylilammi and T. Ranta-aho, *J. Electrochem. Soc.* 141, 1278 (1994).
216. G. S. Higashi and C. G. Flemming, *Appl. Phys. Lett.* 55, 1963 (1989).
217. V. E. Drozd, A. P. Baraban, and I. O. Nikiforova, *Appl. Surf. Sci.* 82–83, 583 (1994).
218. A. W. Ott, K. C. McCarley, J. W. Klaus, J. D. Way, and S. M. George, *Appl. Surf. Sci.* 107, 128 (1996).
219. A. W. Ott, J. W. Klaus, J. M. Johnson, and S. M. George, *Thin Solid Films* 292, 135 (1997).
220. P. Ericsson, S. Begtsson, and J. Skarp, *Microelectron. Eng.* 36, 91 (1997).
221. Y. Kim, S. M. Lee, C. S. Park, S. I. Lee, and M. Y. Lee, *Appl. Phys. Lett.* 71, 3604 (1997).

222. E. P. Gusev, M. Copel, E. Cartier, I. J. R. Baumvol, C. Krug, and M. A. Gribelyuk, *Appl. Phys. Lett.* 76, 176 (2000).
223. M. Juppo, A. Rahtu, M. Ritala, and M. Leskelä, *Langmuir* 16, 4034 (2000).
224. R. Matero, A. Rahtu, M. Ritala, M. Leskelä, and T. Sajavaara, *Thin Solid Films* 368, 1 (2000).
225. J.-F. Fan, K. Sugioka, and K. Toyoda, *Japan. J. Appl. Phys.* 30, L1139 (1991).
226. J.-F. Fan and K. Toyoda, *Appl. Surf. Sci.* 60–61, 765 (1992).
227. J.-F. Fan and K. Toyoda, *Japan. J. Appl. Phys.* 32, L1349 (1993).
228. H. Kumagai, K. Toyoda, M. Matsumoto, and M. Obara, *Japan. J. Appl. Phys.* 32, 6137 (1993).
229. H. Kumagai and K. Toyoda, *Appl. Surf. Sci.* 82–83, 481 (1994).
230. T. M. Mayer, J. W. Rogers, Jr., and T. A. Michalske, *Chem. Mater.* 3, 641 (1993).
231. M. E. Bartram, T. A. Michalske, J. W. Rogers, Jr., and R. T. Paine, *Chem. Mater.* 5, 1424 (1993).
232. H. Liu, D. C. Bertolet, and J. W. Rogers, Jr., *Surf. Sci.* 340, 88 (1995).
233. D. Riihelä, M. Ritala, R. Matero, M. Leskelä, J. Jokinen, and P. Haussalo, *Chem. Vapor Deposition* 2, 277 (1996).
234. J. R. Gong, S. Nakamura, M. Leonard, S. M. Bedair, and N. A. El-Masry, *J. Electron. Mater.* 21, 965 (1992).
235. J. R. Gong, P. C. Colter, D. Jung, S. A. Hussien, C. A. Parker, A. Dip, F. Hyuga, W. M. Duncan, and S. M. Bedair, *J. Cryst. Growth* 107, 83 (1991).
236. N. Hayafuji, G. M. Eldallal, A. Dip, P. C. Colter, N. A. El-Masry, and S. M. Bedair, *Appl. Surf. Sci.* 82–83, 18 (1994).
237. K. Kukli, M. Ritala, M. Leskelä, and J. Jokinen, *J. Vac. Sci. Technol. A* 15, 2214 (1997).
238. A. Niskanen, M. Ritala, and M. Leskelä, unpublished results.
239. M. Ishii, S. Iwai, H. Kawata, T. Ueki, and Y. Aoyagi, *J. Cryst. Growth* 180, 15 (1997).
240. S. Hirose, N. Kano, M. Deura, K. Hara, H. Munekata, and H. Kukimoto, *Japan. J. Appl. Phys.* 34, L1436 (1995).
241. R. Huang and A. H. Kitai, *J. Electron. Mater.* 22, 215 (1993).
242. M. Asif Khan, J. N. Kuznia, R. A. Skogman, D. T. Olson, M. MacMillan, and W. J. Choyke, *Appl. Phys. Lett.* 61, 2539 (1992).
243. M. Asif Khan, J. N. Kuznia, D. T. Olson, T. George, and W. T. Pike, *Appl. Phys. Lett.* 63, 3470 (1993).
244. D. E. Aspnes, I. Kamiya, H. Tanaka, R. Bhat, L. T. Florez, J. P. Harbison, W. E. Quinn, M. Tamargo, S. Gregory, M. A. A. Pudensi, S. A. Schwarz, M. J. S. P. Brasil, and R. E. Nahory, *Thin Solid Films* 225, 26 (1993).
245. N. H. Karam, T. Parodos, P. Colter, D. McNulty, W. Rowland, J. Schetzina, N. El-Masry, and S. M. Bedair, *Appl. Phys. Lett.* 67, 94 (1995).
246. K. S. Boutros, F. G. McIntosh, J. C. Roberts, S. M. Bedair, E. L. Piner, and N. A. El-Masry, *Appl. Phys. Lett.* 67, 1856 (1995).
247. E. L. Piner, M. K. Behbehani, N. A. El-Masry, F. G. McIntosh, J. C. Roberts, K. S. Boutros, and S. M. Bedair, *Appl. Phys. Lett.* 70, 461 (1997).
248. F. G. McIntosh, E. L. Piner, J. C. Roberts, M. K. Behbehani, M. E. Aumer, N. A. El-Masry, and S. M. Bedair, *Appl. Surf. Sci.* 112, 98 (1997).
249. S.-C. Huang, H.-Y. Wang, C.-J. Hsu, J.-R. Gong, C.-I. Chiang, S. L. Tu, and H. Chang, *J. Mater. Sci. Lett.* 17, 1281 (1998).
250. B. T. McDermott, K. G. Reid, N. A. El-Masry, S. M. Bedair, W. M. Duncan, X. Yin, and F. H. Pollak, *Appl. Phys. Lett.* 56, 1172 (1990).
251. B. T. McDermott, N. A. El-Masry, B. L. Jiang, F. Hyuga, S. M. Bedair, and W. M. Duncan, *J. Cryst. Growth* 107, 96 (1991).
252. Y. Sakuma, M. Ozeki, N. Ohtsuka, and K. Kodama, *J. Appl. Phys.* 68, 5660 (1990).
253. M. Ozeki, K. Mochizuki, N. Ohtsuka, and K. Kodama, *Appl. Phys. Lett.* 53, 1509 (1988).
254. K. Mochizuki, M. Ozeki, K. Kodama, and N. Ohtsuka, *J. Cryst. Growth* 93, 557 (1988).
255. J. Nishizawa and T. Kurabayashi, *Appl. Surf. Sci.* 106, 11 (1996).
256. K. Mukai, N. Ohtsuka, H. Shoji, and M. Sugawara, *Appl. Surf. Sci.* 112, 102 (1997).
257. B. Y. Maa and P. D. Dapkus, *Appl. Phys. Lett.* 58, 2261 (1991).
258. R. Arès, S. P. Watkins, P. Yeo, G. A. Horley, P. O'Brien, and A. C. Jones, *J. Appl. Phys.* 83, 3390 (1998).
259. M. Asif Khan, R. A. Skogman, J. M. Van Hove, D. T. Olson, and J. N. Kuznia, *Appl. Phys. Lett.* 60, 1366 (1992).
260. M. Asif Khan, J. N. Kuznia, D. T. Olson, J. M. Van Hove, M. Blasingame, and L. F. Reitz, *Appl. Phys. Lett.* 60, 2917 (1992).
261. M. Ait-Lhouss, J. L. Castaño, B. J. Garcia, and J. Piqueras, *J. Appl. Phys.* 78, 5834 (1995).
262. I. Suemune, *Appl. Surf. Sci.* 82–83, 149 (1994).
263. K. Mori, M. Yoshida, A. Usui, and H. Terao, *Appl. Phys. Lett.* 52, 27 (1988).
264. A. W. Ott, J. M. Johnson, J. W. Klaus, and S. M. George, *Appl. Surf. Sci.* 112, 205 (1997).
265. W. K. Chen, J. C. Chen, L. Anthony, and P. L. Liu, *Appl. Phys. Lett.* 55, 987 (1989).
266. Y. Kobayashi and N. Kobayashi, *Japan. J. Appl. Phys.* 31, L71 (1992).
267. N. Pan, J. Carter, S. Hein, D. Howe, L. Goldman, L. Kupferberg, S. Brierley, and K. C. Hsieh, *Thin Solid Films* 225, 64 (1993).
268. N. Otsuka, J. Nishizawa, H. Kikuchi, and Y. Oyama, *J. Cryst. Growth* 205, 253 (1999).
269. W. G. Jeong, E. P. Menu, and P. D. Dapkus, *Appl. Phys. Lett.* 55, 244 (1989).
270. C. A. Tran, R. Ares, S. P. Watkins, G. Soerensen, and Y. Lacroix, *J. Electron. Mater.* 24, 1597 (1995).
271. V. E. Drozd and V. B. Aleskovski, *Appl. Surf. Sci.* 82–83, 591 (1994).
272. V. Lujala, J. Skarp, M. Tammenmaa, and T. Suntola, *Appl. Surf. Sci.* 82–83, 34 (1994).
273. B. W. Sanders and A. Kitai, *Chem. Mater.* 4, 1005 (1992).
274. A. Hunter and A. H. Kitai, *J. Cryst. Growth* 91, 111 (1988).
275. C. H. Liu, M. Yokoyama, and Y. K. Su, *Japan. J. Appl. Phys.* 35, 5416 (1996).
276. C. T. Hsu, *Thin Solid Films* 335, 284 (1998).
277. C. T. Hsu, *J. Cryst. Growth* 193, 33 (1998).
278. C. T. Hsu, *Mater. Chem. Phys.* 58, 6 (1999).
279. A. Yoshikawa, M. Kobayashi, and S. Tokita, *Appl. Surf. Sci.* 82–83, 316 (1994).
280. I. Bhat and S. Akram, *J. Cryst. Growth* 138, 127 (1994).
281. C.-T. Hsu, *Japan. J. Appl. Phys.* 35, 4476 (1996).
282. M. Yokoyama, N. T. Chen, and H. Y. Ueng, *J. Cryst. Growth* 212, 97 (2000).
283. W.-S. Wang, H. Ehsani, and I. Bhat, *J. Electron. Mater.* 22, 873 (1993).
284. B. Sang and M. Konagai, *Japan. J. Appl. Phys.* 35, L602 (1996).
285. S. Chaisitsak, T. Sugiyama, A. Yamada, and M. Konagai, *Japan. J. Appl. Phys.* 38, 4989 (1999).
286. A. Shimizu, S. Chaisitsak, T. Sugiyama, A. Yamada, and M. Konagai, *Thin Solid Films* 361–362, 193 (2000).
287. E. B. Yousfi, J. Fouache, and D. Lincot, *Appl. Surf. Sci.* 153, 223 (2000).
288. E. B. Yousfi, T. Asikainen, V. Pietu, P. Cowache, M. Powalla, and D. Lincot, *Thin Solid Films* 361–362, 183 (2000).
289. A. Yamada, B. Sang, and M. Konagai, *Appl. Surf. Sci.* 112, 216 (1997).
290. B. Sang, A. Yamada, and M. Konagai, *Solar Energy Mater. Solar Cells* 49, 19 (1997).
291. B. Sang, A. Yamada, and M. Konagai, *Japan. J. Appl. Phys.* 37, L1125 (1998).
292. B. Sang, K. Dairiki, A. Yamada, and M. Konagai, *Japan. J. Appl. Phys.* 38, 4983 (1999).
293. A. W. Ott and R. P. H. Chang, *Mater. Chem. Phys.* 58, 132 (1999).
294. B. Sang, A. Yamada, and M. Konagai, *Japan. J. Appl. Phys.* 37, L206 (1998).
295. E. Soininen, G. Härkönen, and K. Vasama, "3rd International Conference on the Science and Technology of Display Phosphors," Huntington Beach, CA, 1997, p. 105, Extended Abstracts.
296. S. Moehnke, M. Bowen, S.-S. Sun, and R. Tuenge, "4th International Conference on the Science and Technology of Display Phosphors," Bend, OR, 1998, p. 203, Extended Abstracts.
297. H. Fujiwara, H. Kiryu, and I. Shimizu, *J. Appl. Phys.* 77, 3927 (1995).

298. Y. Luo, D. Slater, M. Han, J. Moryl, and R. M. Osgood, Jr., *Appl. Phys. Lett.* 71, 3799 (1997).
299. Y. Luo, D. Slater, M. Han, J. Moryl, R. M. Osgood, Jr., and J. G. Chen, *Langmuir* 14, 1493 (1998).
300. M. Han, Y. Luo, J. E. Moryl, R. M. Osgood, Jr., and J. G. Chen, *Surf. Sci.* 415, 251 (1998).
301. M. Han, Y. Luo, J. E. Moryl, and R. M. Osgood, Jr., *Surf. Sci.* 425, 259 (1999).
302. Y. Luo, M. Han, D. A. Slater, and R. M. Osgood, Jr., *J. Vac. Sci. Technol. A* 18, 438 (2000).
303. N. H. Karam, R. G. Wolfson, I. B. Bhat, H. Ehsani, and S. K. Ghandhi, *Thin Solid Films* 225, 261 (1993).
304. M. Ritala, M. Leskelä, and E. Rauhala, *Chem. Mater.* 6, 556 (1994).
305. J. Aarik, A. Aidla, V. Sammelselg, M. Ritala, and M. Leskelä, *Thin Solid Films* 370, 163 (2000).
306. H. Döring, K. Hashimoto, and A. Fujishima, *Ber. Bunsenges. Phys. Chem.* 96, 620 (1992).
307. M. Ritala, M. Leskelä, L. Niinistö, and P. Haussalo, *Chem. Mater.* 5, 1174 (1993).
308. J. Aarik, A. Aidla, T. Uustare, M. Ritala, and M. Leskelä, *Appl. Surf. Sci.* 161, 385 (2000).
309. M. Schuisky, K. Kukli, M. Ritala, A. Hårsta, and M. Leskelä, *Chem. Vapor Deposition* 6, 139 (2000).
310. K. Kukli, M. Ritala, and M. Leskelä, *Chem. Vapor Deposition* 6, 297 (2000).
311. K. Kukli, M. Ritala, M. Leskelä, and R. Lappalainen, *Chem. Vapor Deposition* 4, 29 (1998).
312. K. Kukli, M. Ritala, and M. Leskelä, *J. Electrochem. Soc.* 142, 1670 (1995).
313. K. Kukli, J. Aarik, A. Aidla, H. Siimon, M. Ritala, and M. Leskelä, *Appl. Surf. Sci.* 112, 236 (1997).
314. H.-J. Song, W. Koh, and S.-W. Kang, *Mater. Res. Soc. Symp. Proc.* 567, 469 (1999).
315. E. Nykänen, J. Laine-Ylijoki, P. Soininen, L. Niinistö, M. Leskelä, and L. G. Hubert-Pfalzgraf, *J. Mater. Chem.* 4, 1409 (1994).
316. T. Hatanpää, J. Ihanus, J. Kansikas, I. Mutikainen, M. Ritala, and M. Leskelä, *Chem. Mater.* 11, 1846 (1999).
317. M. Putkonen, L.-S. Johansson, E. Rauhala, and L. Niinistö, *J. Mater. Chem.* 9, 2449 (1999).
318. M. Tammenmaa, H. Antson, M. Asplund, L. Hiltunen, M. Leskelä, and L. Niinistö, *J. Cryst. Growth* 84, 151 (1987).
319. M. Leskelä, M. Mäkelä, L. Niinistö, E. Nykänen, and M. Tammenmaa, *Chemtronics* 3, 113 (1988).
320. J. Rautanen, M. Leskelä, L. Niinistö, E. Nykänen, P. Soininen, and M. Utriainen, *Appl. Surf. Sci.* 82–83, 553 (1994).
321. T. Hänninen, I. Mutikainen, V. Saanila, M. Ritala, M. Leskelä, and J. C. Hanson, *Chem. Mater.* 9, 1234 (1997).
322. M. Putkonen, A. Kosola, and L. Niinistö, private communication.
323. M. Leskelä, L. Niinistö, E. Nykänen, P. Soininen, and M. Tiitta, *Mater. Res. Soc. Symp. Proc.* 222, 315 (1991).
324. J. Aarik, A. Aidla, A. Jaek, M. Leskelä, and L. Niinistö, *J. Mater. Chem.* 4, 1239 (1994).
325. P. Soininen, E. Nykänen, L. Niinistö, and M. Leskelä, *Chem. Vapor Deposition* 2, 69 (1996).
326. V. Saanila, J. Ihanus, M. Ritala, and M. Leskelä, *Chem. Vapor Deposition* 4, 227 (1998).
327. M. Nieminen, L. Niinistö, and E. Rauhala, *J. Mater. Chem.* 6, 27 (1996).
328. H. Mölsä, L. Niinistö, and M. Utriainen, *Adv. Mater. Opt. Electron.* 4, 389 (1994).
329. M. Putkonen, T. Sajavaara, L.-S. Johansson, and L. Niinistö, *Chem. Vapor Deposition* 7, 44 (2001).
330. K. Kukli, M. Peussa, L.-S. Johansson, E. Nykänen, and L. Niinistö, *Mater. Sci. Forum* 315–317, 216 (1999).
331. K. Kukli, H. Heikkinen, E. Nykänen, and L. Niinistö, *J. Alloys Compd.* 275–277, 10 (1998).
332. H. Seim, M. Nieminen, L. Niinistö, H. Fjellvåg, and L.-S. Johansson, *Appl. Surf. Sci.* 112, 243 (1997).
333. H. Seim, H. Mölsä, M. Nieminen, H. Fjellvåg, and L. Niinistö, *J. Mater. Chem.* 7, 449 (1997).
334. O. Nilsen, M. Peussa, H. Fjellvåg, L. Niinistö, and A. Kjekshus, *J. Mater. Chem.* 9, 1781 (1999).
335. H. Mölsä and L. Niinistö, *Mater. Res. Soc. Symp. Proc.* 335, 341 (1994).
336. M. Tammenmaa, M. Leskelä, T. Koskinen, and L. Niinistö, *J. Less-Common Met.* 126, 209 (1986).
337. M. Leppänen, M. Leskelä, L. Niinistö, E. Nykänen, P. Soininen, and M. Tiitta, *SID 91 Dig.* 22, 282 (1991).
338. M. Leppänen, G. Härkönen, A. Pakkala, E. Soininen, and R. Törnqvist, "Conference Proceedings Eurodisplay 93," Starsbourg, 1993, p. 229.
339. T. Leskelä, K. Vasama, G. Härkönen, P. Sarkio, and M. Lounasmaa, *Adv. Mater. Opt. Electron.* 6, 169 (1996).
340. E. Nykänen, P. Soininen, L. Niinistö, M. Leskelä, and E. Rauhala, "Proceedings of the 7th International Workshop on Electroluminescence," Beijing, 1995, p. 437.
341. M. Utriainen, M. Kröger-Laukkanen, and L. Niinistö, *Mater. Sci. Eng. B* 54, 98 (1998).
342. M. Utriainen, M. Kröger-Laukkanen, L.-S. Johansson, and L. Niinistö, *Appl. Surf. Sci.* 157, 151 (2000).
343. P. Mårtensson and J.-O. Carlsson, *J. Electrochem. Soc.* 145, 2929 (1998).
344. P. Mårtensson and J.-O. Carlsson, *Electrochem. Soc. Proc.* 97-25, 1529 (1997).
345. P. Soininen, E. Nykänen, M. Leskelä, and L. Niinistö, unpublished results.
346. K. Swiatek, M. Godlewski, M. Leskelä, and L. Niinistö, *Acta Phys. Pol. A* 79, 255 (1991).
347. M. Leskelä, L. Niinistö, E. Nykänen, P. Soininen, and M. Tiitta, *J. Less-Common Met.* 153, 219 (1989).
348. K. Swiatek, M. Godlewski, M. Leskelä, and L. Niinistö, *J. Appl. Phys.* 74, 3442 (1993).
349. K. Swiatek, A. Suchocki, A. Stapor, L. Niinistö, and M. Leskelä, *J. Appl. Phys.* 66, 6048 (1989).
350. G. Härkönen, K. Härkönen, and R. Törnqvist, *SID 90 Dig.* 21, 232 (1990).
351. S. J. Yun, S.-D. Nam, J. S. Kang, K.-S. Nam, and H.-M. Park, "3rd International Conference on the Science and Technology of Display Phosphors," Huntington Beach, CA, 1997, p. 167, Extended Abstracts.
352. M. Asplund, J. Hölsä, M. Leskelä, L. Niinistö and E. Nykänen, *Inorg. Chim. Acta* 139, 261 (1987).
353. R. Huang and A. H. Kitai, *Appl. Phys. Lett.* 61, 1450 (1992).
354. R. Huang and A. H. Kitai, *J. Mater. Sci. Lett.* 12, 1444 (1993).
355. M. Putkonen, T. Sajavaara, and L. Niinistö, *J. Mater. Chem.* 10, 1857 (2000).
356. M. Vehkamäki, T. Hatanpää, T. Hänninen, M. Ritala, and M. Leskelä, *Electrochem. Solid-State Lett.* 2, 504 (1999).
357. M. Ritala, K. Kukli, M. Vehkamäki, T. Hänninen, T. Hatanpää, P. I. Räisänen, and M. Leskelä, *Proc. Electrochem. Soc.* 2000-13, 597 (2000).
358. M. Vehkamäki, T. Hänninen, M. Ritala, M. Leskelä, T. Sajavaara, E. Rauhala, and J. Keinonen, *Chem. Vapor Deposition* 7, 75 (2001).
359. J. Ihanus, T. Hänninen, T. Hatanpää, T. Aaltonen, I. Mutikainen, T. Sajavaara, J. Keinonen, M. Ritala, and M. Leskelä, submitted for publication.
360. G. Härkönen, M. Lahonen, E. Soininen, R. Törnqvist, K. Vasama, K. Kukli, L. Niinistö, and E. Nykänen, "4th International Conference on the Science and Technology of Display Phosphors," Bend, OR, 1998, p. 223, Extended Abstracts.
361. M. Tammenmaa, T. Koskinen, L. Hiltunen, L. Niinistö, and M. Leskelä, *Thin Solid Films* 124, 125 (1985).
362. M. Oikkonen, M. Blomberg, T. Tuomi, and M. Tammenmaa, *Thin Solid Films* 124, 317 (1985).
363. K. Kobayashi and S. Okudaira, *Chem. Lett.* 511 (1997).
364. L. Hiltunen, M. Leskelä, M. Mäkelä, and L. Niinistö, *Acta Chem. Scand. A* 41, 548 (1987).
365. H. Liu and J. W. Rogers, Jr., *J. Vac. Sci. Technol. A* 17, 325 (1999).
366. K. Kitahara, N. Ohtsuka, T. Ashino, M. Ozeki, and K. Nakajima, *Japan. J. Appl. Phys.* 32, L236 (1993).

367. J. N. Kidder, Jr., J. S. Kuo, A. Ludviksson, T. P. Pearsall, J. W. Rogers, Jr., J. M. Grant, L. R. Allen, and S. T. Hsu, *J. Vac. Sci. Technol. A* 13, 711 (1995).
368. A. Ludviksson, D. W. Robinson, and J. W. Rogers, Jr., *Thin Solid Films* 289, 6 (1996).
369. J. N. Kidder, Jr., H. K. Yun, J. W. Rogers, Jr., and T. P. Pearsall, *Chem. Mater.* 10, 777 (1998).
370. M. Nagano, S. Iwai, K. Nemoto, and Y. Aoyagi, *Japan. J. Appl. Phys.* 33, L1289 (1994).
371. N. Kano, S. Hirose, K. Hara, J. Yoshino, H. Munekata, and H. Kukimoto, *Appl. Surf. Sci.* 82–83, 132 (1994).
372. S. Hirose, N. Kano, K. Hara, H. Munekata, and H. Kukimoto, *J. Cryst. Growth* 172, 13 (1997).
373. J. Nishizawa, K. Aoki, S. Suzuki, and K. Kikuchi, *J. Electrochem. Soc.* 137, 1898 (1990).
374. J. Nishizawa, K. Aoki, and S. Suzuki, *J. Cryst. Growth* 99, 502 (1990).
375. Y. Takahashi and T. Urisu, *Japan. J. Appl. Phys.* 30, L209 (1991).
376. H. Nagasawa and Y. Yamaguchi, *Thin Solid Films* 225, 230 (1993).
377. H. Nagasawa and Y. Yamaguchi, *Appl. Surf. Sci.* 82–83, 405 (1994).
378. Y. Suda, D. Lubben, T. Motooka, and J. E. Greene, *J. Vac. Sci. Technol. B* 7, 1171 (1989).
379. T. Fuyuki, T. Yoshinobu, and H. Matsunami, *Thin Solid Films* 225, 225 (1993).
380. S. Hara, T. Meguro, Y. Aoyagi, M. Kawai, S. Misawa, E. Sakuma and S. Yoshida, *Thin Solid Films* 225, 240 (1993).
381. S. Imai, S. Takagi, O. Sugiura, and M. Matsumura, *Japan. J. Appl. Phys.* 30, 3646 (1991).
382. P. A. Coon, M. L. Wise, A. C. Dillon, M. B. Robinson, and S. M. George, *J. Vac. Sci. Technol. B* 10, 221 (1992).
383. Y. Takahashi, H. Ishii, and K. Fujinaga, *J. Electrochem. Soc.* 136, 1826 (1989).
384. J.-S. Min, H. S. Park, W. Koh, and S.-W. Kang, *Mater. Res. Soc. Symp. Proc.* 564, 207 (1999).
385. J.-S. Min, H. S. Park, and S.-W. Kang, *Appl. Phys. Lett.* 75, 1521 (1999).
386. J.-S. Min, Y.-W. Son, W.-G. Kang, S.-S. Chun, and S.-W. Kang, *Japan. J. Appl. Phys.* 37, 4999 (1998).
387. W. S. Rees, Jr., O. Just, and D. S. Van Derveer, *J. Mater. Chem.* 9, 249 (1999).
388. W. Gasser, Y. Uchida, and M. Matsumura, *Thin Solid Films* 250, 213 (1994).
389. K. Yamaguchi, S. Imai, N. Ishitobi, M. Takemoto, H. Miki, and M. Matsumura, *Appl. Surf. Sci.* 130–132, 202 (1998).
390. S. Morishita, W. Gasser, K. Usami, and M. Matsumura, *J. Non-Cryst. Solids* 187, 66 (1995).
391. S. Morishita, Y. Uchida, and M. Matsumura, *Japan. J. Appl. Phys.* 34, 5738 (1995).
392. M. Leskelä, L. Niinistö, P. Niemelä, E. Nykänen, P. Soininen, M. Tiitta, and J. Vähäkangas, *Vacuum* 41, 1457 (1990).
393. M. Ritala, K. Kukli, A. Rahtu, P. I. Räisänen, M. Leskelä, T. Sajavaara, and J. Keinonen, *Science* 288, 319 (2000).
394. V. E. Drozd, A. A. Tulub, V. B. Aleskovski, and D. V. Korol'kov, *Appl. Surf. Sci.* 82–83, 587 (1994).
395. K. Kukli, M. Ritala, and M. Leskelä, *Chem. Mater.* 12, 1914 (2000).
396. M. Leskelä and M. Ritala, *J. Phys. IV* 9, Pr8-837 (1999).
397. N. Kobayashi, Y. Kobayashi, Y. Yamauchi, and Y. Horikoshi, *Appl. Surf. Sci.* 60–61, 544 (1992).
398. M. Ritala and M. Leskelä, *Nanotechnology* 10, 19 (1999).
399. M. Aguilera and B. Aitchison, *Solid State Technol.*, Nov., 109 (1996).
400. M. Leskelä, W.-M. Li, and M. Ritala, "*Electroluminescence*," *Semicond., Semimet.* 64, 413 (1999).
401. P. D. Rack and P. H. Holloway, *Mater. Sci. Eng.* R21, 171 (1998).
402. A. Pakkala, EL displays based on ALE grown phosphors and insulator films, www.planar.com.
403. E. Soininen, G. Härkönen, and K. Vasama, "3rd International Conference on the Science and Technology of Display Phosphors," Huntington Beach, CA, 1997, p. 105, Extended Abstracts.
404. L. Hiltunen, M. Leskelä, L. Niinistö, E. Nykänen, P. Soininen, and M. Tiitta, *Acta Polytechnol. Scand. Ser. Appl. Phys.* 170, 233 (1990).
405. P. Soininen, M.Sc. Thesis, Helsinki University of Technology, Espoo, 1990.
406. E. Nykänen, S. Lehto, M. Leskelä, L. Niinistö, and P. Soininen, "Electroluminescence, Proceedings of the 6th International Workshop on Electroluminescence," El-Paso, 1992, p. 199.
407. S. J. Yun, Y. S. Kim, J. S. Kang, S.-H. K. Park, K. I. Cho, and D. S. Ma, *SID 99 Dig.* 30, 1142 (1999).
408. R. Törnqvist, *SID 97 Dig.* 28, 855 (1997); TFEL color by white, www.planar.com.
409. P. Soininen, M. Leskelä, L. Niinistö, E. Nykänen, and E. Rauhala, "Electroluminescence, Proceedings of the 6th International Workshop on Electroluminescence," El-Paso, 1992, p. 217.
410. E. Soininen, private communication.
411. T. Harju, G. Härkönen, M. Lahonen, J. Määttänen, E. Soininen, R. Törnqvist, K. Vasama, J. Viljanen, and T. Flegal, *SID 97 Dig.* 28, 859 (1997); Bright 320 (x3). 240 RGB TFEL display based on "color by white", www.planar.com.
412. J. Haaranen, T. Harju, P. Heikkinen, G. Härkönen, M. Leppänen, T. Lindholm, J. Maula, J. Määttänen, A. Pakkala, E. Soininen, M. Sonninen, R. Törnqvist, and J. Viljanen, *SID 95 Dig.* 26, 883 (1995).
413. R. Törnqvist, J. Antson, J. Skarp, and V. Tanninen, *IEEE Trans. Electron Devices* ED-30, 468 (1983).
414. D. Theis, H. Oppolzer, G. Ebbinghaus, and S. Schild, *J. Cryst. Growth* 63, 47 (1983).
415. Y. Charreire, A. Marbeuf, G. Tourillon, M. Leskelä, L. Niinistö, E. Nykänen, P. Soininen, and O. Tolonen, *J. Electrochem. Soc.* 139, 619 (1992).
416. J. Ihanus, T. Hänninen, M. Ritala, and M. Leskelä, "4th International Conference on the Science and Technology of Display Phosphors," Bend, OR, 1998, p. 263, Extended Abstracts.
417. S.-S. Sun and R. Khormaei, *Proc. SPIE* 1664, 48 (1992).
418. K. Kukli, M. Ritala, and M. Leskelä, *Electrochem. Soc. Proc.* 97-25, 1137 (1997).
419. J. Antson, *SID 82 Dig.* 13, 124 (1982).
420. S. Haukka, M. Tuominen, and E. Granneman, Semicon Europa/ Semieducation, Munich, 5th of April, 2000.
421. M. Houssa, M. Tuominen, M. Naili, V. Afanas'ev, A. Stesmans, S. Haukka, and M. M. Heyns, *J. Appl. Phys.* 87, 8615 (2000).
422. H. Kattelus, H. Ronkainen, and T. Riihisaari, *Int. J. Microcircuits Electron. Packag.* 22, 254 (1999).
423. H. Kattelus, H. Ronkainen, T. Kanniainen, and J. Skarp, "Proceedings of the 28th European Solid-State Device Research Conference ESSDERC'98," Bordeaux, France, 1998, p. 444.
424. M. Ritala, T. Asikainen, M. Leskelä, and J. Skarp, *Mater. Res. Soc. Symp. Proc.* 426, 513 (1996).
425. V. Lujala, J. Skarp, M. Tammenmaa, T. Suntola, and J. Wallinga, "Proceedings of the 12th European Photovoltaic Solar Energy Conference," Amsterdam, The Netherlands, 1994, p. 1511.
426. J. D. Ouwens, R. E. I. Schropp, J. Wallinga, W. F. van der Weg, M. Ritala, M. Leskelä, and J. Hyvärinen, "Proceedings of the 12th European Photovoltaic Solar Energy Conference," Amsterdam, The Netherlands, 1994, p. 1296.
427. H. Antson, M. Grasserbauer, M. Hamilo, L. Hiltunen, T. Koskinen, M. Leskelä, L. Niinistö, G. Stingeder, and M. Tammenmaa, *Fresenius Z. Anal. Chem.* 322, 175 (1985).
428. W. Barrow, R. Coovert, E. Dickey, T. Flegal, M. Fullman, C. King, and C. Laakso, "Conference Record of the 1994 International Display Research Conference," 1994, p. 498.
429. R. Matero, M. Ritala, M. Leskelä, T. Salo, J. Aromaa, and O. Forsen, *J. Phys. IV* 9, Pr8-493 (1999).
430. L. A. Okada and S. M. George, *Appl. Surf. Sci.* 137, 113 (1999).
431. M. Juppo, M. Ritala, and M. Leskelä, unpublished results.
432. J. Skarp, Y. Koskinen, S. Lindfors, A. Rautiainen, and T. Suntola, "Proceedings of the 10th European Photovoltaic Solar Energy Conference," Lisbon, Portugal, 1991, p. 567.

433. J. Skarp, E. Anttila, A. Rautiainen, and T. Suntola, *Int. J. Solar Energy* 12, 137 (1992).
434. T. Suntola, *MRS Bull.* Oct. 45 (1993).
435. D. Riihelä, M. Ritala, R. Matero, and M. Leskelä, *Thin Solid Films* 289, 250 (1996).
436. G. D. Parfitt, *Prog. Surf. Membr. Sci.* 11, 181 (1976).
437. M. Ritala, M. Juppo, K. Kukli, A. Rahtu, and M. Leskelä, *J. Phys. IV* 9, Pr8-1021 (1999).
438. A. Rahtu and M. Ritala, *Electrochem. Soc. Proc.* 2000-13, 105 (2000).
439. R. Matero, A. Rahtu, and M. Ritala, submitted for publication.
440. N. Kobayashi and Y. Kobayashi, *Thin Solid Films* 225, 32 (1993).
441. J. P. Simko, T. Meguro, S. Iwai, K. Ozasa, Y. Aoyagi, and T. Sugano, *Thin Solid Films* 225, 40 (1993).
442. A. Usui, *Thin Solid Films* 225, 53 (1993).
443. A. Koukitu and T. Taki, *Appl. Surf. Sci.* 112, 63 (1997).
444. A. Koukitu, T. Taki, K. Narita, and H. Seki, *J. Cryst. Growth* 198–199, 1111 (1999).
445. B. Y. Maa and P. D. Dapkus, *Thin Solid Films* 225, 12 (1993).
446. N. Kobayashi and Y. Horikoshi, *Japan. J. Appl. Phys.* 28, L1880 (1989).
447. D. E. Aspnes, J. P. Harbison, A. A. Studna, and L. T. Florez, *Phys. Rev. Lett.* 59, 1687 (1987).
448. A. Rosental, P. Adamson, A. Gerst, and A. Niilisk, *Appl. Surf. Sci.* 107, 178 (1996).
449. A. Rosental, P. Adamson, A. Gerst, H. Koppel, and A. Tarre, *Appl. Surf. Sci.* 112, 82 (1997).
450. R. G. van Welzenis, R. A. M. Bink, and H. H. Brongersma, *Appl. Surf. Sci.* 107, 255 (1996).
451. S. T. Ceyer, *Science* 249, 133 (1990).